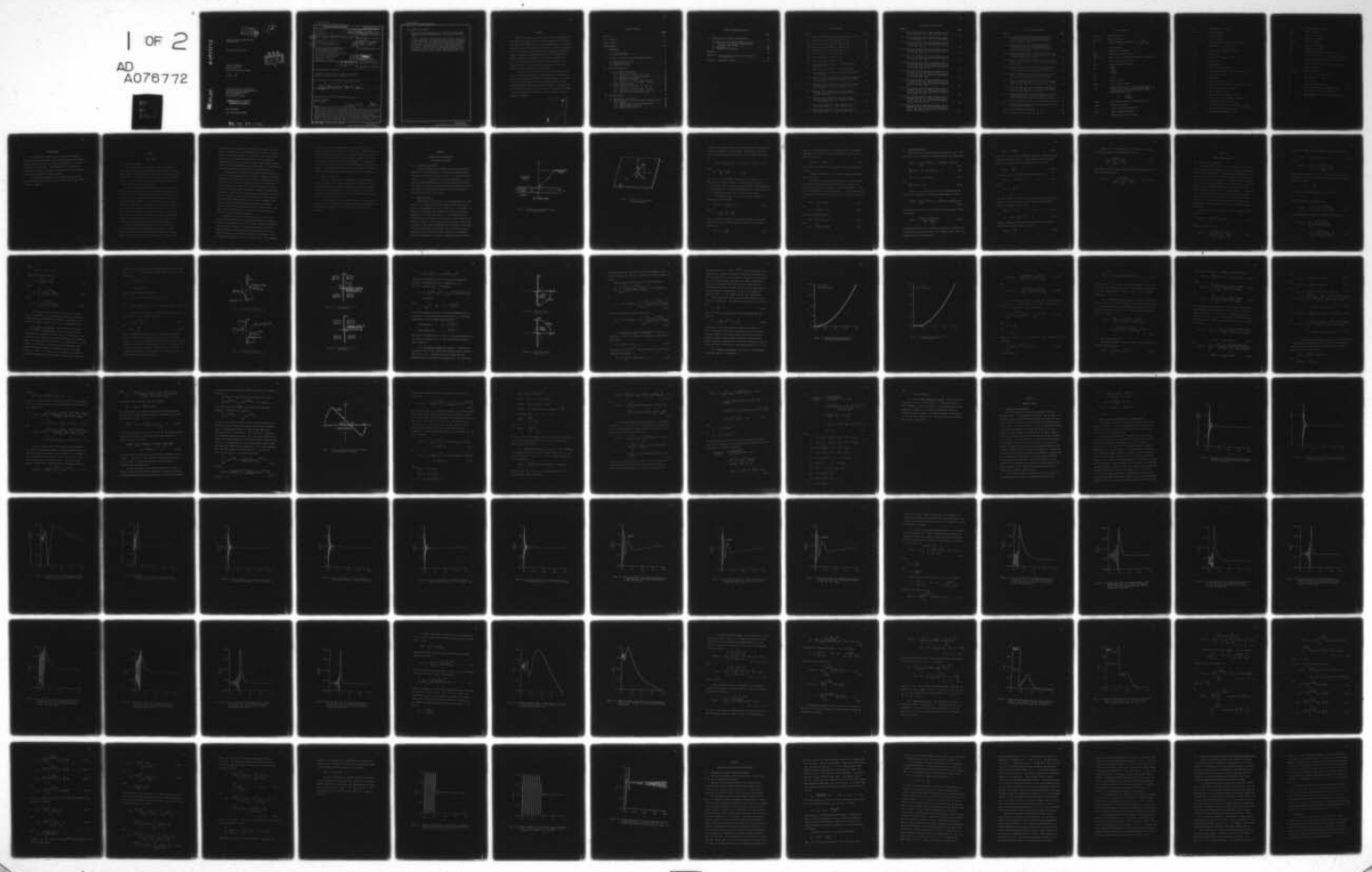
AD-A076 772 PENNSYLVANIA STATE UNIV UNIVERSITY PARK APPLIED RESE--ETC F/G 20/1
TRANSIENT ACOUSTIC RADIATION FROM ELASTIC PLATES.(U)
APR 79 S M SENGERDY N00024-79-C-6043
UNCLASSIFIED ARL/PSU/TM-79-50 NL

1 OF 2
AD A076772



LEVEL II

12

AD A076772

TRANSIENT ACOUSTIC RADIATION FROM ELASTIC PLATES

Seroj Mackertich Sengerdy

DDC
RECEIVED
NOV 15 1979
E

Technical Memorandum
File No. TM 79-50
April 2, 1979
Contract No. N00024-79-C-6043

Copy No. 5

The Pennsylvania State University
Institute for Science and Engineering
APPLIED RESEARCH LABORATORY
Post Office Box 30
State College, PA 16801

DDC FILE COPY

APPROVED FOR PUBLIC RELEASE
DISTRIBUTION UNLIMITED

NAVY DEPARTMENT

NAVAL SEA SYSTEMS COMMAND

79 11 15 001

UNCLASSIFIED

SECURITY CLASSIFICATION OF THIS PAGE (When Data Entered)

REPORT DOCUMENTATION PAGE

READ INSTRUCTIONS BEFORE COMPLETING FORM

1. REPORT NUMBER: TM 79-50
2. GOVT ACCESSION NO.: (9)
3. RECIPIENT'S CATALOG NUMBER: Doctoral thesis
4. TITLE (and Subtitle): (6) TRANSIENT ACOUSTIC RADIATION FROM ELASTIC PLATES
5. TYPE OF REPORT & PERIOD COVERED: PhD Thesis, May 1979
6. PERFORMING ORG. REPORT NUMBER: TM 79-50
7. AUTHOR(s): (10) Seroj Mackertich Sengerdy
8. CONTRACT OR GRANT NUMBER(s): (15) N00024-79-C-6043
9. PERFORMING ORGANIZATION NAME AND ADDRESS: The Pennsylvania State University, Applied Research Laboratory, P. O. Box 30, State College, PA 16801
10. PROGRAM ELEMENT, PROJECT, TASK AREA & WORK UNIT NUMBERS:
11. CONTROLLING OFFICE NAME AND ADDRESS: Navsl Sea Systems Command, Department of the Navy, Washington, DC 20362
12. REPORT DATE: Apr[redacted]979
13. NUMBER OF PAGES: 110 pages & figures
14. MONITORING AGENCY NAME & ADDRESS (if different from Controlling Office): (12) 112
15. SECURITY CLASS. (of this report): Unclassified, Unlimited
15a. DECLASSIFICATION/DOWNGRADING SCHEDULE:
16. DISTRIBUTION STATEMENT (of this Report):

Approved for public release, distribution unlimited, per NSSC (Naval Sea Systems Command), 5/2/79

17. DISTRIBUTION STATEMENT (of the abstract entered in Block 20, if different from Report):
18. SUPPLEMENTARY NOTES: (14) ARL/PSU/TM-79-50
19. KEY WORDS (Continue on reverse side if necessary and identify by block number):

acoustic radiation
elastic plates

391 007

20. ABSTRACT (Continue on reverse side if necessary and identify by block number):

An expression for the acoustic radiated pressure emanating from an infinite elastic plate excited by a unit impulse load for different observation angles and distances is obtained analytically. The solution is obtained by use of Fourier transform on time and Hankel transform on the radial coordinate. Using Cauchy contour integration theorem and regular and modified saddle-point methods, the inverse Fourier and Hankel transforms were evaluated. The unit impulse response and convolution theorem was then utilized to obtain an →

DD FORM 1 JAN 73 1473 EDITION OF 1 NOV 65 IS OBSOLETE

UNCLASSIFIED

SECURITY CLASSIFICATION OF THIS PAGE (When Data Entered)

20. ABSTRACT (Continued)

expression for radiated pressure of an infinite elastic plate excited by constant magnitude load, square pulse and CW-pulse loads.

The first arrival of acoustic wave at an observer point in the acoustic medium due to an impulse load was shown to correspond to the time of travel for the normal distance from the observer to the plate. After the first arrival, the acoustic pressure was shown to decay sinusoidally with an increasing period of oscillation. The decay rate for long times was shown to be the reciprocal of elapsed time. Similar response was shown for a square pulse and for a CW-pulse after the removal of the load.

ABSTRACT

An expression for the acoustic radiated pressure emanating from an infinite elastic plate excited by a unit impulse load for different observation angles and distances is obtained analytically. The solution is obtained by use of Fourier transform on time and Hankel transform on the radial coordinate. Using Cauchy contour integration theorem and regular and modified saddle-point methods, the inverse Fourier and Hankel transforms were evaluated. The unit impulse response and convolution theorem was then utilized to obtain an expression for radiated pressure of an infinite elastic plate excited by constant magnitude load, square pulse and CW-pulse loads.

The first arrival of acoustic wave at an observer point in the acoustic medium due to an impulse load was shown to correspond to the time of travel for the normal distance from the observer to the plate. After the first arrival, the acoustic pressure was shown to decay sinusoidally with an increasing period of oscillation. The decay rate for long times was shown to be the reciprocal of elapsed time. Similar response was shown for a square pulse and for a CW-pulse after the removal of the load.

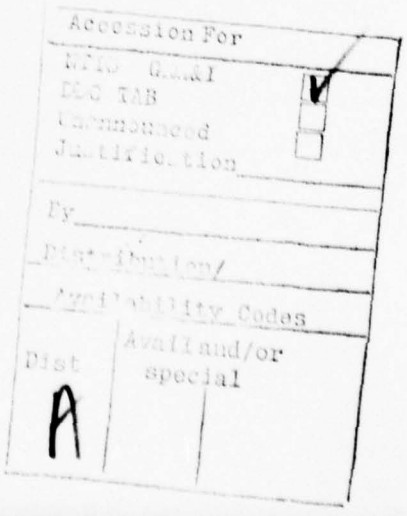


TABLE OF CONTENTS

	Page
Abstract	iii
List of Figures	vi
List of Symbols	ix
Acknowledgments	xii
I. INTRODUCTION	1
1.1 Literature Review	1
1.2 Goals of the Study	3
II. STATEMENT OF THE PROBLEM AND THE MATHEMATICAL MODEL	4
2.1 Statement of the Problem	4
2.2 Mathematical Model	4
2.3 Transformed Equations	9
III. INVERSE TRANSFORMATION	12
3.1 Inverse Fourier Transform	12
3.1.1 Choice of Branch Cuts	14
3.1.2 Evaluation of Integrals $\bar{P}_1$ and $\bar{P}_2$	18
3.1.3 Evaluation of the Pole Contributions	20
3.1.4 Computation of Residues	21
3.1.5 Evaluation of Integrals C_{R1} and C_{R2}	24
3.1.6 Final Solution of the Integral $I^*(k,z,t)$	25
3.2 Inverse Hankel Transform	25
3.2.1 Evaluation of Integrals I_{12} and I_{22}	27
3.2.2 Evaluation of Integrals I_{11} and I_{21}	33
3.2.3 Final Solution of the Integral $I(R,\phi,t)$	34
3.2.4 Special Case and Approximate Method	37
IV. NUMERICAL RESULTS	38
4.1 Introduction and Input Data	38
4.2 Radiated Pressure for Different Types of Applied Force	39
4.2.1 Impulse	39
4.2.2 Applied Force with a Constant Magnitude	51
4.2.3 Applied Square Pulse Force	63
4.2.4 Applied CW-Pulse Force	65

TABLE OF CONTENTS (Continued)

Page

V. DISCUSSIONS OF THE RESULTS AND CONCLUSIONS 77

5.1 Discussion of the Impulse Response Solutions 77
5.2 Discussion of the Radiated Pressure Due to Different Applied Loads 82
5.3 Conclusions 83
5.4 Suggested Future Research 84

REFERENCES 86

APPENDIX A: Acoustic Pressure Response in the Vicinity of the Vertical Axis 88

APPENDIX B: Approximate Solutions 90

LIST OF FIGURES

Figure		Page
2.1	Geometry and Coordinates Defining the Observation Point . . .	5
2.2	Geometry of the Plate and Coordinate System	6
3.1a	Branch Cuts in the Ω-Plane for Integral $\bar{P}_1$	16
3.1b	Branch Cuts in the Ω-Plane for Integral $\bar{P}_2$	16
3.2a	Branch Cuts for $\varepsilon = 0$ for Integral $\bar{P}_1$	17
3.2b	Branch Cuts for $\varepsilon = 0$ for Integral $\bar{P}_2$	17
3.3a	Integration Path in Ω-Plane for $\bar{P}_1$	19
3.3b	Integration Path in Ω-Plane for $\bar{P}_2$	19
3.4	Normalized Frequency Spectrum Ω Versus Normalized Wavenumber $\bar{k}$	22
3.5	Normalized Axial Wavenumber $\bar{\Gamma}$ Versus Wavenumber $\bar{k}$	23
3.6	Path of Integration and Path of Steepest Descent (PSD) in the k-Plane	31
4.1	Magnitude of the First Term of the Unit Impulse Response Versus Time for the Observation Point at $\phi = 30^\circ$ and $R/h = 50$	40
4.2	Magnitude of the First Term of the Unit Impulse Response Versus Time for the Observation Point at $\phi = 60^\circ$ and $R/h = 50$	41
4.3	Magnitude of the Second Term of the Unit Impulse Response Versus Time for the Observation Point at $\phi = 30^\circ$ and $R/h = 50$	42
4.4	Magnitude of the Second Term of the Unit Impulse Response Versus Time for the Observation Point at $\phi = 60^\circ$ and $R/h = 50$	43
4.5	Plot of the Acoustic Unit Impulse Response for the Observation Point at $\phi = 30^\circ$ and $R/h = 50$	44
4.6	Plot of the Acoustic Unit Impulse Response for the Observation Point at $\phi = 60^\circ$ and $R/h = 50$	45

LIST OF FIGURES (Continued)

Figure		Page
4.7	Plot of the Acoustic Unit Impulse Response for the Observation Point at $\phi = 30^{o}$ and R/h = 100	46
4.8	Plot of the Acoustic Unit Impulse Response for the Observation Point at $\phi = 30^{o}$ and R/h = 1000	47
4.9	Plot of the Acoustic Unit Impulse Response with an Expanded Time Scale for the Observation Point at $\phi = 30^{o}$ and R/h = 50	48
4.10	Plot of the Acoustic Unit Impulse Response with an Expanded Time Scale for the Observation Point at $\phi = 30^{o}$ and R/h = 100	49
4.11	Plot of the Acoustic Unit Impulse Response with an Expanded Time Scale for the Observation Point at $\phi = 30^{o}$ and R/h = 1000	50
4.12	Plot of the Acoustic Unit Impulse Response with an Expanded Time Scale for the Observation Point at $\phi = 30^{o}$ and R/h = 50 Obtained by the Modified Saddle-Point Method (MSP)	52
4.13	Plot of the Acoustic Unit Impulse Response with an Expanded Time Scale for the Observation Point at $\phi = 60^{o}$ and R/h = 50 Obtained by the Modified Saddle-Point Method (MSP)	53
4.14	Plot of the Acoustic Unit Impulse Response with an Expanded Time Scale for the Observation Point at $\phi = 30^{o}$ and R/h = 100 Obtained by the Modified Saddle-Point Method (MSP)	54
4.15	Plot of the Acoustic Unit Impulse Response with an Expanded Time Scale for the Observation Point at $\phi = 60^{o}$ and R/h = 100 Obtained by the Modified Saddle-Point Method (MSP)	55
4.16	Plot of the Acoustic Unit Impulse Response with an Expanded Time Scale for the Observation Point at $\phi = 30^{o}$ and R/h = 50 Obtained by the Regular Saddle-Point Method (RSP)	56
4.17	Plot of the Acoustic Unit Impulse Response with an Expanded Time Scale for the Observation Point at $\phi = 30^{o}$ and R/h = 100 Obtained by the Regular Saddle-Point Method (RSP)	57

LIST OF FIGURES (Continued)

Figure		Page
4.18	Plot of the Acoustic Unit Impulse Response with an Expanded Time Scale for the Observation Point at $\phi = 60^{o}$ and $R/h = 50$ Obtained by the Regular Saddle-Point Method (RSP)	58
4.19	Plot of the Acoustic Unit Impulse Response with an Expanded Time Scale for the Observation Point at $\phi = 60^{o}$ and $R/h = 100$ Obtained by the Regular Saddle-Point Method (RSP)	59
4.20	Normalized Radiated Pressure Versus Expanded Time Scale at the Observation Point $\phi = 30^{o}$ and $R/h = 50$ for a Constant Magnitude Applied Load	61
4.21	Normalized Radiated Pressure Versus Time at Observation Point $\phi = 30^{o}$ and $R/h = 50$ for a Constant Magnitude Applied Load	62
4.22	Normalized Radiated Pressure Versus Time at Observation Point $\phi = 30^{o}$ and $R/h = 50$ for a Square Pulse Applied Load with Pulse Length $T_o = 0.5 \cos\phi$	66
4.23	Normalized Radiated Pressure Versus Time at Observation Point $\phi = 30^{o}$ and $R/h = 50$ for a Square Pulse Applied Load with Pulse Length $T_o = \cos\phi - 0.1$	67
4.24	Normalized Radiated Pressure Versus Time at Observation Point $\phi = 30^{o}$ and $R/h = 50$ for a CW-Pulse Applied Load with Pulse Length $T_o = 0.5 \cos\phi$	74
4.25	Normalized Radiated Pressure Versus Time at Observation Point $\phi = 30^{o}$ and $R/h = 50$ for a CW-Pulse Applied Load with Pulse Length $T_o = \cos\phi - 0.1$	74
4.26	Normalized Radiated Pressure Versus Expanded Time Scale at Observation Point $\phi = 30^{o}$ and $R/h = 50$ for a CW-Pulse Applied Load with Pulse Length $T_o = \cos\phi - 0.1$.	76
B.1	Branch Cuts and Branch Points in the k-Plane for Integral $\bar{P}$.	92
B.2	Path of Integration and Path of Steepest Descent (PSD) in the k-Plane for Integral $\bar{P}$	93
B.3a	Integration Path in Ω-Plane for $\tau_1 > 0$	95
B.3b	Integration Path in Ω-Plane for $\tau_1 < 0$	95

LIST OF SYMBOLS

A_1 and A_2	defined on page 36
B_1 and B_2	defined on page 36
D	flexural rigidity of the plate: $D = \frac{Eh^3}{12(1 - \nu^2)}$
E	Young's modulus
F_o	amplitude of the impulse
H(t)	Heaviside unit step function
$H_o^{(1),(2)}$	Hankel function of first and second kind of degree zero
J_o	Bessel function of degree zero
MSP	modified saddle-point method
N_1	$= \frac{\beta\alpha c_o}{4\pi h^2 R}$
N_2	$= \frac{\alpha R \sin^2\phi}{4h}$
N_3	$= \omega_1 N_2$
P	acoustic pressure
PSD	path of steepest descent
P_o	radiated pressure from an infinite elastic plate excited by time harmonic point force of amplitude f_o at coincidence frequency and evaluated at the observation angle $\phi = 0$, $P_o = \frac{f_o \alpha R}{2\pi (R/h) h^2}$
Q(t)	time dependent amplitude of the applied force
(R,ϕ)	spherical coordinates
R	radius in spherical coordinates
RSP	regular saddle-point method
T	nondimensional time ($T = c_o t/R$)

T_o	nondimensional pulse length
X_1 and X_2	defined on page 36
Y_o	Neumann functions
Z_I and Z_{II}	defined on page 35
a	nondimensional retarded time ($a = T - \cos\phi$)
c_p	plate speed, $c_p = \frac{E}{\sqrt{12(1 - \nu^2)\rho}}$
c_o	phase velocity of the acoustic medium
f(r,t)	applied force
f_o	amplitude of the applied force
h	plate thickness
i	imaginary unit $\sqrt{-1}$
k	Hankel transform parameter
$\bar{k}$	nondimensional Hankel transform parameter ($\bar{k} = kh$)
k_p	pole in the k-plane
k_s	saddle point
k_o	acoustic wave number ($k_o = \omega/c_o$)
m	mass density of the plate, per unit area ($m = \rho h$)
r	radius in cylindrical coordinates
t	time variables, seconds
t_o	duration of the applied load, seconds
z	axial component in cylindrical coordinates
Ω	nondimensional frequency ($\Omega = \omega/\omega_o$)
Ω_1	nondimensional excitation frequency ($\Omega = \omega_1/\omega_o$)
Γ	wavenumber perpendicular to plate $\Gamma = (k^2 - \frac{\alpha^2\Omega^2}{h^2})^{1/2}$
$\bar{\Gamma}$	nondimensional wavenumber ($\bar{\Gamma} = \Gamma h$)

Φ	acoustic velocity potential
$\bar{\Phi}_I(k_s)$	defined on page 33
$\bar{\Phi}_1$	is equal to $Re[\bar{\Phi}_I(k_s)]$
$\bar{\Phi}_2$	is equal to $Im[\bar{\Phi}_I(k_s)]$
$\bar{\Phi}''_I(k_s)$	defined on page 33
$\bar{\Phi}''_a$	is equal to $Re[\bar{\Phi}''_I(k_s)]$
$\bar{\Phi}''_b$	is equal to $Im[\bar{\Phi}''_I(k_s)]$
τ_1	nondimensional retarded time ($\tau = T - 1.0$)
α	ratio of acoustic speed to plate speed ($\alpha = c_o/c_p$)
β	ratio of acoustic medium mass density to plate mass density ($\beta = \rho_o/\rho$)
ϕ	observation angle measured from vertical axis
$\delta(x)$	Dirac delta function
ψ_1, ψ_2 and ξ	defined on page 36
ρ_o	mass density of the fluid medium
ρ	mass density of the plate
ν	Poisson's ratio
ω	Fourier transform parameter
ω_o	coincidence frequency ($\omega_o = c_o^2\sqrt{m/D} = c_o^2/c_p h$)
ω_1	radian frequency of applied tone burst
$\bar{\omega}_1$	nondimensional frequency of applied tone burst ($\bar{\omega}_1 = \omega_1 R/c_o$)

ACKNOWLEDGMENTS

The author wishes to express his sincere appreciation to his thesis advisor, Professor Sabih I. Hayek, for his guidance and assistance throughout the entire study. He also wishes to thank Dr. A. D. Stuart for many helpful discussions. Acknowledgments are also extended to Professors V. H. Neubert, N. Davids, W. Thompson Jr. and E. J. Skudrzyk for serving on the author's doctoral committee.

This research was supported by the Applied Research Laboratory of The Pennsylvania State University under contract with the U. S. Naval Sea Systems Command.

CHAPTER I

INTRODUCTION

1.1 Literature Review

The acoustic radiation from elastic structures has occupied acousticians interested in radiated noise. Many structures are either large compared to the wavelength, or highly damped so that outgoing waves do not reflect from the boundaries, effectively making the structure infinite in extent. In this section, only the acoustic radiation from an infinite elastic plate will be reviewed.

The first solution to the radiated power from an elastic plate modeled by the classical plate theory was performed by Skudrzyk [1, 2] and by Heckl [3-5] for a point force, and Thompson and Rattaya [6] for point-moment. The solution for the acoustic radiated pressure from a point-excited plate using the classical theory was given by Gutin [7], Feit [8], and Skudrzyk [9]. The influence of fluid on the radiation from elastic plates was investigated by Maidanik and Kerwin [10]. All of these investigation employ the classical plate theory. Such a theory fails at high frequencies where the phase and group velocities become infinite as the frequency becomes unbounded. Such a plate theory is useful only up to frequencies where wavelength/plate thickness > 8.

To improve the high frequency predictions of elastic plates, Feit [11] employed the Timoshenko-Mindlin plate theory for such a prediction. This theory adds shear deformation and rotatory inertia effects to the classical flexural deformation theory. There are two

dispersion curves for this plate. The flexural (acoustic) branch has phase and group velocities approaching the shear velocity of the plate material as frequency increases. Stuart [12-14] explored the solution for the same plate further with new insights into the leaky waves emanating from the plate and obtained a more accurate solution when the angle of observation approaches the coincidence angle. This new solution would be accurate at closer observer distances than Feit's [11].

Sound radiation from beam-reinforced plates excited by point or line forces has been investigated by few authors. Romanov [15] obtained the solution of the radiated pressure from a plate reinforced with beams and excited by a line force. Feit and Saurenman [16] analyzed the acoustic radiation of a point-excited plate reinforced with beam, but confined their interest to high frequencies. Gorman [17] obtained the solution for a plate reinforced by many beams and excited by a line force parallel to beams. His solution thus makes the beam's influence purely as rotatory and transverse impedances with no waves travelling in the beams. Garrelick and Lin [18] analyzed the radiation from beam-reinforced plate and confined their attention to on-axis response. Lin and Hayek [19] obtained the exact solution for the radiation from a point-excited plate reinforced by one beam.

Investigations into the transient acoustic radiation from a plate under the influence of time dependent point forces were investigated by Magrab and Reader [20] and Stuart [12]. Magrab and Reader [20] predicted the time signature of the radiated pressure for a CW pulse. However, the solution was valid only after the acoustic arrival and there was an error in the choice of the poles in the solution. Stuart [12] predicted the impulse response of an elastic plate. His formulation

accounts for shear and rotary inertia effects of the plate, and the fluid loading coupling of the acoustic medium. The resulting far-field radiated pressure as determined from the standard saddle point method is for times before and after the acoustic arrival. However, the origin of the first arrival is not predictable by his method. The solution after the acoustic arrival was predicted to be monotonically decaying solution. However, it is more physically reasonable to assume that the plate will vibrate freely, generating an oscillating and decaying time signature.

1.2 Goals of the Study

Because of the inaccuracies or ambiguities in the prediction of the time signature of the radiated pressure emitted from a transiently excited plate, this study undertakes to predict the solution of such a problem exactly. Furthermore, since the exact solution is bound to be complicated, approximate solutions will be sought that are more accurate than the currently available ones.

The time signature of the radiated pressure is to be computed for an impulse force, a constant force, a square pulse, and a CW pulse. The behavior of the solutions at short times and for long times will be examined.

CHAPTER II

STATEMENT OF THE PROBLEM AND THE MATHEMATICAL MODEL

2.1 Statement of the Problem

Consider an infinite thin, undamped elastic plate excited by a point force as shown in Figure 2.1. The plate is in contact with an infinite acoustic medium occupying the space $z > 0$ and has vacuum in the space $z < 0$. The point force is applied dynamically at $t = 0$ with a prescribed amplitude versus time history, generating transient elastic waves in the plate and transient acoustic pressure in the fluid. The transient radiated pressure time history is to be evaluated at different points in the acoustic medium.

2.2 Mathematical Model

An infinite thin elastic plate, initially undeformed and at rest is excited by a dynamic point force as shown in Figures 2.1 and 2.2. Because of the axisymmetry of the force field, i.e., a point force, the geometric configuration can be expressed in cylindrical coordinates independent of circumferential angle θ. The assumption of thin lossless elastic plate allows one to use the Euler plate theory as the mathematical model for the governing equations of motion. However, the assumption of a thin plate breaks down when the wavelength in the plate is less than eight times the thickness. Thus, the Euler plate theory would lead to incorrect group and phase velocities for wavelengths shorter than eight times the thickness. Therefore, one would expect a

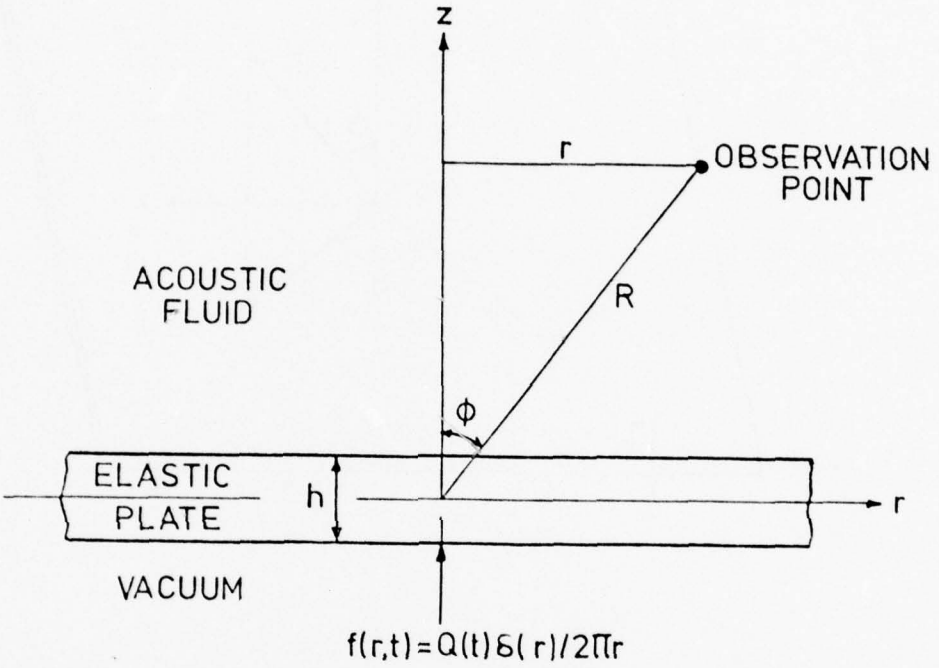


Figure 2.1 Geometry and Coordinates Defining the Observation Point

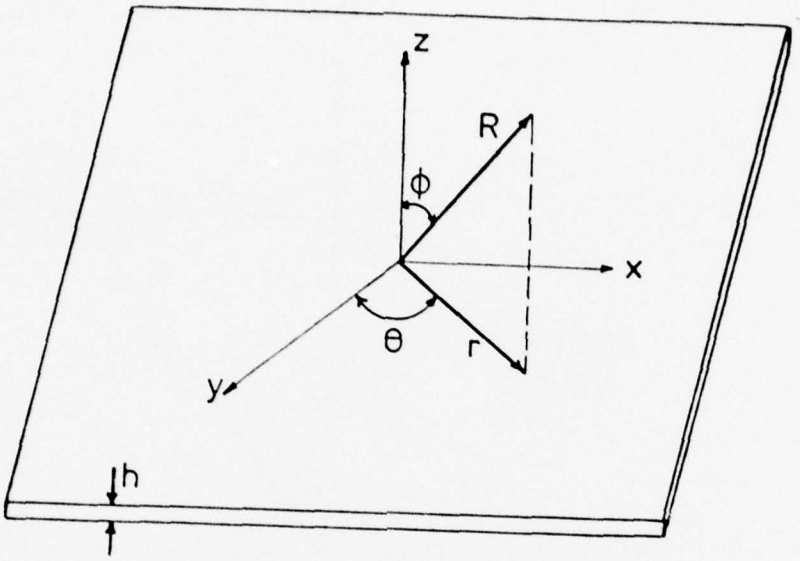


Figure 2.2 Geometry of the Plate and Coordinate Systems

slight error in the prediction of the first arrival which corresponds to an infinite frequency or zero wavelength. The equation of motion for the classical plate under the influence of a force field can be written as:

$$\nabla^4 W(r,t) + \frac{1}{c^2}\frac{1}{h^2 c_p^2}\frac{\partial^2 W}{\partial t^2}(r,t) = \frac{1}{D}[f(r,t) - P(r,o,t)] \quad , \quad (2.1)$$

where

$$\nabla^4 = \left[\frac{\partial^2}{\partial n^2} + \frac{1}{r}\frac{\partial}{\partial r}\right]^2 \quad , \qquad \begin{matrix} t > 0 \\ r \geq 0 \end{matrix}$$

where $W(r,t)$ is the transverse displacement of the plate, $f(r,t)$ is the applied force field, $P(r,o,t)$ is surface acoustic pressure, $D = (Eh^3)/[12(1-\nu^2)]$ is the plate flexural rigidity, $c_p^2 = E/[12(1-\nu^2)\rho]$ is the plate velocity, E is the Young's modulus, h is the thickness, ρ is the plate mass density, and ν is the Poisson's ratio.

The velocity potential $\Phi(r,z,t)$ of the acoustic medium is governed by the wave equation:

$$\nabla^2\phi(r,z,t) - \frac{1}{c_o^2}\frac{\partial^2\phi}{\partial t^2}(r,z,t) = 0 \quad , \quad (2.2)$$

where

$$\nabla^2 = \left[\frac{\partial^2}{\partial r^2} + \frac{1}{r}\frac{\partial}{\partial r} + \frac{\partial^2}{\partial z^2}\right] \quad ,$$

and c_o is the phase velocity of the acoustic medium. The acoustic pressure $P(r,z,t)$ in the fluid medium is related to the velocity potential by:

$$P(r,z,t) = \rho_o \frac{\partial\phi}{\partial t} \quad , \quad (2.3)$$

where ρ_o is the mass density of the acoustic medium. The boundary condition to be satisfied is continuity of normal velocity at fluid-plate interface, i.e.,

$$-\frac{\partial \phi}{\partial z}(r,o,t) = \frac{\partial W}{\partial t}(r,t) \quad . \tag{2.4}$$

The acoustic medium and plate are considered initially undisturbed and at rest.

In addition to Equation (2.4), the outward radiation condition must be satisfied.

The radiated pressure from an infinite elastic plate excited by an impulsive point force will be obtained by using transforms. The Fourier complex transform is applied to the temporal variable t, and the Hankel transform to the spatial variable r. These transform pairs are given by the following relations; the Fourier complex transform pair is:

$$F^*(\omega) = \int_{-\infty}^{\infty} f(t) e^{i\omega t} dt \quad , \tag{2.5a}$$

and

$$f(t) = \frac{1}{2\pi} \int_{-\infty}^{\infty} F^*(\omega) e^{-i\omega t} d\omega \quad , \tag{2.5b}$$

and the Hankel transform pair is:

$$\bar{F}(k) = \int_{o}^{\infty} r f(r) \, J_o(kr) dr \quad , \tag{2.6a}$$

and

$$f(r) = \int_{o}^{\infty} k \bar{F}(k) \, J_o(kr) dk \quad . \tag{2.6b}$$

2.3 Transformed Equations

Applying Fourier and Hankel transforms to Equations (2.1), (2.2), (2.3), and (2.4), the resulting transformed equations are, respectively:

$$k^4 \bar{W}^*(k,\omega) + \frac{1}{h^2 c_p^2}[-\omega^2 \bar{W}^*(k,\omega)] = \frac{1}{D}[\bar{f}^*(k,\omega) - \bar{P}^*(k,o,\omega)] \quad , \tag{2.7}$$

$$\frac{d^2 \bar{\Phi}^*}{dz^2}(k,z,\omega) - (k^2 - k_o^2)\,\bar{\Phi}^*(k,z,\omega) = 0 \quad , \tag{2.8}$$

$$\bar{P}^*(k,z,\omega) = -i\omega\rho_o\,\bar{\Phi}^*(k,z,\omega) \quad , \tag{2.9}$$

and

$$\frac{\partial \bar{\Phi}^*}{\partial z}(k,o,\omega) = i\omega \bar{W}^* \quad . \tag{2.10}$$

Equating z to zero in Equation (2.9), and substituting into Equation (2.7), results in the following coupled algebraic equation:

$$k^4 \bar{W}^*(k,\omega) + \frac{1}{h^2 c_p^2}[-\omega^2 \bar{W}^*(k,\omega)] = \frac{1}{D}[\bar{f}^*(k,\omega) + i\omega\rho_o \bar{\Phi}^*(k,o,\omega)] \quad . \tag{2.11}$$

Solving Equation (2.11) for the transformed plate displacement $\bar{W}^*(k,\omega)$, one obtains:

$$\bar{W}^*(k,\omega) = \frac{\bar{f}^*(k,\omega) + i\omega\rho_o \bar{\Phi}^*(k,o,\omega)}{D[k^4 - \frac{\omega^2}{h^2 c_p^2}]} \quad . \tag{2.12}$$

The applied force field to be considered in this study is assumed to be a point force acting at the origin of the coordinate system. Hence, the applied force can be represented by:

$$f(r,t) = \frac{Q(t)\delta(r)}{2\pi r} \quad , \tag{2.13}$$

where $\delta(r)$ is the Dirac delta function, and $Q(t)$ represents the time dependent amplitude of the force. Again applying Fourier and Hankel transforms to the force field in Equation (2.13), one obtains:

$$\bar{f}^*(k,\omega) = \frac{\bar{Q}(\omega)}{2\pi} \quad . \tag{2.14}$$

The general solution to Equation (2.8) can be written as:

$$\bar{\Phi}^*(k,z,\omega) = Ae^{\Gamma z} + Be^{\Gamma z} \quad , \qquad z > 0 \quad , \tag{2.15}$$

where

$$\Gamma = (k^2 - k_o^2)^{1/2}$$

and

$$k_o = \omega/c_o \quad .$$

The two solutions of $\bar{\Phi}^*(k,z,\omega)$ represent progressive waves that travel outward and inward in the z-direction. Imposing outward radiation condition on Equation (2.15) yields:

$$\bar{\Phi}^*(k,z,\omega) = Ae^{\Gamma z} \quad , \qquad z > 0 \quad , \tag{2.16}$$

and

$$\mathrm{Im}\Gamma = \mathrm{Im}[k^2 - k_o^2]^{1/2} > 0 \quad . \tag{2.17}$$

Applying Fourier and Hankel transform to Equation (2.4), and then equating with Equation (2.16), one obtains:

$$\bar{W}^*(k,\omega) = \frac{A\Gamma}{i\omega} \quad . \tag{2.18}$$

Solving for A from Equations (2.12) and (2.18), one obtains an expression for the pressure amplitude transform:

$$A = \frac{i\omega \overline{f}^{*}(k,\omega)}{L\left\{\left[k^4 - \frac{\omega^2}{h^2 c_p^2}\right]\Gamma + \frac{\omega^2 \rho_o}{D}\right\}} \quad . \tag{2.19}$$

From Equations (2.9), (2.14), (2.16), and (2.18), the transform of the pressure field is given by:

$$\overline{P}^{*}(k,z,\omega) = \frac{\rho_o \omega^2 Q(\omega) e^{\Gamma z}}{2\pi D\left\{(k^4 - \frac{\omega^2}{h^2 c_p^2})\Gamma + \frac{\omega^2 \rho_o}{D}\right\}} \quad , \quad z > 0 \ . \tag{2.20}$$

CHAPTER III

INVERSE TRANSFORMATION

3.1 Inverse Fourier Transform

One has a choice of which of the inverse transforms to perform first. It was decided to perform the inverse Fourier transform exactly first so that the integrand in the Hankel inverse transform is exact. Any approximations performed in the Hankel inverse transformation would thus be of known order. However, taking the Hankel inverse transform first and performing an approximation in its evaluations, as was done by Stuart [12], would lead to an approximate integrand in the Fourier inverse transform and hence would lead to an unknown order of approximation. Furthermore, the first arrival time would be unknown and the solution before the acoustic arrival would not have an initial value. In addition, the solution after the acoustic arrival would show an exponentially decaying signature, which is contrary to known experimental data.

Applying inverse Fourier transform on time to Equation (2.20), one obtains:

$$\bar{P}(k,z,t) = \frac{1}{2\pi}\int_{-\infty}^{\infty} \bar{P}^{*}(k,z,\omega)e^{-i\omega t}d\omega \quad . \tag{3.1}$$

Substituting for $\bar{P}^{*}(k,z,\omega)$:

$$\bar{P}(k,z,t) = \frac{\rho_o}{4\pi^2 D}\int_{-\infty}^{\infty} \frac{\omega^2 Q(\omega)e^{\Gamma z - i\omega t}\,d\omega}{(k^4 - \frac{\omega^2}{h^2 c_p^2})\,\Gamma + \frac{\omega^2\rho_o}{D}} \quad . \tag{3.2}$$

Using the convolution theorem, Equation (3.2) can be written as:

$$\bar{P}(k,z,t) = \int_o^t I^*(k,z,\tau)Q(t-\tau)d\tau \quad , \tag{3.3}$$

where

$$I^*(k,z,t) = \frac{\rho_o}{4\pi^2 D} \int_{-\infty}^{\infty} \frac{\omega^2 \, e^{\Gamma z - i\omega t} d\omega}{(k^4 - \frac{\omega^2}{h^2 c_p^2})\ \Gamma + \frac{\omega^2 \rho_o}{D}} \tag{3.4}$$

is the impulse response of the system. It will be convenient to normalize the angular frequency to that of the classical coincidence frequency defined by:

$$\omega_o = c_o^2 \sqrt{\frac{m}{D}} = \frac{c_o^2}{c_p h}$$

such that the normalized frequency Ω is defined as:

$$\Omega = \frac{\omega}{\omega_o} \quad .$$

Thus, Equation (3.4) can be rewritten as:

$$I^*(k,z,t) = \frac{\beta\alpha^5 c_o}{4\pi^2 h} \int_{-\infty}^{\infty} \frac{\Omega^2 \, e^{\Gamma z - i\omega_o \Omega t} d\Omega}{(\bar{k}^4 - \alpha^4\Omega^2)\ \bar{\Gamma} + \alpha^4\Omega^2\beta} \quad , \tag{3.5}$$

or, by dividing the integration path, Equation (3.5) becomes:

$$I^*(k,z,t) = \left\{ \int_{-\infty}^{o} \frac{\Omega^2 \, e^{\Gamma z - i\omega_o \Omega t} d\Omega}{(\bar{k}^4 - \alpha^4\Omega^2)\ \bar{\Gamma} + \alpha^4\Omega^2\beta} + \int_o^{\infty} \frac{\Omega^2 e^{\Gamma z - i\omega_o \Omega t} d\Omega}{(\bar{k}^4 - \alpha^4\Omega^2)\ \Gamma + \alpha^4\Omega^2\beta} \right\} \quad , \tag{3.5a}$$

where

$$\bar{k} = kh \quad \text{and} \quad \bar{\Gamma} = \Gamma h \quad .$$

Equation (3.5a) may be written as:

$$I^* = \frac{\beta\alpha^5 c_o}{4\pi^2 h} \left\{ \bar{P}_1 + \bar{P}_2 \right\} \quad , \tag{3.6}$$

where

$$\bar{P}_1 = \int_o^\infty \frac{\Omega^2 \, e^{\Gamma z - i\omega_o \Omega t} \, d\Omega}{(\bar{k}^4 - \alpha^4\Omega^2)\,\bar{\Gamma} + \alpha^4\Omega^2\beta} \tag{3.7}$$

and

$$\bar{P}_2 = \int_o^\infty \frac{\Omega^2 \, e^{\Gamma z + i\omega_o \Omega t} \, d\Omega}{(\bar{k}^4 - \alpha^4\Omega^2)\,\bar{\Gamma} + \alpha^4\Omega^2\beta} \quad . \tag{3.8}$$

To evaluate integrals in Equations (3.7) and (3.8), one can extend the variable Ω into the complex plane and use the method of Cauchy contour integration for their evaluation. The choice of the branch cuts, contour integration paths, etc., are enumerated below.

3.1.1 Choice of Branch Cuts. The existence of the function $\Gamma = \sqrt{k^2 - \alpha^2\Omega^2/h^2}$ in the integrals requires that integrand be made single-valued functions before Cauchy's theorem is to be applied. This requirement can be satisfied by introducing branch cuts in the complex plane. The branch points are defined by $\Gamma = 0$, which yields $\Omega_B = \pm \frac{\bar{k}}{\alpha}$ located on the real axis. To allow an effective application of the methods of operational analysis, a complex value of the wave number $\bar{k} = \bar{k}_1 + i\varepsilon$ (where $\varepsilon << 1$) has to be used instead of real valued k in order to avoid difficulties in constructing the paths of integration.

After the branch cut integrals have been determined, one may then take a limit as $\varepsilon \to 0$. For determination of branch cuts, one can start with the equation:

$$\bar{\Gamma} = (\bar{k}^2 - \alpha^2\Omega^2)^{1/2}$$

or

$$\bar{\Gamma}^2 = (\bar{k}^2 - \alpha^2\Omega^2) \quad ,$$

which in complex form may be written as:

$$h^2(\Gamma_1 + i\Gamma_2)^2 = (\bar{k}_1 + i\varepsilon)^2 - \alpha^2(\Omega_1 + i\Omega_2)^2$$

or

$$h^2(\Gamma_1^2 - \Gamma_2^2 + 2i\Gamma_1\Gamma_2) = \bar{k}_1^2 - \varepsilon^2 - \alpha^2\Omega_1^2 + \alpha^2\Omega_2^2 + 2i(\bar{k}_1\varepsilon - \alpha^2\Omega_1\Omega_2) \quad .$$

Applying the condition $\mathrm{Im}\Gamma = 0$, which will separate the $\mathrm{Im}\Gamma > 0$ plane from the $\mathrm{Im}\Gamma < 0$ plane, one obtains:

$$\Omega_1^2 - \Omega_2^2 < \frac{\bar{k}_1^2 - \varepsilon^2}{\alpha^2} \quad , \tag{3.9}$$

and

$$\Omega_1\Omega_2 = \frac{\bar{k}_1\varepsilon}{\alpha^2} \quad . \tag{3.10}$$

These two equations restrict the choice of a branch cut as shown in Figures 3.1a and 3.1b for integrations $\bar{P}_1$ and $\bar{P}_2$, respectively. Letting $\varepsilon \to 0$, the branch points will fall on the real Ω-axis, and the branch cuts will extend from branch points to $\pm i\infty$ on imaginary Ω-axis as shown in Figures 3.2a and 3.2b. The sign of the $\mathrm{Re}\Gamma$ in each quadrant of the top ($\mathrm{Im}\Gamma > 0$) and bottom ($\mathrm{Im}\Gamma < 0$) Riemann sheets can be obtained by the following procedure.

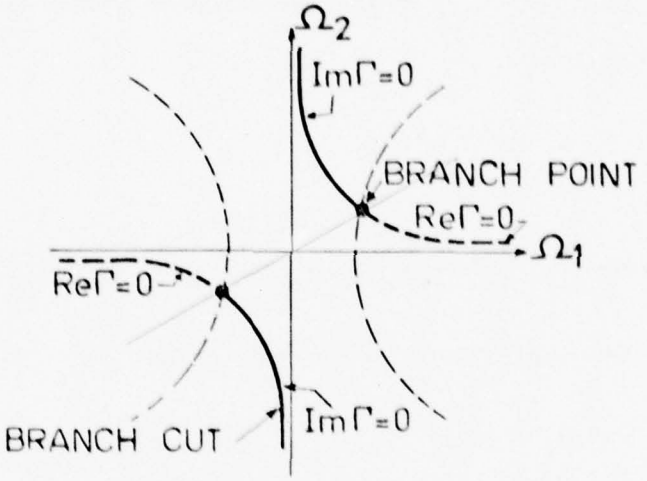


Figure 3.1a Branch Cuts in the Ω-Plane for Integral $\bar{P}_1$

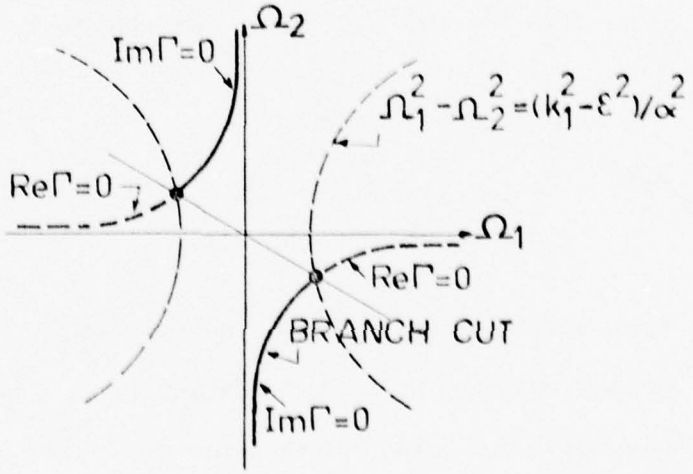


Figure 3.1b Branch Cuts in the Ω-Plane for Integral $\bar{P}_2$

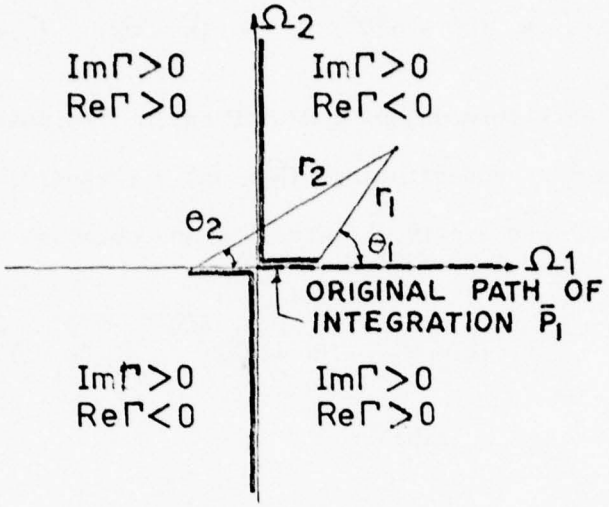


Figure 3.2a Branch Cuts for $\varepsilon = 0$ for Integral $\bar{P}_1$

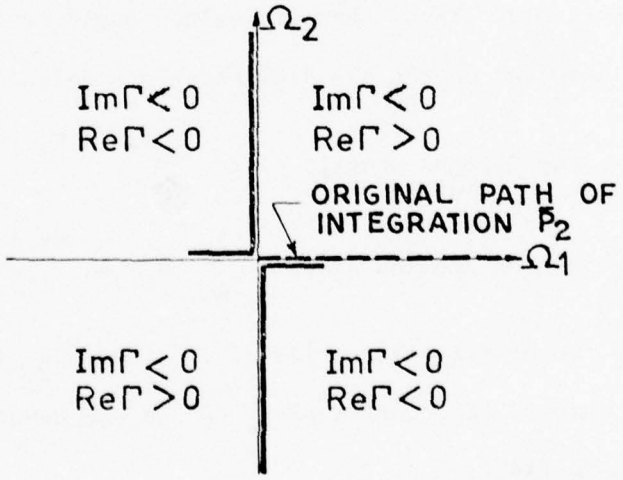


Figure 3.2b Branch Cuts for $\varepsilon = 0$ for Integral $\bar{P}_2$

Let

$$\bar{\Gamma} = (\bar{k}^2 - \alpha^2\Omega^2)^{1/2} = (\bar{k} - \alpha\Omega)^{1/2}(\bar{k} + \alpha\Omega)^{1/2} ,$$

where each term associated with one of the pair of branch points $\Omega_B = \pm \frac{\bar{k}}{\alpha}$. Substituting $(\bar{k} - \alpha\Omega) = r_1 \exp(i\theta_1 \pm i\pi)$ and $(\bar{k} + \alpha\Omega) = r_2 \exp(i\theta_2)$ into Γ , one obtains:

$$\bar{\Gamma} = (\bar{k} - \alpha\Omega)^{1/2}(\bar{k} + \alpha\Omega)^{1/2} = (r_1 r_2)^{1/2} \exp\left\{\frac{i(\theta_1 + \theta_2 \pm \pi)}{2}\right\}$$

$$= r_o \exp(i\theta_o) ,$$

where

$$r_o = (r_1 r_2)^{1/2} \quad \text{and} \quad \theta_o = \frac{\theta_1 + \theta_2 \pm \pi}{2}$$

are the amplitude and phase angle of the polar representation of Γ , respectively. Thus, the multivalued angle function θ_o can be made single-valued on the two Riemann sheets defined by:

top Riemann sheet $\quad \theta_o = \frac{\theta_1 + \theta_2 + \pi}{2}$

bottom Riemann sheet $\quad \theta_o = \frac{\theta_1 + \theta_2 - \pi}{2}$,

where the positive direction of θ_1 and θ_2 is measured from positive real axis of the complex plane Ω in the counterclockwise sense as shown in Figure 3.2.

3.1.2 Evaluation of Integrals $\bar{P}_1$ and $\bar{P}_2$. Examining the integrands in $\bar{P}_1$ and $\bar{P}_2$ together with outward radiation conditions $\mathrm{Im}\Gamma > 0$ and $\mathrm{Im}\Gamma < 0$, respectively, it can be shown that the integrations must be performed on top Riemann sheet. The closed paths

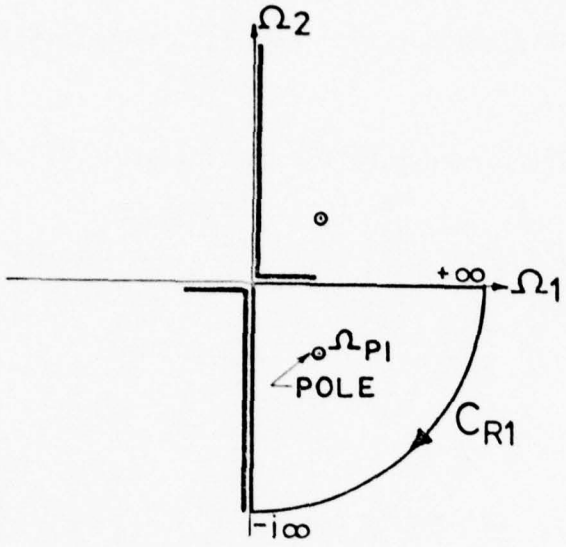


Figure 3.3a Integration Path in Ω-Plane for $\underline{P}_1$

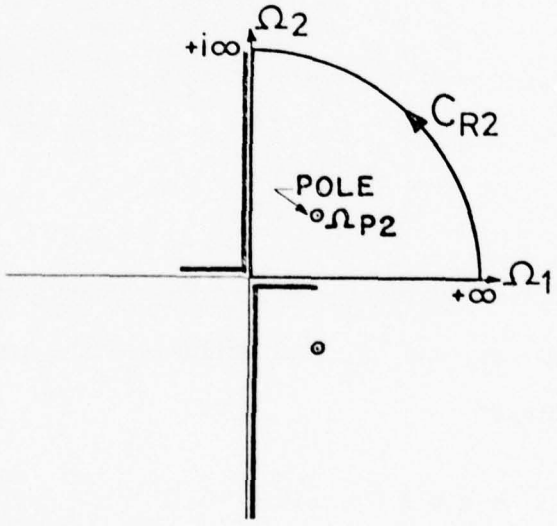


Figure 3.3b Integration Path in Ω-Plane for $\underline{P}_2$

of integration must be in the fourth and the first quadrants of the complex Ω-plane for $\bar{P}_1$ and $\bar{P}_2$, respectively, as shown in Figures 3.3a and 3.3b.

The closed path for the integral $\bar{P}_1$ may be written as:

$$\left\{ \int_0^{\infty} + \int_{C_{R1}} + \int_{-i\infty}^{0} \right\} \left[\frac{\Omega^2 \, e^{\Gamma z - i\omega_o \Omega t} \, d\Omega}{(\bar{k}^4 - \alpha^4\Omega^2)\,\bar{\Gamma} + \alpha^4\Omega^2\beta} \right] = -2\pi i \{ \Sigma \text{ Residues} \}_1$$

or

$$\bar{P}_1 = -2\pi i \{ \Sigma \text{ Residue} \}_1 - \left\{ \int_{cR_1} + \int_{-i\infty}^{0} \right\} \left[\frac{\Omega^2 \, e^{\Gamma z - i\omega_o \Omega t} \, d\Omega}{(\bar{k}^4 - \alpha^4\Omega^2)\,\bar{\Gamma} + \alpha^4\Omega^2\beta} \right] . \tag{3.11}$$

Similarly, the integral $\bar{P}_2$ may be written as:

$$\bar{P}_2 = +2\pi i \{ \Sigma \text{ Residues} \}_2 - \left\{ \int_{C_{R2}} + \int_{i\infty}^{0} \right\} \left[\frac{\Omega^2 \, e^{\Gamma z + i\omega_o \Omega t} \, d\Omega}{(\bar{k}^4 - \alpha^4\Omega^2)\,\bar{\Gamma} + \alpha^4\Omega^2\beta} \right] . \tag{3.12}$$

3.1.3 Evaluation of the Pole Contributions. The poles of integrals $\bar{P}_1$ and $\bar{P}_2$ are defined as the homogeneous roots of their denominators:

$$(\bar{k}^4 - \alpha^4\Omega^2)\,\bar{\Gamma} + \alpha^4\Omega^2\beta = 0 \quad . \tag{3.13}$$

Substituting $\alpha\Omega = (\bar{k}^2 - \bar{\Gamma}^2)^{1/2}$ into Equation (3.13), one obtains the following cubic equation:

$$\bar{\Gamma}^3 - \beta\bar{\Gamma}^2 + \frac{\bar{\Gamma}}{\alpha^2}(\bar{k}^4 - \alpha^2\bar{k}^2) + \bar{k}^2\beta = 0 \quad . \tag{3.14}$$

The multivaluedness of $\bar{\Gamma} = (\bar{k}^2 - \alpha^2\Omega^2)^{1/2}$ indicates that there are six complex Ω-poles. Numerical computation of these roots shows that four of these complex poles fall on top Riemann sheet ($Im\Gamma > 0$) and two real poles fall on bottom Riemann sheet ($Im\Gamma < 0$). However, only the two poles on top Riemann sheet that fall inside the closed contour of integration are needed in the Residue theorem. Let the poles that fall inside the contour of integration of $\bar{P}_1$ and $\bar{P}_2$ be designed as $\Omega_{p1}(Re\Gamma > 0,\ Im\Gamma > 0)$ and $\Omega_{p2}(Re\Gamma > 0,\ Im\Gamma < 0)$, respectively.

One can approximate the position of the pole that falls inside the paths of integration. The approximate expressions for Ωp and $\bar{\Gamma} p$ are:

$$\Omega p \approx \frac{\bar{k}^2}{\alpha^2} \quad , \tag{3.15a}$$

which represents the frequency spectrum for an unloaded Euler plate model, and

$$\bar{\Gamma} p \approx \pm i\left(\frac{k^4}{\alpha^2} - k^2\right)^{1/2} \approx \pm i\,\frac{\bar{k}^2}{\alpha} \quad , \tag{3.15b}$$

respectively. These approximations are good for large values of k. Closer examination of these expressions shows that they are valid for frequencies above the coincidence frequency where the acoustic mass loading is minimal. Comparing these approximate values with exact values computed from Equations (3.13) and (3.14), in Figures 3.4 and 3.5, one can conclude that these are very good approximations for $k > 1.0$.

3.1.4 Computation of Residues. The residue of the integrands at the simple poles are, respectively:

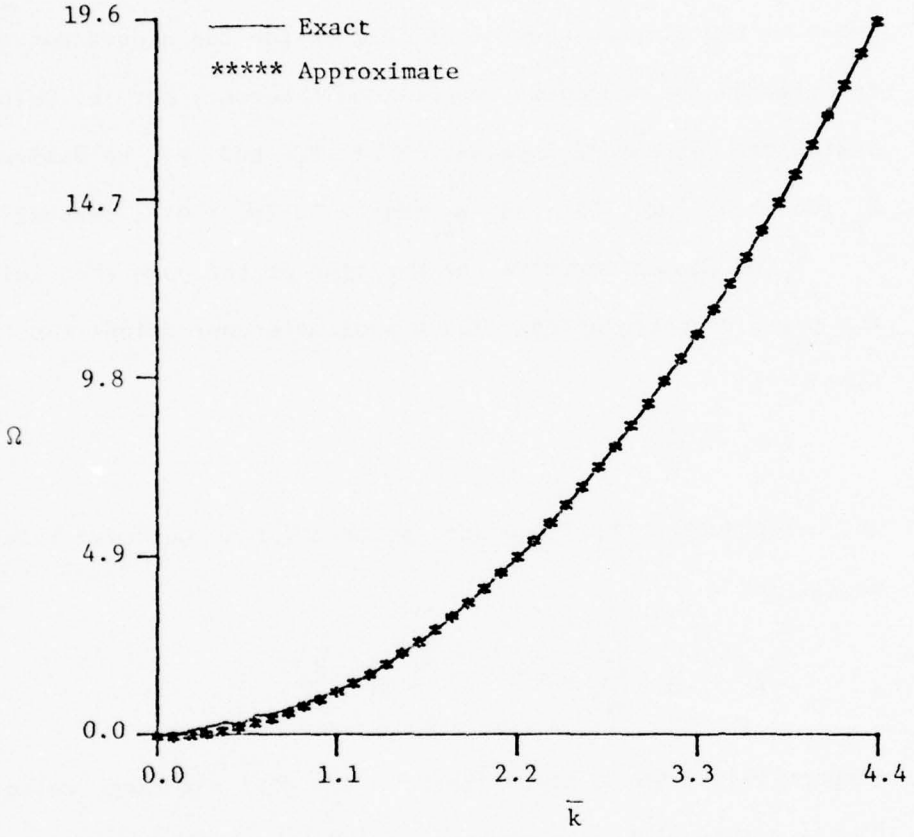


Figure 3.4 Normalized Frequency Spectrum $\bar{\Omega}$ Versus Normalized Wavenumber $\bar{k}$

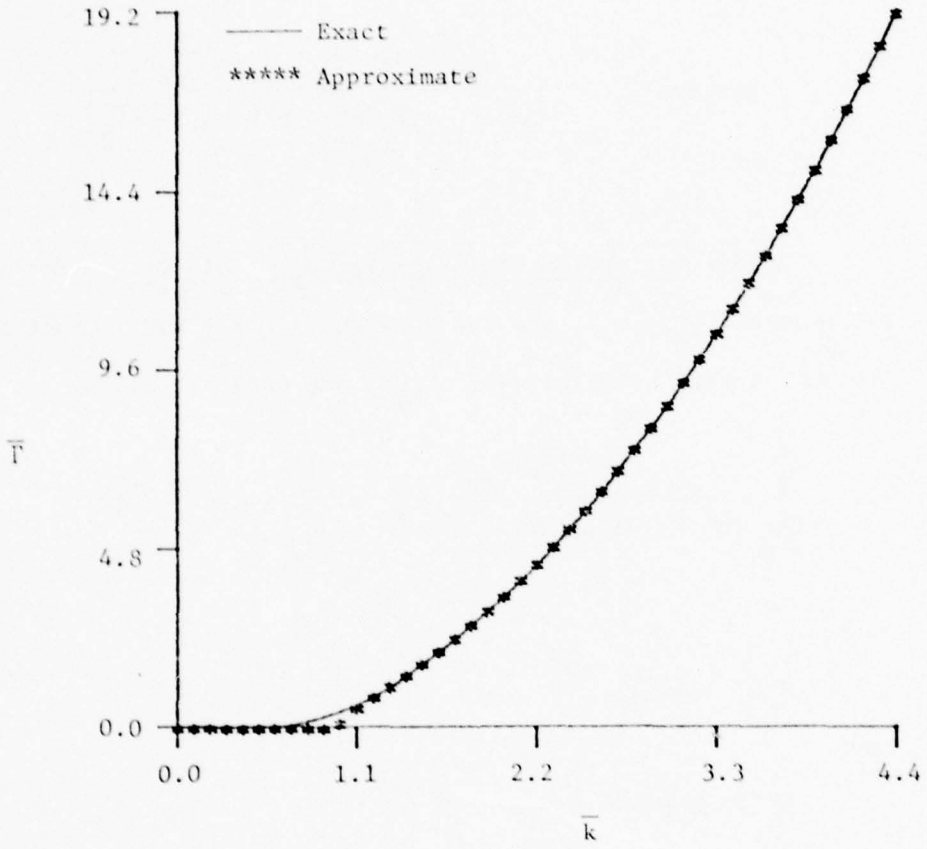


Figure 3.5 Normalized Axial Wavenumber $\bar{\Gamma}$ Versus Wavenumber $\bar{k}$

$$\{ \text{Residue} \}_1 = \frac{\Omega_{p1}\bar{\Gamma}_{p1}\exp\{\Gamma_{p1}z - i\omega_o\Omega_{p1}t\}}{3\alpha^6\Omega_{p1}^2 - 2\alpha^4\bar{k}^2 - \alpha^2\bar{k}^4 + 2\alpha^4\beta\bar{\Gamma}_{p1}} \quad , \qquad (3.16a)$$

and

$$\{ \text{Residue} \}_2 = \frac{\Omega_{p2}\bar{\Gamma}_{p2}\exp\{\Gamma_{p2}z + i\omega_o\Omega_{p2}t\}}{3\alpha^6\Omega_{p1}^2 - 2\alpha^4\bar{k}^2 - \alpha^2\bar{k}^4 + 2\alpha^4\beta\bar{\Gamma}_{p2}} \quad . \qquad (3.16b)$$

3.1.5 Evaluation of Integrals C_{R1} and C_{R2}. For large value of Ω (i.e., $\Omega \to \infty$), one can show that $\bar{\Gamma} \to \pm i\alpha\Omega$. Substituting $\bar{\Gamma} = i\alpha\Omega$ in the integral over C_{R1}, one obtains:

$$\int_{C_{R1}} \frac{\Omega^2 e^{i\alpha\Omega z - i\omega_o\Omega t} d\Omega}{(\bar{k}^4 - \alpha^4\Omega^2)(i\alpha\Omega) + \alpha^4\beta\Omega^2} = \int_{C_{R1}} A(\Omega)e^{-i\alpha\Omega\tau} d\Omega \quad , \qquad (3.17)$$

where

$$A(\Omega) \sim 0\left(\frac{1}{\Omega}\right)$$

and

$$\tau = c_o t - z \quad .$$

Changing the variable Ω to θ by letting $\Omega = \rho_1 e^{i\theta}$ in Equation (3.17), one obtains:

$$\int_0^{-\pi/2} A(\rho_1 e^{i\theta})\, e^{-i\alpha\tau\rho_1 e^{i\theta}} (i\rho_1 e^{i\theta}) d\theta \quad . \qquad (3.18)$$

One can show that:

$$\lim_{\rho_1 \to \infty} \int_0^{-\pi/2} A(\rho_1 e^{i\theta}) i\rho_1 e^{i\theta} \exp(-i\alpha\tau\rho_1 e^{i\theta}) d\theta \to 0 \quad , \tag{3.19}$$

provided that $\tau = c_o t - z \geq 0$, and becomes unbounded if $c_o t - z < 0$. Similarly, one can show that the integration on the large circular path C_{R2} will vanish for large Ω , when $\tau = c_o t - z \geq 0$, and becomes unbounded if $c_o t - z < 0$.

3.1.6 Final Solution of the Integral $I^*(k,z,t)$. Substituting Equations (3.15) and (3.16) into Equations (3.11) and (3.12), respectively, and substituting the resulting equations into Equation (3.6), and using the relationship $\int_{i\infty}^{o} + \int_{-i\infty}^{o} = 0$, then the final expression for $I^*(K,z,t)$ becomes:

$$I^*(k,z,t) = \frac{i\beta\alpha^5 c_o}{2\pi h} \left\{ \frac{\Omega_{p1}\bar{\Gamma}_{p1} \exp[\Gamma_{p1} z - i\omega_o \Omega_{p1} t]}{3\alpha^6\Omega_{p1}^2 - 2\alpha^4\bar{k}^2 - \alpha^2\bar{k}^4 + 2\alpha^4 \bar{\Gamma}_{p1}\beta} \right.$$

$$\left. + \frac{\Omega_{p2}\bar{\Gamma}_{p2} \exp[\Gamma_{p2} z + i\omega_o \Omega_{p2} t]}{3\alpha^6\Omega_{p2}^2 - 2\alpha^4\bar{k}^2 - \alpha^2\bar{k}^4 + 2\alpha^4\beta\bar{\Gamma}_{p2}} \right\} H(c_o t - z) \quad . \tag{3.20}$$

3.2 Inverse Hankel Transform

Applying inverse Hankel transform to inverse Fourier transform in Equation (3.20), one obtains:

$$I(r,z,t) = \int_0^{\infty} k I^*(k,z,t) J_o(kr) \, dk \quad . \tag{3.21}$$

Substituting for $I^*(k,z,t)$ from Equation (3.20), one obtains:

$$I(r,z,t) = \frac{i\beta\alpha^5 c_o}{2\pi h} \{-I_1(r,z,t) + I_2(r,z,t)\} H(c_o t - z) \quad (3.22)$$

where

$$I_1(r,z,t) = \int_o^\infty \frac{\Omega_{p1}\bar{\Gamma}_{p1} k \exp\{\Gamma_{p1} z - i\omega_o \Omega_{p1} t\} J_o(kr)dk}{3\alpha^6\Omega_{p1}^2 - 2\alpha^4\bar{k}^2 - \alpha^2\bar{k}^4 + 2\alpha^4\beta\bar{\Gamma}_{p1}} , \quad (3.23)$$

and

$$I_2(r,z,t) = \int_o^\infty \frac{\Omega_{p2}\bar{\Gamma}_{p2} k \exp\{\Gamma_{p2} z + i\omega_o \Omega_{p2} t\} J_o(kr)dk}{3\alpha^6\Omega_{p2}^2 - 2\alpha^4\bar{k}^2 - \alpha^2\bar{k}^4 + 2\alpha^4\beta\bar{\Gamma}_{p2}} . \quad (3.24)$$

It should be noted that the degree of the polynomials in the numerator and denominator of the integrands of Equations (3.23) and (3.24) are equal. The two must be divided so that the remainder function has a denominator that is at least one degree higher than the numerator and consequently, Hankel inverse transformation would converge. Dividing out, one obtains:

$$I_1(r,z,t) = \int_o^\infty \left\{ \frac{i}{2\alpha^5} + \frac{2\alpha^5\Omega_{p1}\bar{\Gamma}_{p1} - i[3\alpha^6\Omega_{p1}^2 - 2\alpha^4\bar{k}^2 - \alpha^2\bar{k}^4 + 2\alpha^4\beta\bar{\Gamma}_{p1}]}{2\alpha^5(3\alpha^6\Omega_{p1}^2 - 2\alpha^4\bar{k}^2 - \alpha^2\bar{k}^4 + 2\alpha^4\beta\bar{\Gamma}_{p1})} \right\}$$

$$\times \exp\{\Gamma_{p1} z - i\omega_o \Omega_{p1} t\} kJ_o(kr)dk \quad (3.25a)$$

and

$$I_2(r,z,t) = \int_o^\infty \left\{ \frac{-i}{2\alpha^5} + \frac{2\alpha^5\Omega_{p2}\bar{\Gamma}_{p2} + i[3\alpha^6\Omega_{p2}^2 - 2\alpha^4\bar{k}^2 - \alpha^2\bar{k}^4 + 2\alpha^4\beta\bar{\Gamma}_{p2}]}{2\alpha^5(3\alpha^6\Omega_{p2}^2 - 2\alpha^4\bar{k}^2 - \alpha^2\bar{k}^4 + 2\alpha^4\beta\bar{\Gamma}_{p2})} \right\}$$

$$\times \exp\{\Gamma_{p2} z + i\omega_o \Omega_{p2} t\} kJ_o(kr)dk . \quad (3.25b)$$

Let

$$I_1(r,z,t) = I_{11}(r,z,t) + I_{12}(r,z,t) \tag{3.26}$$

and

$$I_2(r,z,t) = I_{21}(r,z,t) + I_{22}(r,z,t) \quad , \tag{3.27}$$

where

$$I_{11}(r,z,t) = \frac{i}{2\alpha^5} \int_o^\infty k\, J_o(kr)\, \exp\{\Gamma_{p1} z - i\omega_o \Omega_{p1} t\}\, dk \quad , \tag{3.28}$$

$$I_{12}(r,z,t) = \int_o^\infty \left\{ \frac{2\alpha^5 \Omega_{p1} \overline{\Gamma}_{p1} - i[3\alpha^6 \Omega_{p1}^2 - 2\alpha^4 \overline{k}^2 - \alpha^2 \overline{k}^4 + 2\alpha^4 \beta \overline{\Gamma}_{p1}]}{2\alpha^5 (3\alpha^6 \Omega_{p1}^2 - 2\alpha^4 \overline{k}^2 - \alpha^2 \overline{k}^4 + 2\alpha^4 \beta \overline{\Gamma}_{p1})} \right\}$$

$$\times\ k\, J_o(kr)\, \exp\{\Gamma_{p1} z - i\omega_o \Omega_{p1} t\}\, dk \quad , \tag{3.29}$$

$$I_{21}(r,z,t) = \frac{-i}{2\alpha^5} \int_o^\infty \left\{ k\, J_o(kr)\, \exp[\Gamma_{p2} z + i\omega_o \Omega_{p2} t] \right\} dk \tag{3.30}$$

and

$$I_{22}(r,z,t) = \int_o^\infty \left\{ \frac{2\alpha^5 \Omega_{p2} \overline{\Gamma}_{p2} + i[3\alpha^6 \Omega_{p2}^2 - 2\alpha^4 \overline{k}^2 - \alpha^2 \overline{k}^4 + 2\alpha^4 \beta \overline{\Gamma}_{p2}]}{2\alpha^5 (3\alpha^6 \Omega_{p2}^2 - 2\alpha^4 \overline{k}^2 - \alpha^2 \overline{k}^4 + 2\alpha^4 \beta \overline{\Gamma}_{p2})} \right\}$$

$$\times\ k\, J_o(kr)\, \exp\{\Gamma_{p2} z + i\omega_o \Omega_{p2} t\}\, dk \quad . \tag{3.31}$$

3.2.1 Evaluation of Integrals I_{12} and I_{22}. In the evaluation of the integral in Equations (3.29) and (3.31), it is advantageous to change from Bessel functions to Hankel functions in the integrands. Thus, use is made of the identity:

$$J_o(kr) = \frac{1}{2} [H_o^{(1)}(kr) + H_o^{(2)}(kr)]$$

and

$$H_o^{(1)}(kr) = - H_o^{(2)}(-kr) \quad .$$

Letting

$$H_o^{(1),(2)}(kr) \approx \sqrt{\frac{2}{\pi kr}}\ \exp\{\pm i(kr - \tfrac{\pi}{4})\} \quad ,$$

which is the asymptotic form of the Hankel functions for large arguments ($kr > 1$), and neglecting higher order terms, Equations (3.29) and (3.31) can be written as:

$$I_{12}(r,z,t) = \sqrt{\frac{1}{2\pi r}} \int_{-\infty}^{\infty} \frac{[2\alpha^5 \Omega_{p1} \bar{\Gamma}_{p1} - i(3\alpha^6 \Omega_{p1}^2 - 2\alpha^4 \bar{k}^2 - \alpha^2 \bar{k}^4 + 2\alpha^4 \beta \bar{\Gamma}_{p1}]}{2\alpha^5 (3\alpha^6 \Omega_{p1}^2 - 2\alpha^4 \bar{k}^2 - \alpha^2 \bar{k}^4 + 2\alpha^4 \beta \bar{\Gamma}_{p1})}$$

$$\times\ k^{1/2} \exp\{\Gamma_{p1} z - i\omega_o \Omega_{p1} t + ikr - \tfrac{\pi}{4}\}\, dk \qquad (3.32)$$

and

$$I_{22}(r,z,t) = \sqrt{\frac{1}{2\pi r}} \int_{-\infty}^{\infty} \frac{\{2\alpha^5 \Omega_{p2} \bar{\Gamma}_{p2} + i[3\alpha^6 \Omega_{p2}^2 - 2\alpha^4 \bar{k}^2 - \alpha^2 \bar{k}^4 + 2\alpha^4 \beta \bar{\Gamma}_{p2}]\}}{2\alpha^5 (3\alpha^6 \Omega_{p2}^2 - 2\alpha^4 \bar{k}^2 - \alpha^2 \bar{k}^4 + 2\alpha^4 \beta \bar{\Gamma}_{p2})}$$

$$\times\ k^{1/2} \exp\{\Gamma_{p2} z + i\omega_o \Omega_{p2} t - ikr + i\tfrac{\pi}{4}\}\, dk \quad . \qquad (3.33)$$

Equations (3.32) and (3.33) are written in a form that permits evaluation by the saddle-point method. It will be found convenient to transform the observer coordinates from cylindrical (r,z) to spherical (R,ϕ) coordinates by the relations $z = R\cos\phi$ and $r = R\sin\phi$, where R is the radial distance from the origin and ϕ is the polar angle measured from the z-axis. Equation (3.32) can be written in the form:

$$I_{12}(R,\phi,t) = \sqrt{\frac{1}{2\pi R\sin\phi}}\ \frac{e^{-\frac{i\pi}{4}} h^5}{2\alpha^5} \int_{-\infty}^{\infty} F_I(k) e^{R\Phi_I(k)}\, dk \quad , \qquad (3.34)$$

where

$$F_I(k) = \frac{k^{1/2}\{2\alpha^5\Omega_{p1}\bar{\Gamma}_{p1} - i[3\alpha^6\Omega_{p1}^2 - 2\alpha^4\bar{k}^2 - \alpha^2\bar{k}^4 + 2\alpha^4\beta\bar{\Gamma}_{p1}]\}}{(3\alpha^6\Omega_{p1}^2 - 2\alpha^4\bar{k}^2 - \alpha^2\bar{k}^4 + 2\alpha^4\beta\bar{\Gamma}_{p1})} ,$$

and the term in the exponential function is defined by:

$$\Phi_I(k) = \Gamma_{p1}\cos\phi - i\frac{\omega_o t}{R}\Omega_{p1} + ik\sin\phi \quad .$$

The saddle point(s) k_s of the above integral is (are) defined as the value(s) of k for which the first derivative with respect to k of the exponential term $\Phi_I(k)$ is zero, i.e.,

$$\frac{d\Phi(k)}{dk} = (\Gamma'_{p1}\cos\phi - i\frac{\omega_o t}{R}\Omega'_{p1} + i\sin\phi)\Big|_{k=k_s} = 0 . \qquad (3.35a)$$

If one substitutes Equation (3.15) for Ω_p and $\bar{\Gamma}_p$ into Equation (3.35a), one obtains a fourth-degree polynomial equation whose roots are the saddle points k_s as follows:

$$\bar{k}^4(\frac{4\cos\phi}{\alpha^4} - \frac{4T^2}{\alpha^4}) + \bar{k}^3(\frac{4\sin\phi}{\alpha^3}) + \bar{k}^2(-\frac{4\cos^2\phi}{\alpha^2} - \frac{\sin^2\phi}{\alpha^2} + \frac{4T^2}{\alpha^2})$$
$$+ \bar{k}(-\frac{4T\sin\phi}{\alpha}) + 1.0 = 0 \quad . \qquad (3.35b)$$

The saddle points' locations in the complex plane are functions of R/h, ϕ and T. Thus, as T or R/h decrease, the saddle point moves far from the origin. It can be shown that only three of the roots of Equation (3.35b) are saddle points.

The path of steepest descent (PSD) is defined as (a) $Im\Gamma_1(k) = Im\Gamma_I(k_s)$, and (b) the value of the exponential is largest at the saddle point and decreases most rapidly along the path. From numerical analysis,

the proper path of steepest descent (PSD) and saddle point are shown in Figure 3.6.

The integral of Equation (3.34) can be written in the form:

$$\int_{-\infty}^{\infty} F_I(k) e^{R\Phi_I(k)}\, dk + \int_{PSD} F_I(k) e^{R\Phi_I(k)}\, dk = 2\pi i \; \Sigma \text{ Residues} \quad .$$

Since no poles are located inside the closed path of integration, therefore, Σ Residues = 0 , one obtains:

$$\int_{-\infty}^{\infty} F_I(k) e^{R\Phi_I(k)}\, dk = -\int_{PSD} F_I(k) e^{R\Phi_I(k)}\, dk \quad .$$

To evaluate the integral in the PSD, either one of two methods must be employed. Since the integrand of Equation (3.34) has poles located at $k_p(\phi)$, the integrand may become very large when the saddle point approaches the pole. As the distance R/h or the time T increases, the saddle point approaches the pole. Hence, the regular saddle point (RSP) method would be appropriate if the saddle point is located far from the pole. If the saddle point is located near the pole, then the modified saddle point (MSP) method is appropriate. Thus, for such distances where the saddle point is far from the pole, i.e., $T \gtrsim \cos\phi$ and $R/h < 100$, the solution can be obtained as follows:

$$-\int_{PSD} F_I(k) e^{R\Phi_I(k)}\, dk = \sqrt{\frac{-2\pi}{R\Phi_I''(k_{s1})}}\, \frac{h^5}{2\alpha^5}\, F_I(k_{s1}) e^{R\Phi_I(k_{s1})} \quad , \tag{3.36}$$

and hence,

$$I_{12}(R,\phi,t) = \sqrt{\frac{1}{2\pi R\sin\phi}}\, \frac{h^5}{2\alpha^5}\, e^{\frac{-i\pi}{4}} \left\{ \sqrt{\frac{-2}{R\Phi_I''(k_{s1})}}\, F_{II}(k_{s1}) e^{R\Phi_I(k_{s1})} \right\} \quad , \tag{3.37}$$

valid for $\phi > 0$.

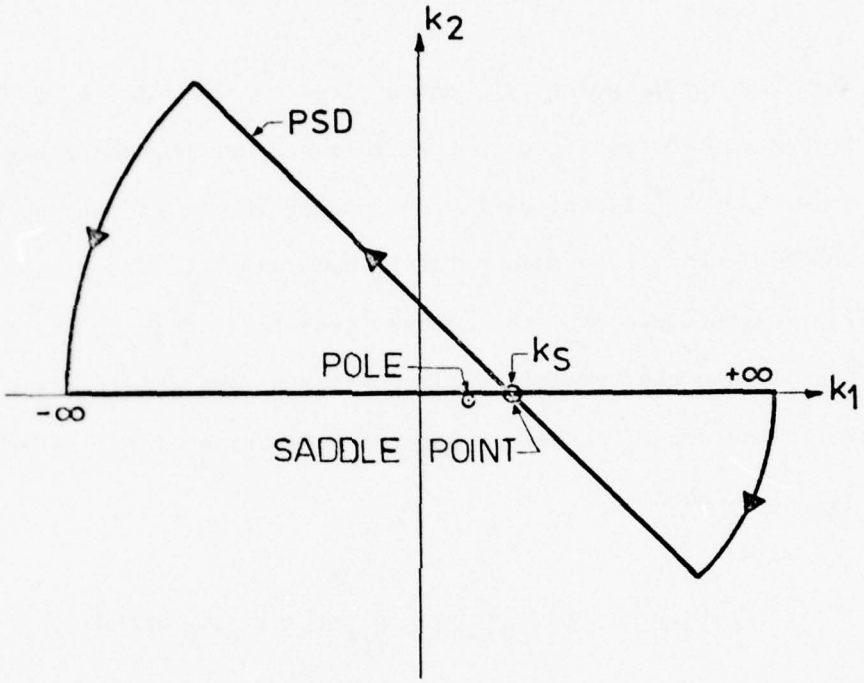


Figure 3.6 Path of Integration and Path of Steepest Descent (PSD) in the k-Plane

Following the same procedure for the evaluation of the integral I_{22}, one obtains:

$$I_{22}(R,\phi,t) = \sqrt{\frac{1}{2\pi R\sin\phi}}\,\frac{h^5 e^{\frac{i\pi}{4}}}{2\alpha^5}\left\{-\sqrt{\frac{-2\pi}{R\Phi''_{II}(k_{s2})}}\,F_{II}(k_{s2})e^{R\Phi_{II}(k_{s2})}\right\} . \tag{3.38}$$

When the saddle point k_s comes close to the pole k_p, the saddle-point method must be modified to take into account the contribution of this pole. Jones [21] has outlined a procedure for evaluating this type of an integral when the saddle point is near a pole. The procedure is to isolate the pole k_p that occurs near the saddle point, and then to approximate the remainder by its value at the saddle point k_s. Following Jones' procedure for the evaluation of the integrals I_{12} and I_{22}, one obtains:

$$I_{12}(R,\phi,t) = \sqrt{\frac{\pi}{2R\sin\phi}}\,\frac{h^5 e^{\frac{-i\pi}{4}}}{2\alpha^5}\left\{-ih_I(k_s)\exp[R\Phi_I(k_s) + \tfrac{1}{2}RZ_I^2]\right\} \times \operatorname{erfc}\{-(\tfrac{1}{2}R)^{1/2}Z_I\} , \tag{3.39}$$

and

$$I_{22}(R,\ ,t) = \sqrt{\frac{\pi}{2R\sin\phi}}\,\frac{h^5}{2\alpha^5}\,e^{\frac{i\pi}{4}}\left\{-ih_{II}(k_s)\exp[R\Phi_{II}(k_s) + \tfrac{1}{2}RZ_{II}^2]\right\} \times \operatorname{erfc}\{-(\tfrac{1}{2}R)^{1/2}Z_{II}\} , \tag{3.40}$$

where

$$h_I(k_s) = (k_s - k_p)\,F_I ,$$

$$h_{II}(k_s) = (k_s - k_p)\,F_{II} ,$$

$$Z_I = (k_p - k_s)\,\{\Phi''_I(k_s)\}^{1/2} ,$$

$$Z_{II} = (k_p - k_s)\{\Phi''_{II}(k_s)\}^{1/2} ,$$

$$\Phi_I(k_s) = \Gamma_{p1}\cos\phi - i\tau_o\Omega_{p1} + ik_s\sin\phi ,$$

$$\Phi_{II}(k_s) = \Gamma_{p2}\cos\phi + i\tau_o\Omega_{p2} - ik_s\sin\phi ,$$

erfc(x) = the complementary error function, $\tau_o = \frac{\omega_o t}{R}$,

the saddle point = $k_{s1} = k_{s2} = k_s$,

$$\Phi''_I(k_s) = \left.\frac{d^2\Phi_I(k)}{dk^2}\right|_{k=k_s}$$

and

$$\Phi''_{II}(k_s) = \left.\frac{d^2\Phi_{II}(k)}{dk^2}\right|_{k=k_s} .$$

For large values of the argument of the error function, the simplified expressions in Equations (3.37) and (3.38) can be used instead of Equations (3.39) and (3.40).

3.2.2 Evaluation of Integrals I_{11} and I_{21}. Using Gradshteyn and Ryzhik [22] table of integrals to evaluate the integrals I_{11} and I_{21}, and letting $z = R\cos\phi$ and $r = R\sin\phi$ in Equations (3.28) and (3.30), one obtains:

$$I_{11}(r,\phi,t) = \frac{ih^5}{2\alpha^5}\int_o^\infty kJ_o(kR\sin\phi)\exp\{\Gamma_{p1}R\cos\phi - i\omega_o\Omega_{p1}t\}\,dk .$$

Substituting for Ω_{p1} and Γ_{p1} by their approximate values and evaluating the integral, one obtains:

$$I_{11}(R,\phi,t) = \frac{ih^4}{2\alpha^5}\left\{\frac{\alpha}{2R[T-\cos\phi]}\exp\left[-i\left\{\frac{\pi}{2}-\frac{\alpha R\sin^2\phi}{4h[T-\cos\phi]}\right\}\right]\right\} \quad , \phi > 0, \tag{3.41}$$

and

$$I_{21}(R,\phi,t) = \frac{-ih^5}{2\alpha^5}\int_0^\infty kJ_o(kR\sin\phi)\exp\{\Gamma_{p2}R\cos\phi + i\omega_o\Omega_{p2}t\}\,dk = \frac{-ih^4}{2\alpha^5}\left\{\frac{\alpha}{2R[T-\cos\phi]}\exp\left[i\left\{\frac{\pi}{2}-\frac{\alpha R\sin^2}{4h[T-\cos\phi]}\right\}\right]\right\}. \quad 0. \tag{3.42}$$

3.2.3 Final Solution of the Integral $I(R,\phi,t)$. Substituting Equations (3.37), (3.38), (3.41), and (3.42) into Equations (3.26) and (3.27), and substituting the resulting equations into Equation (3.22), then the final simplified solution becomes:

$$I(R,\phi,t) = \frac{\alpha\beta c_o}{4\pi Rh^2(T-\cos\phi)}\sin\left[\frac{\alpha R\sin^2\phi}{4h(T-\cos\phi)}\right]H(T-\cos\phi) + \frac{i\beta c_o}{4\pi Rh\sqrt{\sin\phi}}\left\{\frac{e^{\frac{-i\pi}{4}}}{\sqrt{-\phi''_I(k_s)}}F_I(k_s)\exp[R\phi_I(k_s)] + \frac{e^{\frac{i\pi}{4}}}{\sqrt{-\phi''_{II}(k_s)}}F_{II}(k_s)\exp[R\phi_{II}(k_s)]\right\}H(T-\cos\phi) \quad . \tag{3.43}$$

Similarly, substituting Equations (3.39), (3.40), (3.41), and (3.42) into Equations (3.26) and (3.27), and substituting the resulting equations into Equation (3.22), then the final solution becomes:

$$I(R,\phi,t) = \frac{\alpha\beta c_o}{4\pi R h^2 (T - \cos\phi)} \sin\left[\frac{\alpha R \sin^2\phi}{4h(T - \cos\phi)}\right] H(T - \cos\phi) +$$

$$+ \frac{\beta c_o}{4h\sqrt{2\pi R \sin\phi}} \left\{\left[h_I(k_s)\exp\left(R\Phi_I(k_s) + \frac{R}{2}Z_I^2 - i\frac{\pi}{4}\right)\right]\right.$$

$$\times \operatorname{erfc}\left[\left(\frac{1}{2}R\right)^{1/2} Z_I\right] + \left[h_{II}(k_s)\exp\left(R\Phi_{II}(k_s) + \frac{1}{2}RZ_{II}^2 + \frac{i\pi}{4}\right)\right]$$

$$\left.\times \operatorname{erfc}\left[-\left(\frac{1}{2}R\right)^{1/2} Z_{II}\right]\right\} H(T - \cos\phi) \quad , \qquad (3.44)$$

where

$$Z_I = (k_p - k_s)\{\Phi_I''(k_s)\}^{1/2}$$

and

$$Z_{II} = (k_p - k_s)\{\Phi_{II}''(k_s)\}^{1/2} \quad .$$

The simplified and more exact expressions for the normalized radiated pressure from an infinite elastic plate excited by an impulse point force $Q(t) = F_o\delta(t)$ are given respectively by:

$$\frac{P(2\pi h^2)(R/h)}{F_o(c_o/h)} = \frac{\beta\alpha \sin\left[\frac{\alpha(R/h)\sin^2\phi}{4(T - \cos\phi)}\right]}{2(T - \cos\phi)} H(T - \cos\phi)$$

$$+ \frac{\beta\alpha^3 k^{-1/2}(A_1^2 + A_2^2)^{1/2} \exp(R\bar{\Phi}_1/h)}{\sqrt{\sin\phi}(\bar{\Phi}_1''^2 + \bar{\Phi}_2''^2)^{1/4}(B_1^2 + B_2^2)^{1/2}}$$

$$\times \cos\left\{\psi_1 - \psi_2 + \frac{R}{h}\bar{\Phi}_2 - \frac{\pi}{4} - \frac{\theta_1}{2}\right\} H(T - \cos\phi) \quad , \qquad (3.45)$$

and

$$\frac{P(2\pi h^2)(R/h)}{F_o(c_o/h)} = \frac{\beta\alpha \sin\left[\frac{\alpha(R/h)\sin^2\phi}{2(T-\cos\phi)}\right]}{2(T-\cos\phi)} H(T-\cos\phi)$$

$$+ \frac{\beta\alpha^3\sqrt{\pi(R/h)\bar{k}_s}\,(\bar{k}_s - \bar{k}_p)(A_1^2 + A_2^2)^{1/2}(x_1^2 + x_2^2)^{1/2}}{\sqrt{2\sin\phi}\,(B_1^2 + B_2^2)^{1/2}}$$

$$\times \exp\left\{\frac{R}{h}\left[\bar{\Phi}_1 + \frac{1}{2}(\bar{k}_p - \bar{k}_s)^2\,\bar{\Phi}''_a\right]\right\}$$

$$\times \cos\left\{\psi_1 - \psi_2 + \bar{\Phi}_2\left(\frac{R}{h}\right) + \frac{R}{2h}(\bar{k}_p - \bar{k}_s)^2\,\bar{\Phi}''_b - \frac{\pi}{4} - \xi\right\}$$

$$\times H(T-\cos\phi) \quad , \tag{3.46}$$

where

$$A_1 = \mathrm{Re}\{2\alpha\bar{\Omega}_{p1}\bar{\Gamma}_{p1} - i[3\alpha^6\bar{\Omega}_{p1}^2 - 2\alpha^4\bar{k}^2 - \alpha^2\bar{k}^4 + 2\alpha^4\beta\bar{\Gamma}_{p1}]\} \quad ,$$

$$A_2 = \mathrm{Im}\{2\alpha\bar{\Omega}_{p1}\bar{\Gamma}_{p1} - i[3\alpha^6\bar{\Omega}_{p1}^2 - 2\alpha^4\bar{k}^2 - \alpha^2\bar{k}^4 + 2\alpha^4\beta\bar{\Gamma}_{p1}]\} \quad ,$$

$$B_1 = \mathrm{Re}\{2\alpha^5[3\alpha^6\bar{\Omega}_{p1}^2 - 2\alpha^4\bar{k}^2 - \alpha^2\bar{k}^4 + 2\alpha^4\beta\bar{\Gamma}_{p1}]\} \quad ,$$

$$B_2 = \mathrm{Im}\{2\alpha^5[3\alpha^6\bar{\Omega}_{p1}^2 - 2\alpha^4\bar{k}^2 - \alpha^2\bar{k}^4 + 2\alpha^4\beta\bar{\Gamma}_{p1}]\} \quad ,$$

$$\psi_1 = \arctan(A_2/A_1) \quad , \quad \psi_2 = \arctan(B_2/B_1) \quad ,$$

$$\bar{\Phi}_1 = \mathrm{Re}\{\bar{\Phi}_I(k_s)\} \quad , \quad \bar{\Phi}_2 = \mathrm{Im}\{\bar{\Phi}_I(k_s)\} \quad ,$$

$$\bar{\Phi}_1 = h\Phi_I \quad , \quad \bar{\Phi}''_I(k_s) = \bar{\Phi}''_a + i\,\bar{\Phi}''_b \quad ,$$

$$x_1 = \mathrm{Re}\{\mathrm{erfc}[(\tfrac{1}{2}R)^{1/2}\,z_I]\}$$

$$x_2 = \mathrm{Im}\{\mathrm{erfc}[(\tfrac{1}{2}R)^{1/2}\,z_I]\} \quad ,$$

$$\xi = \arctan(x_2/x_1)$$

and

$$\theta_1 = \arctan\left(\bar{\Phi}''_2/\bar{\Phi}''_1\right) \quad .$$

3.2.4 Special Case and Approximate Method. In the case when the observation point is on vertical axis $\phi = 0$, the Hankel function $H_o^{(1),(2)}(kR\sin\phi)$ would become infinite. To avoid this problem, one can substitute $J_o(kR\sin\phi) = 1.0$ in Equations (3.29) and (3.31), and evaluate the radiated pressure. For detailed solution, see Appendix A. For the approximate solution of the radiated pressure from an infinite elastic plate, see Appendix B.

CHAPTER IV

NUMERICAL RESULTS

4.1 Introduction and Input Data

Numerical evaluation of the radiated pressure at different observation angles ϕ and nondimensional distance R/h and time T is performed. Since the transient acoustic pressure is a function of all of these variables, one can only plot the pressure at a specific value of R/h and ϕ as a function of time T. To investigate the influence of one of these parameters on the total time signature, the other parameters are kept constant. The solution for the acoustic radiated pressure time signature for different load histories are also presented in this chapter. In all of these plots, the variation of the pressure as a function of time is very rapid for times just after the first arrival. This made it very difficult for the computer plotter to plot a smooth sinusoidal curve as predicted by the solutions. To avoid this problem, the relative maxima and minima were connected by straight lines. The resulting curves look smooth near the first arrival, but become saw-tooth shaped for longer times. However, the location of these relative maxima and minima are known from the solutions, such as those given in Equation (3.44). Thus, the connected points fall on the envelope of the smoothly predicted curves.

For the sake of numerical computation, the plate was taken as a steel plate immersed in water. The relevant physical data are:

$$E = 30 \times 10^6 \text{ psi, or } 20.68 \times 10^{10} \text{ N/m}^2 \quad ,$$

$$\rho = 7.28 \times 10^4 \frac{\text{lb-sec}^2}{\text{in}^4} \text{, or } 7.68 \text{ kg/m}^3 \quad ,$$

$$\rho_o = 0.948 \times 10^4 \frac{\text{lb-sec}^2}{\text{in}^4} \text{, or } 1 \text{ kg/m}^3 \quad ,$$

$$c_o = 6.0 \times 10^4 \text{ in/sec , or } 1500 \text{ m/sec}$$

and

$$\nu = 0.3 \quad .$$

4.2 Radiated Pressure for Different Types of Applied Force

4.2.1 Impulse. Numerical values for the radiated pressure of an infinite elastic plate excited by an impulsive point force, for different observation angles and distances were obtained by using the above data and Equations (3.45), (3.46), and (A.4).

In order to examine the relative contribution of the first and second terms in Equations (3.45) and (3.46), their numerical values were plotted. Thus, plots of the contribution of the first term for $R/h = 50$ and $\phi = 30^o$ and $\phi = 60^o$ are shown in Figures 4.1 and 4.2, respectively. Plots of the numerical contribution of the second term of these equations are similarly plotted in Figures 4.3 and 4.4 and the sum of the two terms shown in Figures 4.5 and 4.6. In order to examine the influence of R/h, plots of the impulse response are shown for $R/h = 100$ and 1000 in Figures 4.7 and 4.8, respectively. To examine the oscillatory nature of the impulse response for long times, the time scale was expanded and the result plotted in Figures 4.9 through 4.11 for $\phi = 30^o$ and $R/h = 50$, 100 and 1000, respectively. Using Equations (B.8) and (B.9) for the solution (RSP), Equations (B.13) and (B.14) for the solutions MSP, numerical results were obtained for radiated pressure predicted from these

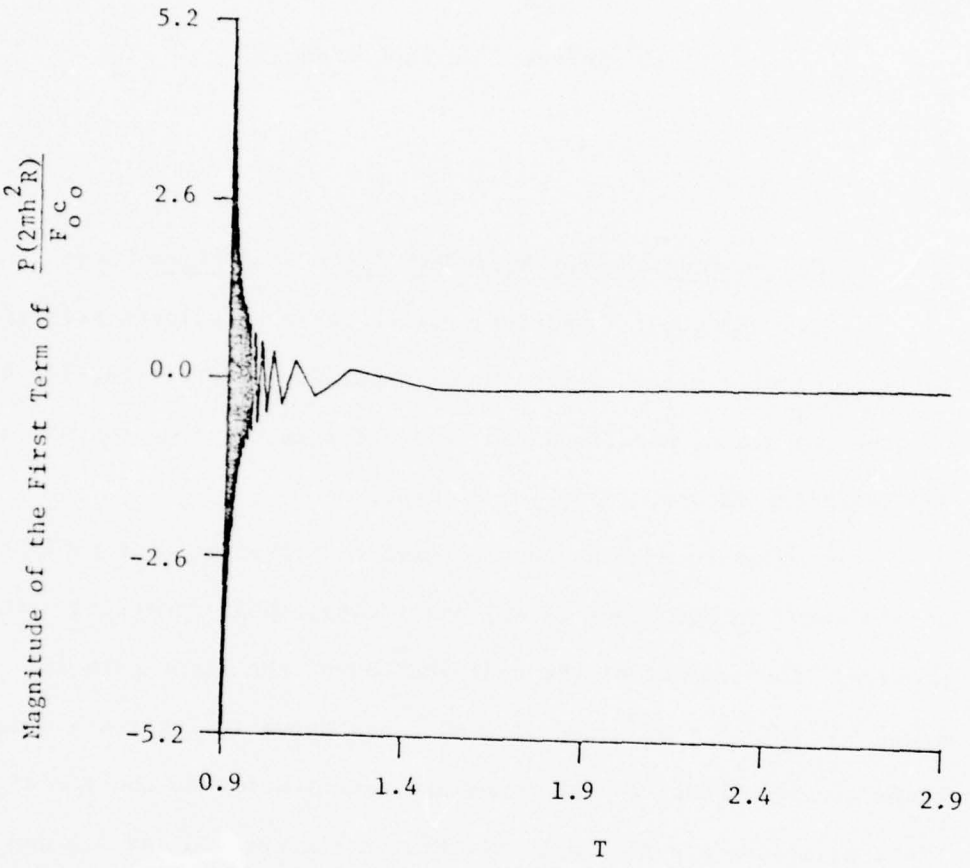


Figure 4.1 Magnitude of the First Term of the Unit Impulse Response Versus Time for Observation Point at $\phi = 30^o$ and $R/h = 50$

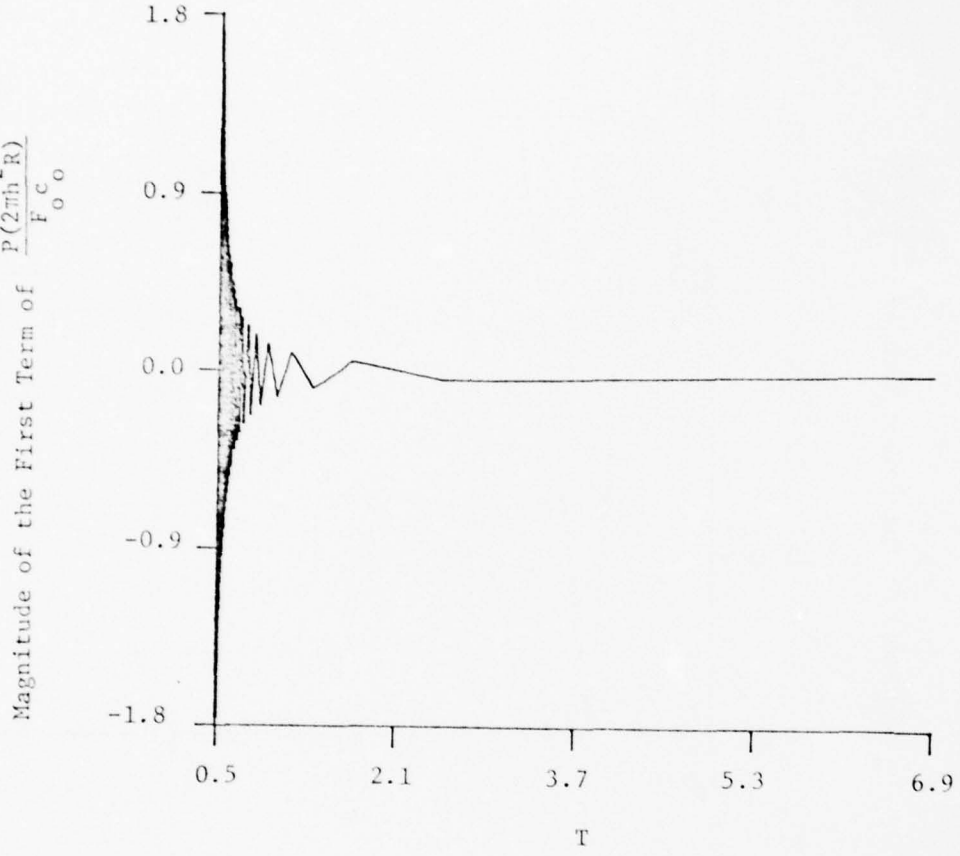


Figure 4.2 Magnitude of the First Term of the Unit Impulse Response Versus Time for Observation Point at $\phi = 60^o$ and $R/h = 50$

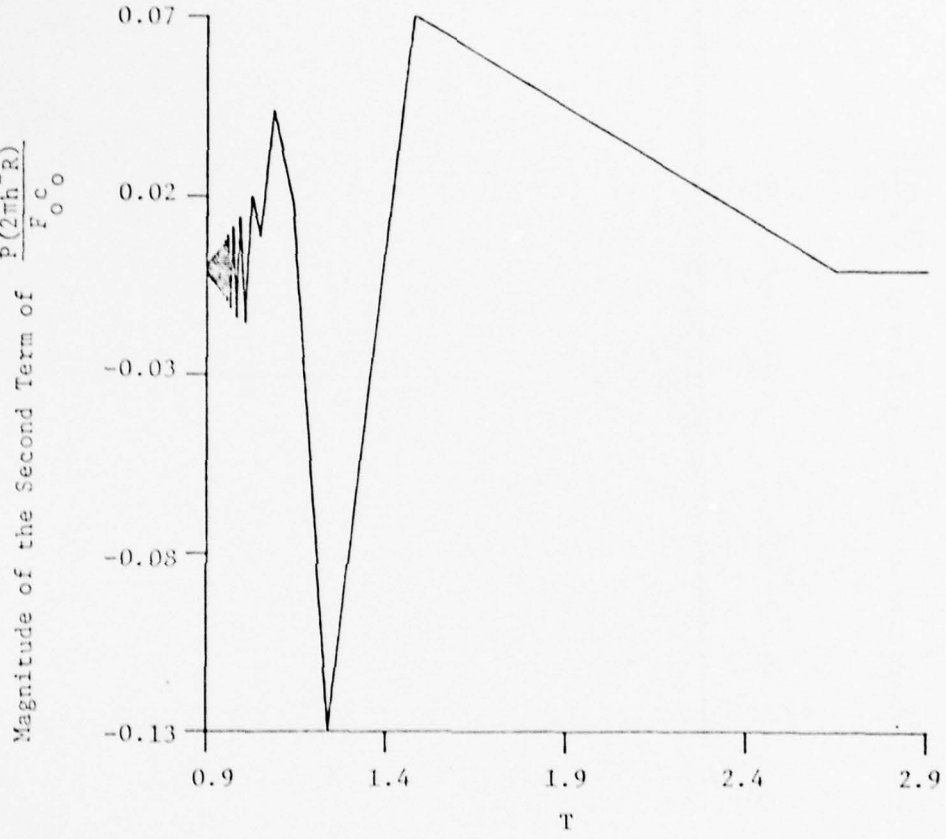


Figure 4.3 Magnitude of the Second Term of Unit Impulse Response Versus Time for Observation Point at $\phi = 30^{o}$ and R/h = 50

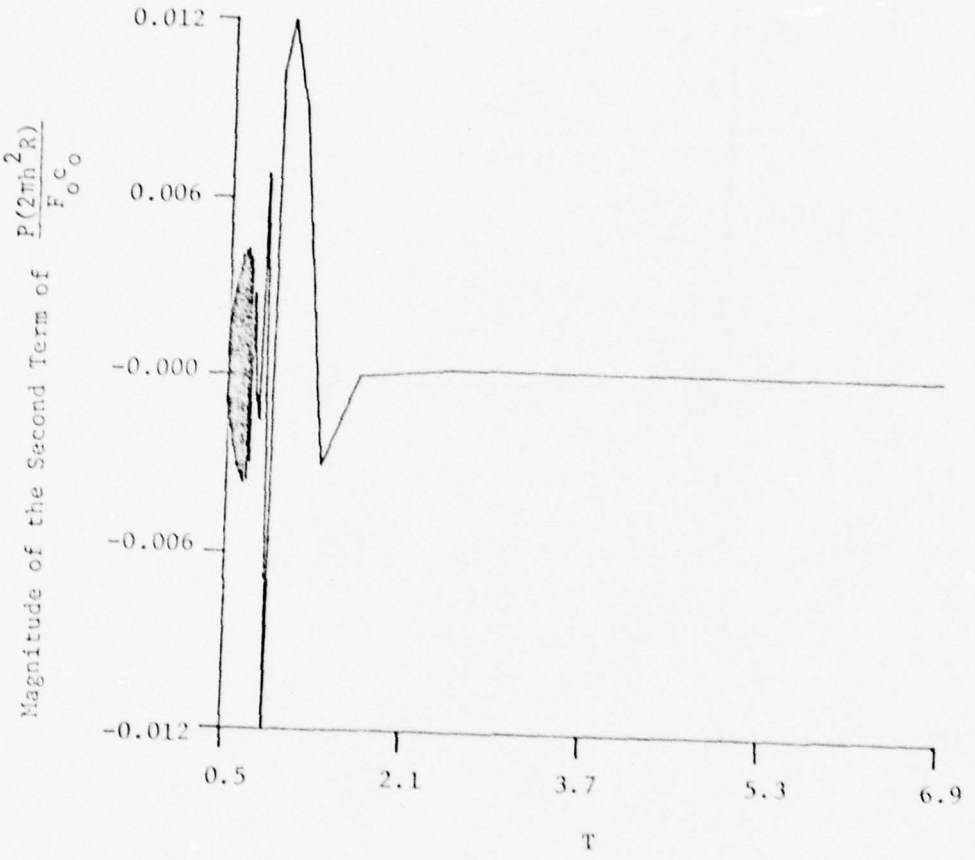


Figure 4.4 Magnitude of the Second Term of the Unit Impulse Response Versus Time for the Observation Point at $= 60^o$ and $R/h = 50$

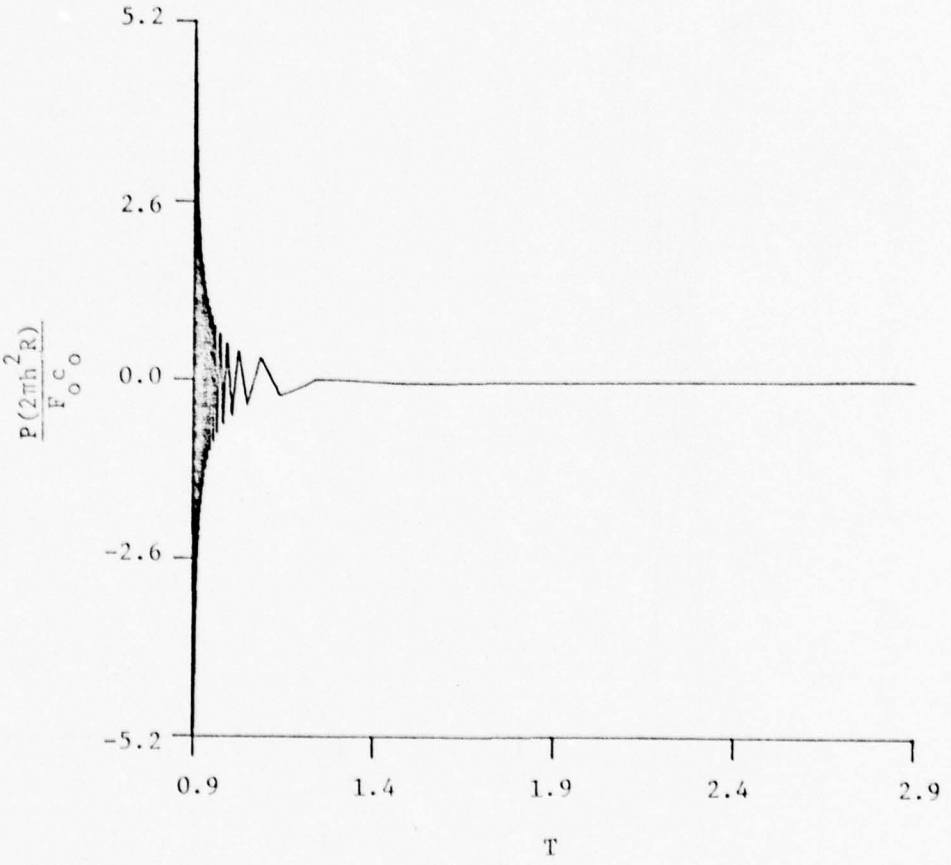


Figure 4.5 Plot of the Acoustic Unit Impulse Response for the Observation Point at $\phi = 30^{o}$ and $R/h = 50$

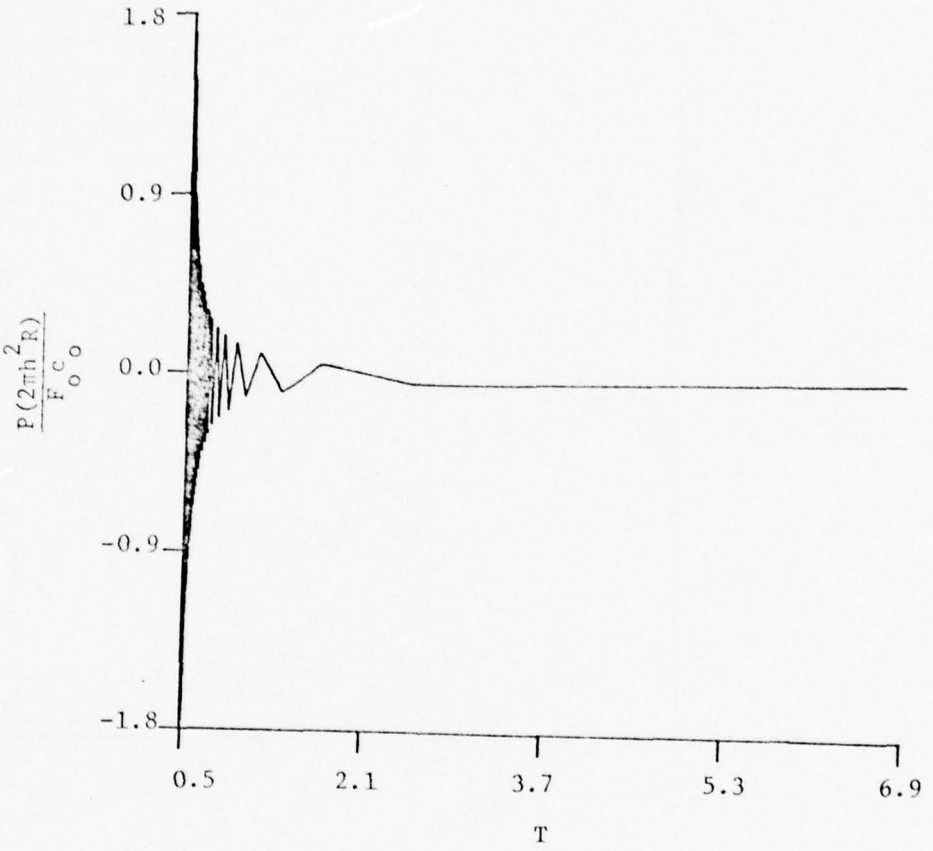


Figure 4.6 Plot of the Acoustic Unit Impulse Response for the Observation Point at $\phi = 60^o$ and $R/h = 50$

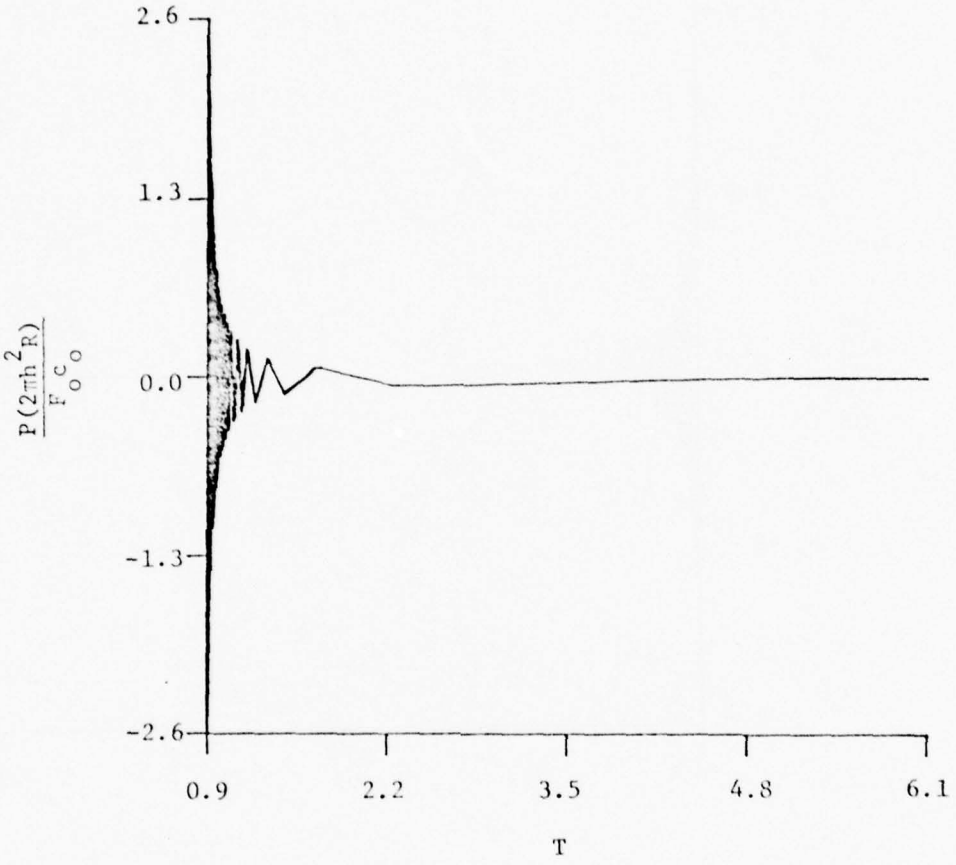


Figure 4.7 Plot of the Acoustic Unit Impulse Response for the Observation Point at $\phi = 30^{o}$ and R/h = 100

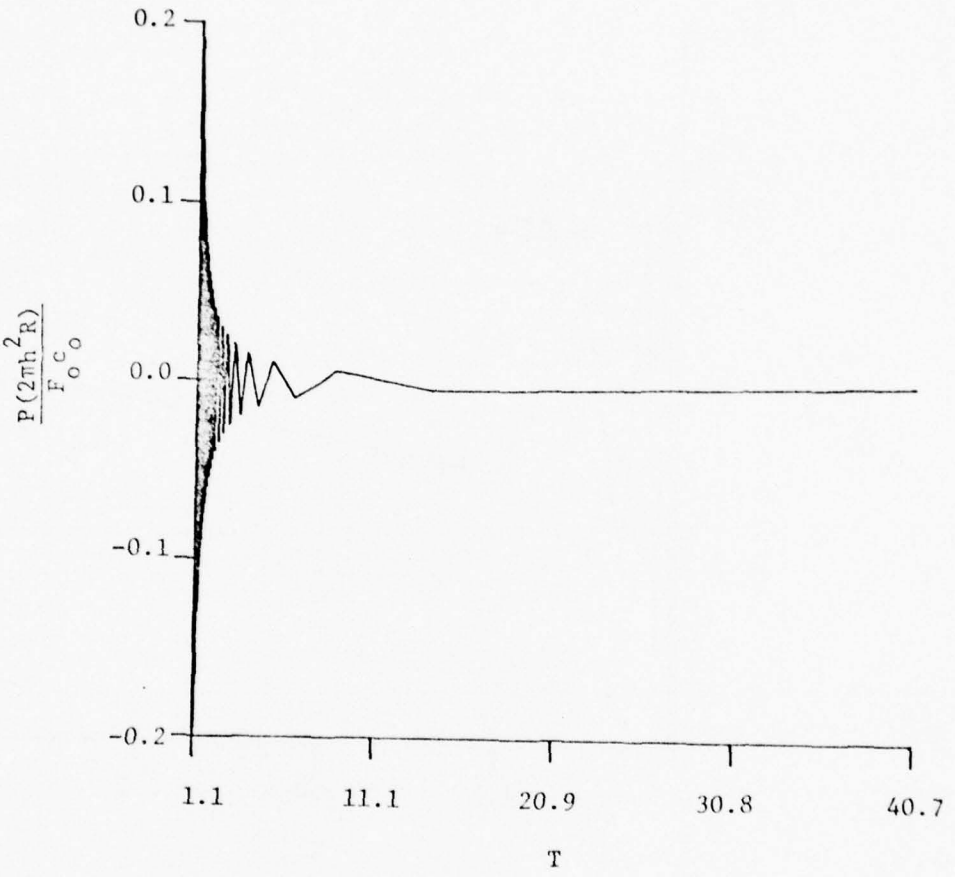


Figure 4.8 Plot of the Acoustic Unit Impulse Response for the Observation Point at $\phi = 30^o$ and $R/h = 1000$

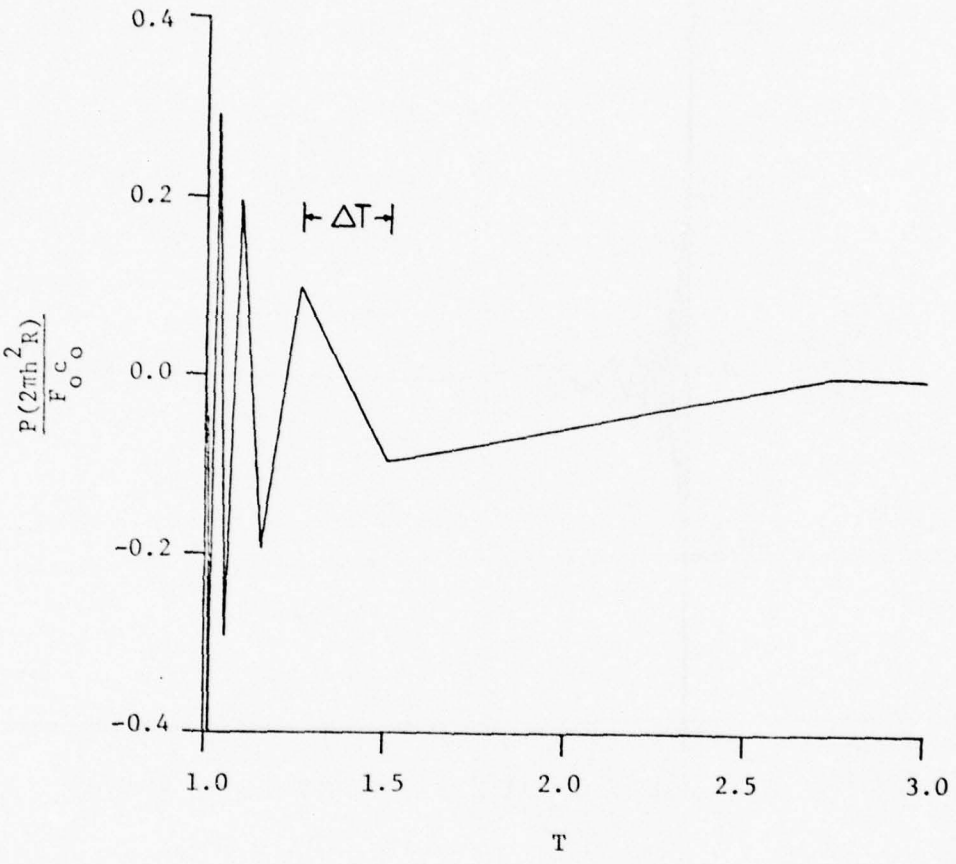


Figure 4.9 Plot of the Acoustic Unit Impulse Response with an Expanded Time Scale for the Observation Point at $\phi = 30^{o}$ and $R/h = 50$

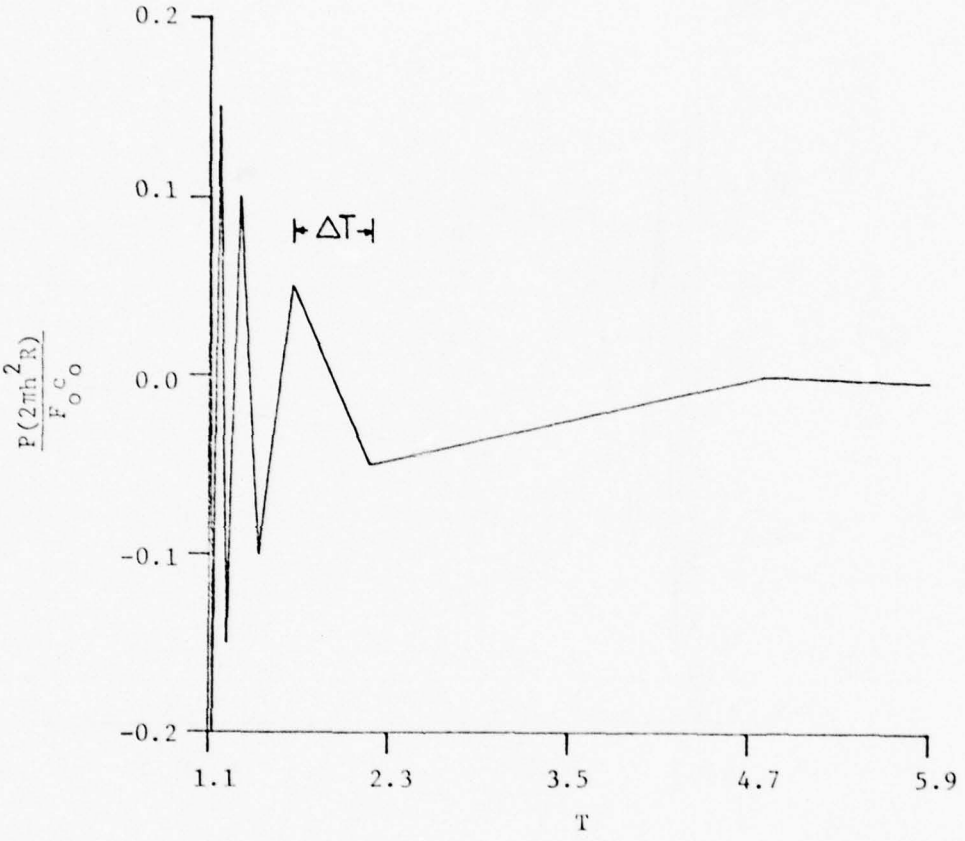


Figure 4.10 Plot of the Acoustic Unit Impulse Response with an Expanded Time Scale for the Observation Point at $\phi = 30^{o}$ and $R/h = 100$

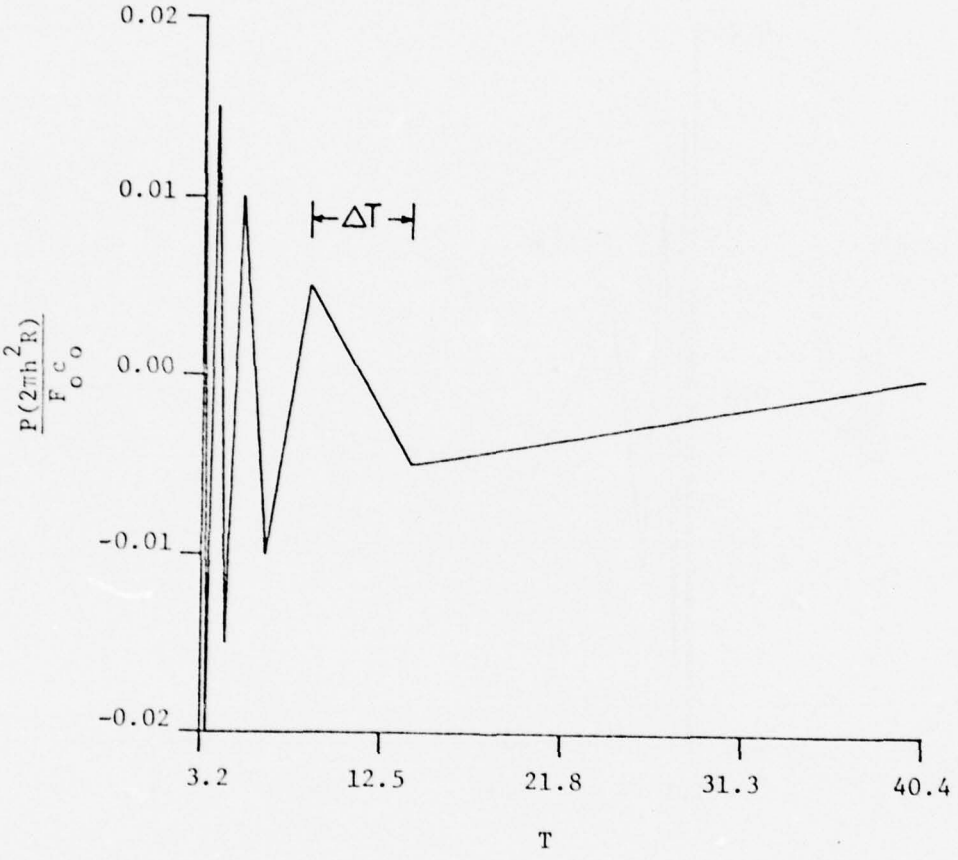


Figure 4.11 Plot of the Acoustic Unit Impulse Response with an Expanded Time Scale for the Observation Point at $\phi = 30^{o}$ and R/h = 1000

approximate solutions. Figures 4.12 through 4.15 and Figures 4.16 through 4.19 show the impulse response of the radiated pressure versus time for different observation angles and observer distances for MSP and RSP solutions, respectively.

4.2.2 Applied Force with a Constant Magnitude. Such an applied force is defined by $Q(t) = f_o H(t)$. Substituting applied force and Equation (3.43) into the convolution integral in Equation (3.3), and neglecting the very small contribution of the second term of Equation (3.43), one obtains:

$$P(R,\phi,t) = f_o \int_0^t \frac{N_1 \sin\left[\dfrac{N_2}{T - \dfrac{\tau c_o}{R} - \cos\phi}\right]}{\left[T - \dfrac{\tau c_o}{R} - \cos\phi\right]} H(T - \frac{\tau c_o}{R} - \cos\phi)\, d\tau \quad , \tag{4.1}$$

where

$$N_1 = \frac{\alpha\beta c_o}{4\pi R h^2}$$

and

$$N_2 = \frac{\alpha R \sin^2\phi}{4h} \quad .$$

Transferring the integration variable τ to u by letting

$$u = \frac{N_2}{T - \dfrac{\tau c_o}{R} - \cos\phi} \qquad \text{and} \qquad du = \frac{c_o N_2\, d\tau}{R(T - \dfrac{\tau c_o}{R} - \cos\phi)^2} \quad ,$$

Equation (4.1) can be written as:

$$P(R,\phi,t) = \frac{-f_o N_1 R}{c_o} \int_0^{\frac{N_2}{T-\cos\phi}} \frac{\sin u}{u} H(T - \cos\phi)\, du \quad . \tag{4.2}$$

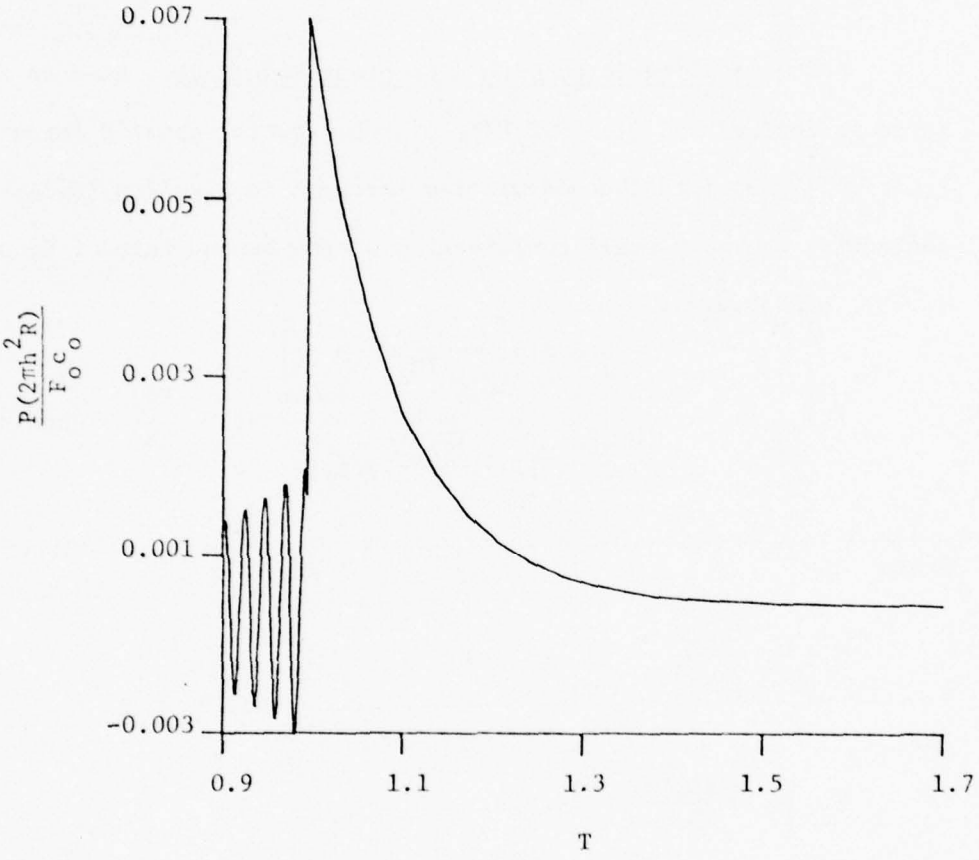


Figure 4.12 Plot of the Acoustic Unit Impulse Response with an Expanded Time Scale for the Observation Point at $\phi = 30^{o}$ and $R/h = 50$ Obtained by the Modified Saddle-Point Method (MSP)

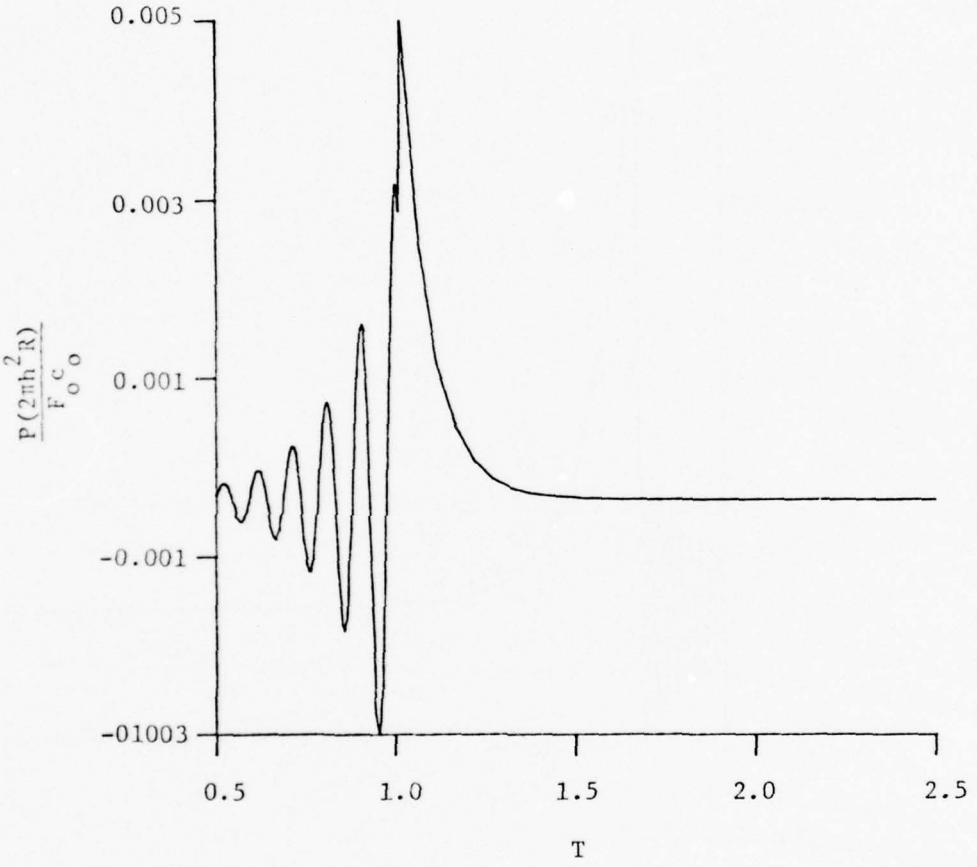


Figure 4.13 Plot of the Acoustic Unit Impulse Response with an Expanded Time Scale for the Observation Point at $\phi = 60^{o}$ and $R/h = 50$ Obtained by the Modified Saddle-Point Method (MSP)

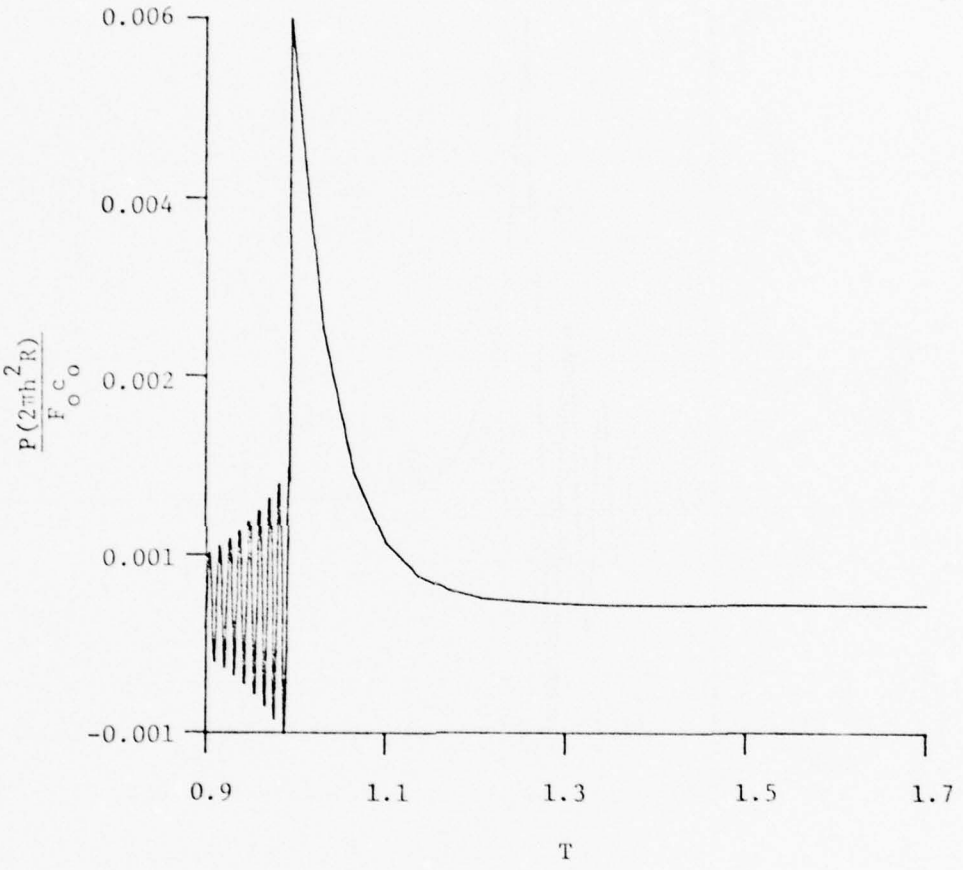


Figure 4.14 Plot of the Acoustic Unit Impulse Response with an Expanded Time Scale for the Observation Point at $\phi = 30^{o}$ and $R/h = 100$ Obtained by the Modified Saddle-Point Method (MSP)

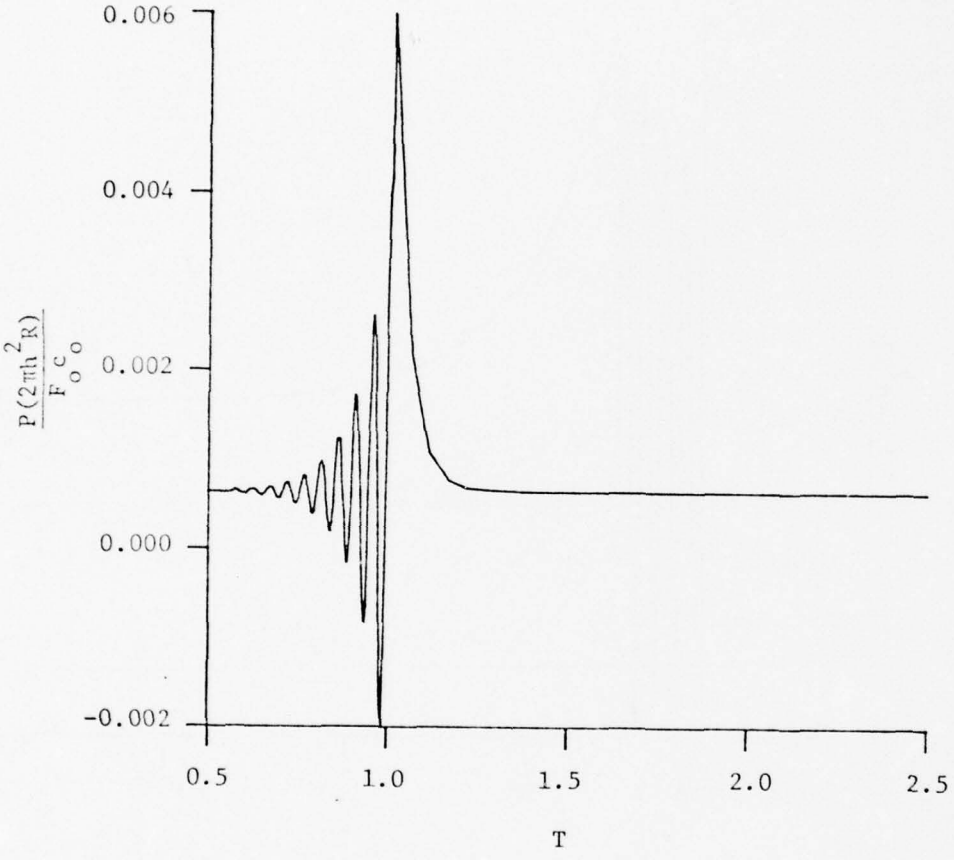


Figure 4.15 Plot of the Acoustic Unit Impulse Response with an Expanded Time Scale for the Observation Point at $\phi = 60^{o}$ and $R/h = 100$ Obtained by the Modified Saddle-Point Method (MSP)

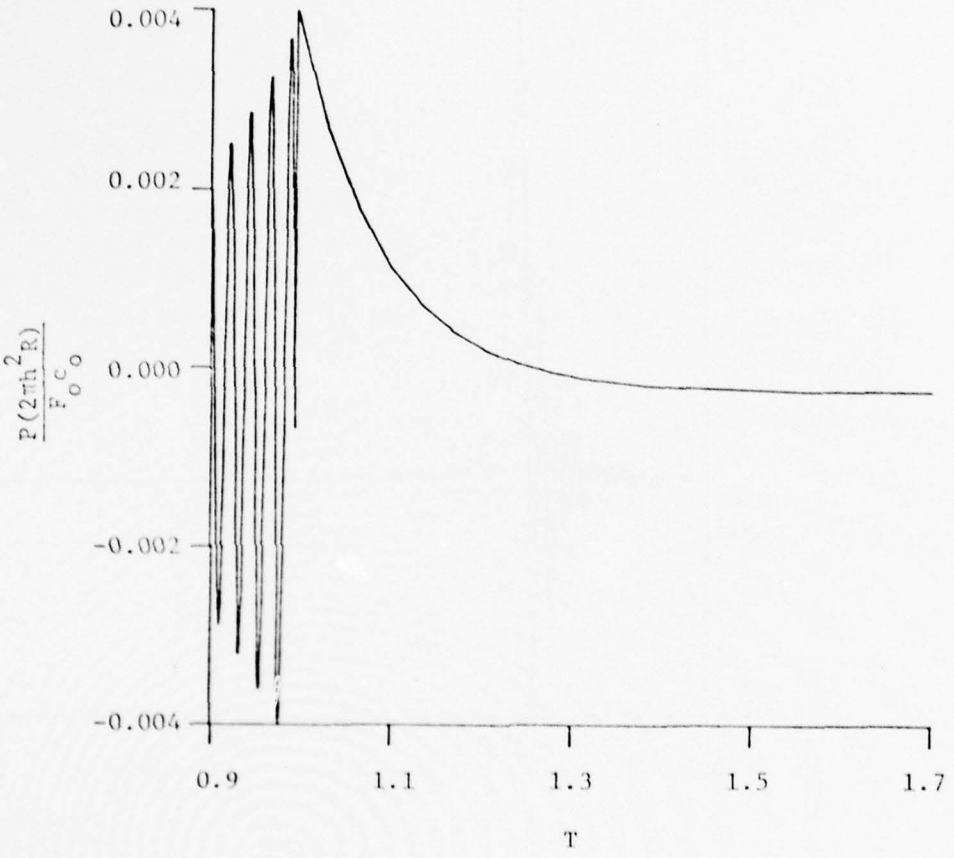


Figure 4.16 Plot of the Acoustic Unit Impulse Response with an Expanded Time Scale for the Observation Point at $\phi = 30^{o}$ and $R/h = 50$ Obtained by the Regular Saddle-Point Method (RSP)

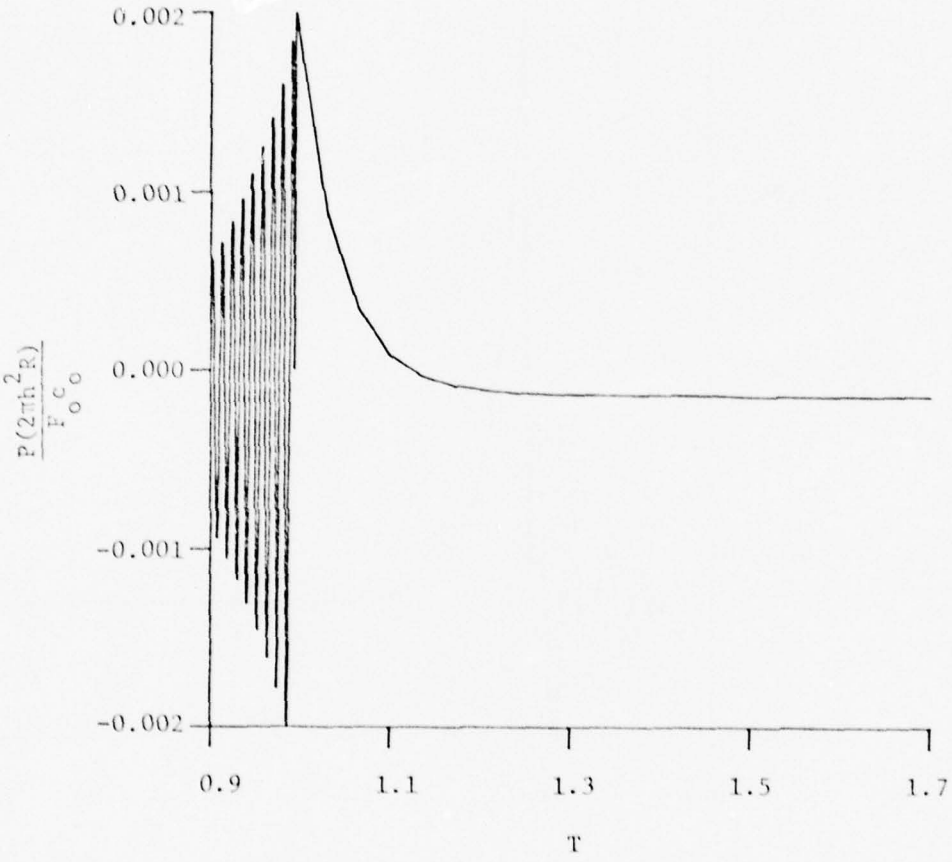


Figure 4.17 Plot of the Acoustic Unit Impulse Response with an Expanded Time Scale for the Observation Point at $\phi = 30^{o}$ and $R/h = 100$ Obtained by the Regular Saddle-Point Method (RSP)

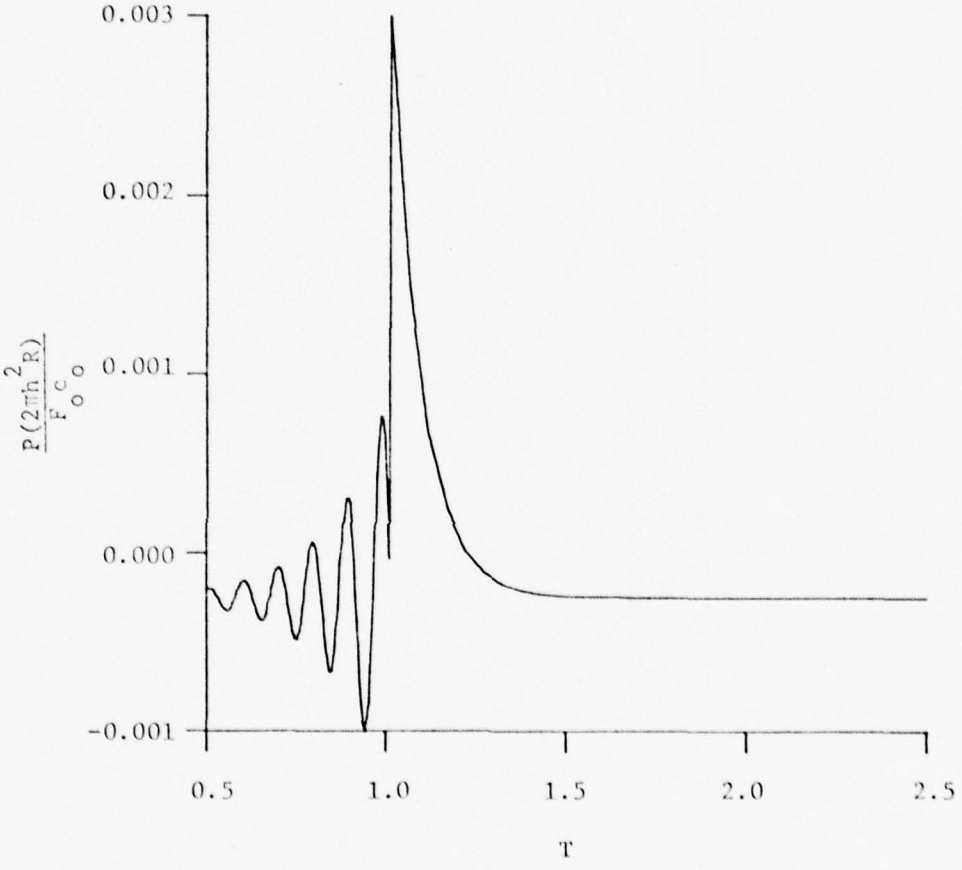


Figure 4.18 Plot of the Acoustic Unit Impulse Response with an Expanded Time Scale for the Observation Point at $\phi = 60^{o}$ and $R/h = 50$ Obtained by the Regular Saddle-Point Method (RSP)

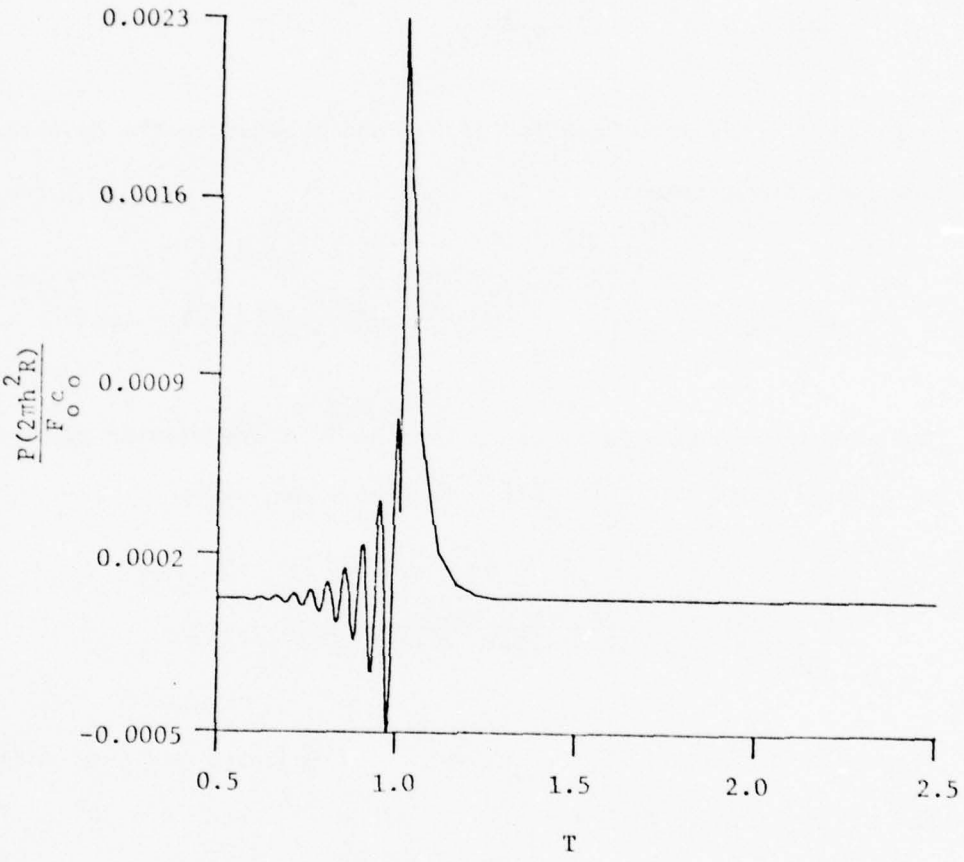


Figure 4.19 Plot of the Acoustic Unit Impulse Response with an Expanded Time Scale for the Observation Point at $\phi = 60^o$ and $R/h = 100$ Obtained by the Regular Saddle-Point Method (RSP)

To evaluate the integral of Equation (4.2), one can substitute sin u/u , with its power series expansion, and then integrate term by term. Letting

$$\frac{\sin u}{u} = \sum_{n=0}^{\infty} (-1)^n \frac{u^{2n}}{(2n+1)!} \quad ,$$

and substituting into Equation (4.2), and evaluating the resulting integral, one obtains:

$$P(R,\phi,t) = \frac{f_o \alpha\beta}{4\pi h^2} \sum_{n=0}^{\infty} \frac{(-1)^n \left[\frac{N_2}{T - \cos\phi}\right]^{2n+1}}{(2n+1)(2n+1)!} H(T - \cos\phi) \quad . \quad (4.3)$$

The normalized radiated pressure from an infinite elastic plate excited by a point force $Q(t) = f_o H(t)$ is then given by:

$$\frac{P}{P_o} = \frac{1}{2}\left(\frac{R}{h}\right) \sum_{n=0}^{\infty} \frac{(-1)^n \left[\frac{N_2}{T - \cos\phi}\right]^{2n+1}}{(2n+1)(2n+1)!} H(T - \cos\phi) \quad . \quad (4.4)$$

Figure (4.20) and (4.21) are the plots of radiated pressure versus time for applied force $Q(t) = f_o H(t)$, $R/h = 50^o$ and $\phi = 30^o$. The normalization pressure P_o is the pressure computed for an infinite elastic plate excited by a time harmonic point force of amplitude f_o at coincidence frequency and evaluated at the observer angle $\phi = 0^o$ given by:

$$|P_o| = \frac{f_o \alpha\beta}{2\pi (R/h) h^2} \quad .$$

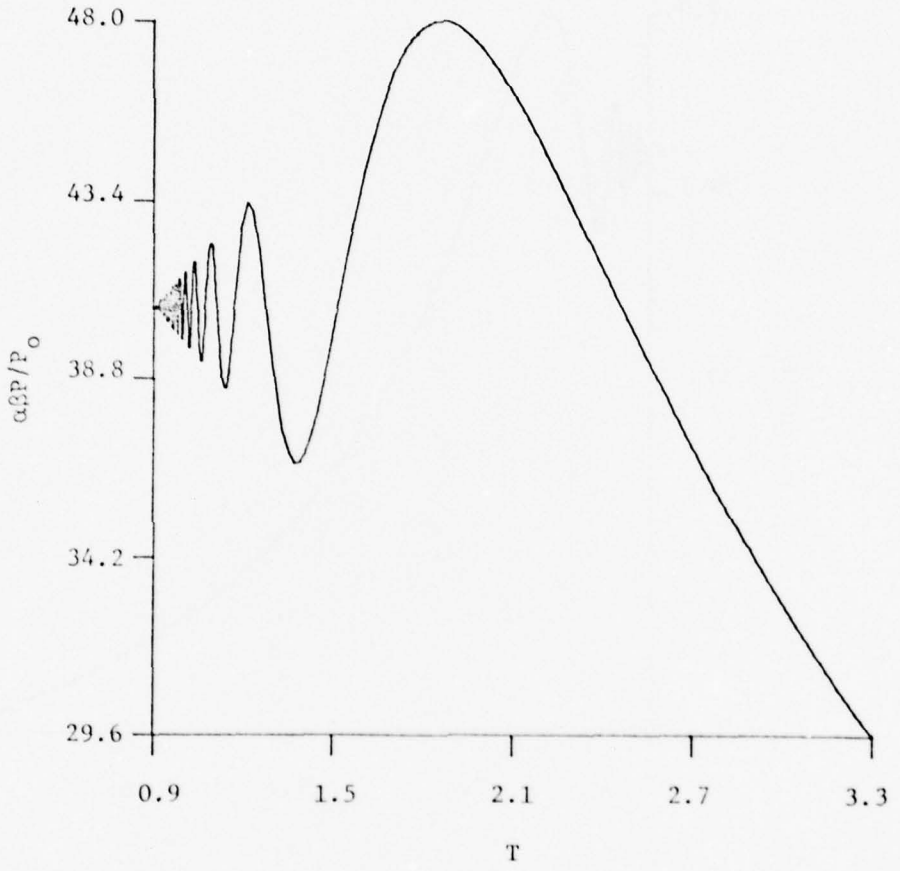


Figure 4.20 Normalized Radiated Pressure Versus Expanded Time Scale at the Observation Point $\phi = 30^{o}$ and $R/h = 50$ for a Constant Magnitude Applied Load

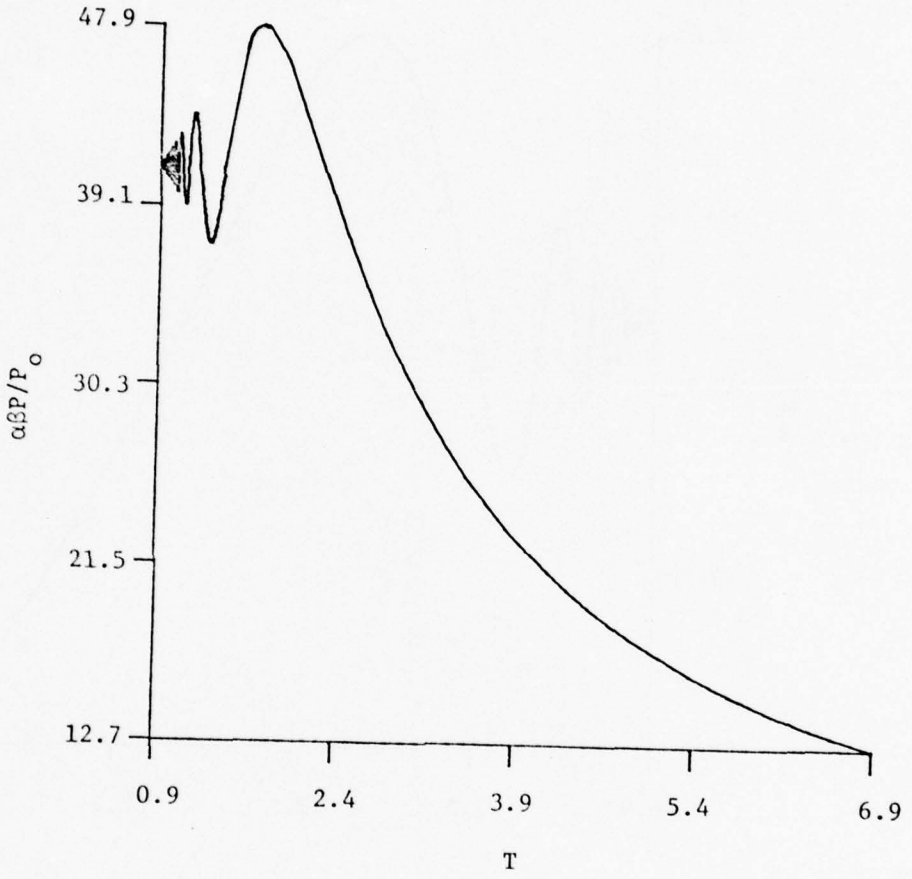


Figure 4.21 Normalized Radiated Pressure Versus Time at Observation Point $\phi = 30^{o}$ and $R/h = 50$ for a Constant Magnitude Applied Load

4.2.3 Applied Square Pulse Force. Such an applied force can be represented by $Q(t) = f_o H(t_o - t)$. Substituting applied force and Equation (3.43) into the convolution integral Equation (3.3), and neglecting the very small contribution of the second term of Equation (3.43), one obtains:

$$P(R,\phi,t) = f_o N_1 \int_0^t \frac{\sin\left[\dfrac{N_2}{T - \frac{\tau c_o}{R} - \cos\phi}\right]}{\left[T - \frac{\tau c_o}{R} - \cos\phi\right]} H(T - \frac{c_o}{R} - \cos\phi)\, d\tau \,,$$

$$\text{for } T \leq T_o \,, \quad (4.5)$$

and

$$P(R,\phi,t) = f_o N_1 \int_0^{t_o} \frac{\sin\left[\dfrac{N_2}{T - \frac{\tau c_o}{R} - \cos\phi}\right]}{\left[T - \frac{\tau c_o}{R} - \cos\phi\right]} H(T - \frac{\tau c_o}{R} - \cos\phi)\, d\tau \,,$$

$$\text{for } T > T_o \,, \quad (4.6)$$

where $T_o = \dfrac{c_o t_o}{R}$.

The integral in Equation (4.5) is similar to the integral in Equation (4.1), therefore, following the same procedure to evaluate the integration, one obtains:

$$P(R,\phi,t) = \frac{\alpha\beta f_o}{4\pi h^2} \sum_{n=0}^{\infty} \frac{(-1)^n \left[\dfrac{N_2}{T - \cos\phi}\right]^{2n+1}}{(2n+1)(2n+1)!} H(T - \cos\phi) \,,$$

$$\text{for } T \leq T_o \,. \quad (4.7)$$

For $T \leq T_o$, the normalized radiated pressure from an infinite elastic plate excited by a point force $Q(t) = f_o H(t_o - t)$ is then given by:

$$\frac{P}{P_o} = \frac{1}{2}\left(\frac{R}{h}\right) \sum_{n=0}^{\infty} \frac{(-1)^n \left[\dfrac{N_2}{T - \cos\phi}\right]^{2n+1}}{2(n+1)(2n+1)!} H(T - \cos\phi) \quad , \text{ for } T \leq T_o \quad . \tag{4.8}$$

Transferring the integration variable τ to u by letting

$$u = \frac{N_2}{\dfrac{\tau c_o}{R} - T - \cos\phi} \qquad \text{and} \qquad du = \frac{c_o N_2 \, d\tau}{R\left(T - \dfrac{\tau c_o}{R} - \cos\phi\right)^2} \quad .$$

Equation (4.6) can be written as:

$$P(R,\phi,t) = f_o N_1 \int_{\frac{N_2}{T-\cos\phi}}^{\frac{N_2}{T-T_o-\cos\phi}} \frac{R}{c_o} \frac{\sin u}{u} H\left(\frac{N_2}{u}\right) du \quad , \quad T > T_o \quad , \tag{4.9}$$

or

$$P(R,\phi,t) = -\frac{f_o N_1 R}{c_o} \int_{o}^{\frac{N_2}{T-\cos\phi}} \frac{\sin u}{u} H\left(\frac{N_2}{u}\right) du + \frac{f_o N_1 R}{c_o} \int_{o}^{\frac{N_2}{T-T_o-\cos\phi}} \frac{\sin u}{u} H\left(\frac{N_2}{u}\right) du \quad , \quad T > T_o \quad . \tag{4.10}$$

The integrals of Equation (4.10) are similar to the integral of Equation (4.1), therefore, following the same procedure to evaluate the integration, one obtains:

$$P(R,\phi,t) = -\frac{\alpha\beta f_o}{4\pi h^2}\left\{\sum_{n=0}^{\infty}\frac{(-1)^n}{(2n+1)(2n+1)!}\left[\left[\frac{N_2}{T-\cos\phi}\right]^{2n+1}\right.\right.$$

$$\left.\left.\times H(T-\cos\phi) - \left[\frac{N_2}{T-T_o-\cos\phi}\right]^{2n+1} H(T-T_o-\cos\phi)\right]\right\}$$

$$\text{for } T > T_o . \quad (4.11)$$

The normalized radiated pressure from an infinite elastic plate excited by a point force $Q(t) = f_o H(t_o - t)$ is given by

$$\frac{P}{P_o} = \frac{1}{2}\left(\frac{R}{h}\right)\left\{\sum_{n=0}^{\infty}\frac{(-1)^n}{(2n+1)(2n+1)!}\left[\left[\frac{N_2}{T-\cos\phi}\right]^{2n+1}\right.\right.$$

$$\left.\left.\times H(T-\cos\phi) - \left[\frac{N_2}{T-T_o-\cos\phi}\right]^{2n+1} H(T-T_o-\cos\phi)\right]\right\},$$

$$\text{for } T > T_o . \quad (4.12)$$

Figures 4.22 and 4.23 are the plots of radiated pressure versus time for applied force $Q(t) = f_o H(t_o - t)$ and $T > T_o$ for $T_o = \cos\phi - 0.1$ and $T_o = 0.5\cos\phi$, respectively, the forcing frequency $\Omega_1 = \omega_1/\omega_2 = 1.5$, $R/h = 50$ and $\phi = 30^o$.

4.2.4 Applied CW-Pulse Force. Such an applied force can be represented by $Q(t) = f_o \cos\omega_1 t H(t_o - t)$. Substituting applied force and Equation (3.43) into the convolution integral Equation (3.3), and neglecting the very small contribution of the second term of Equation (3.43), one obtains:

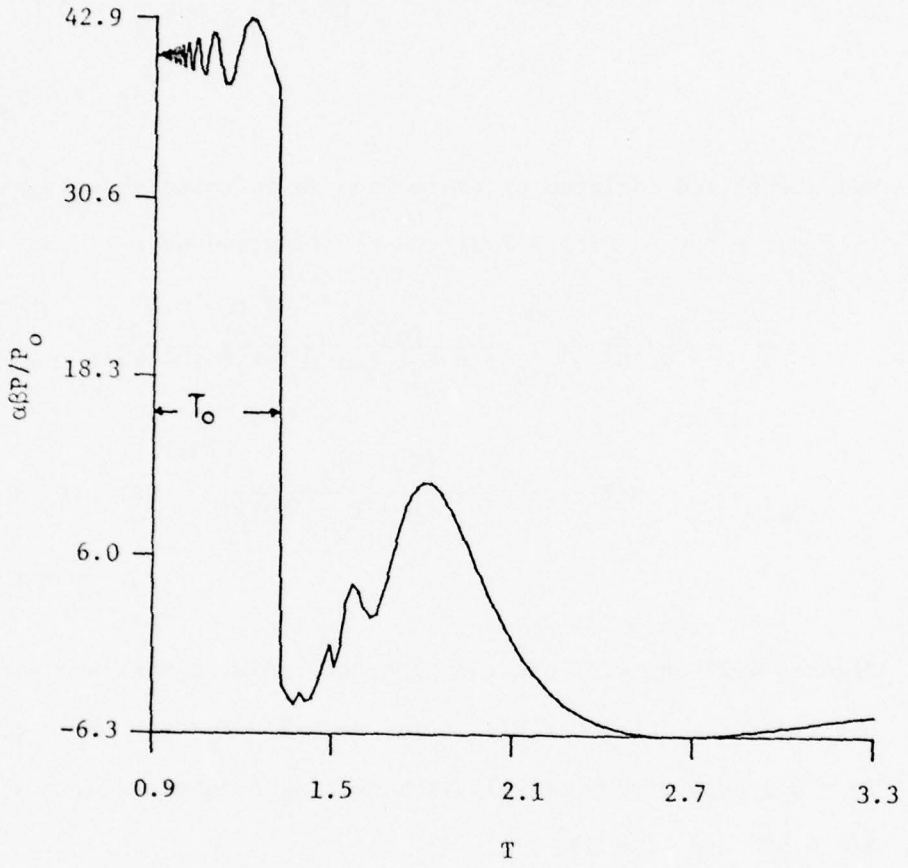


Figure 4.22 Normalized Radiated Pressure Versus Time at Observation Point $\phi = 30^o$ and $R/h = 50$ for a Square Pulse Applied Load with Pulse Length $T_o = 0.5 \cos\phi$

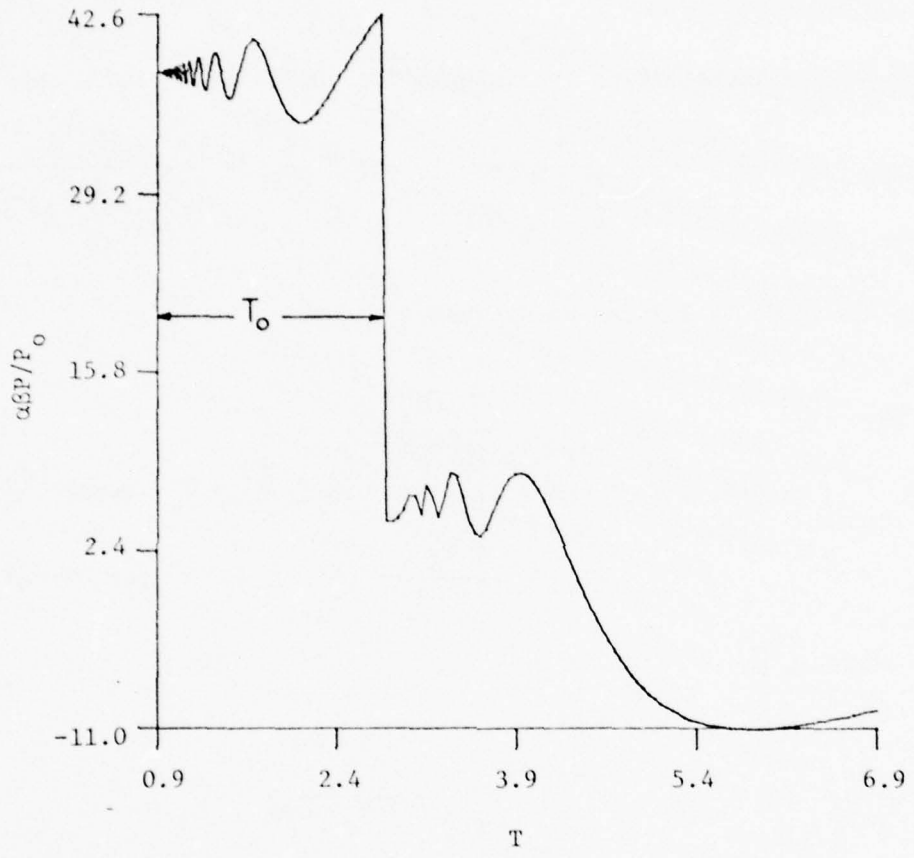


Figure 4.23 Normalized Radiated Pressure Versus Time at Observation Point $\phi = 30^o$ and $R/h = 50$ for a Square Pulse Applied Load with Pulse Length $T_o = \cos\phi - 0.1$

$$P(R,\phi,t) = N_1 f_o \int_0^{t_o} \frac{\cos\omega_1\left[\sin \dfrac{N_2}{T - \frac{\tau c_o}{R} - \cos\phi}\right]}{\left[T - \frac{\tau c_o}{R} - \cos\phi\right]} H(T - \frac{c_o}{R} - \cos\phi)\,d\tau \ ,$$

for $T > T_o$. (4.13)

Transferring the integration variable τ to u by letting

$$u = \frac{N_2}{T - \frac{\tau c_o}{R} - \cos\phi} \quad \text{and} \quad du = \frac{c_o N_2\, d}{R\left(T - \frac{\tau c_o}{R} - \cos\phi\right)^2} \ ,$$

Equation (4.13) can be written as:

$$P(R, \ ,t) = \frac{f_o N_1 R}{c_o} \int_{\frac{N_2}{T-\cos\phi}}^{\frac{N_2}{T-T_o-\cos\phi}} \cos\bar{\omega}_1[-\frac{N_2}{u} + T - \cos\phi] \frac{\sin u}{u} H(\frac{N_2}{u})\,du \ ,$$

for $T > T_o$, (4.14)

where $\bar{\omega}_1 = \dfrac{R\omega_1}{c_o}$,

or

$$P(R,\phi,t) = \frac{f_o N_1 R}{c_o} \left\{ \left[\int_0^{\frac{N_2}{T-T_o-\cos\phi}} \cos(\bar{\omega}_1 a)\cos(\bar{\omega}_1 \frac{N_2}{u}) \frac{\sin u}{u}\,du \right.\right.$$

$$\left.\left. + \int_0^{\frac{N_2}{T-T_o-\cos\phi}} \sin(\bar{\omega}_1 a)\ \sin(\bar{\omega}_1 \frac{N_2}{u}) \frac{\sin u}{u}\,du \right] \times \right.$$

$$\times H(T - T_o - \cos\phi) - \left[\int_0^{\frac{N_2}{T-\cos\phi}} \cos(\bar{\omega}_1 a)\cos(\bar{\omega}_1 \frac{N_2}{u}) \frac{\sin u}{u}\, du \right.$$

$$\left. + \int_0^{\frac{N_2}{T-\cos\phi}} \sin(\bar{\omega}_1 a)\sin(\bar{\omega}_1 \frac{N_2}{u}) \frac{\sin u}{u}\, du \right] H(T - \cos\phi) \Bigg\} ,$$

$$\text{for } T > T_o , \quad (4.15)$$

where $a = T - \cos\phi$.

Equation (4.15) can be rewritten as follows:

$$P(R,\phi,t) = \frac{f_o N_1 R}{c_o} \Big\{ [P_{11} + P_{12} + P_{21} - P_{22}] H(T - \cos\phi)$$

$$- [P_{31} + P_{32} + P_{41} - P_{42}] H(T - T_o - \cos\phi) \Big\}, \quad (4.16)$$

where

$$P_{11} = \frac{\cos\bar{\omega}_1 a}{2} \int_0^{\frac{N_2}{T-\cos\phi}} \sin(u + \frac{N_3}{u}) \frac{du}{u} , \quad (4.17)$$

$$P_{12} = \frac{\cos\bar{\omega}_1 a}{2} \int_0^{\frac{N_2}{T-\cos\phi}} \sin(u - \frac{N_3}{u}) \frac{du}{u} , \quad (4.18)$$

$$P_{21} = \frac{\sin\bar{\omega}_1 a}{2} \int_0^{\frac{N_2}{T-\cos\phi}} \cos(u - \frac{N_3}{u}) \frac{du}{u} , \quad (4.19)$$

$$P_{22} = \frac{\sin\bar{\omega}_1 a}{2} \int_0^{\frac{N_2}{T-\cos\phi}} \cos(u + \frac{N_3}{u}) \frac{du}{u} , \quad (4.20)$$

$$P_{31} = \frac{\cos\bar{\omega}_1 a}{2} \int_0^{\frac{N_2}{T-T_o-\cos\phi}} \sin\left(u + \frac{N_3}{u}\right) \frac{du}{u} \quad , \tag{4.21}$$

$$P_{32} = \frac{\cos\bar{\omega}_1 a}{2} \int_0^{\frac{N_2}{T-T_o-\cos\phi}} \sin\left(u - \frac{N_3}{u}\right) \frac{du}{u} \quad , \tag{4.22}$$

$$P_{41} = \frac{\sin\bar{\omega}_1 a}{2} \int_0^{\frac{N_2}{T-T_o-\cos\phi}} \cos\left(u - \frac{N_3}{u}\right) \frac{du}{u} \tag{4.23}$$

and

$$P_{42} = \frac{\sin\bar{\omega}_1 a}{2} \int_0^{\frac{N_2}{T-T_o-\cos\phi}} \cos\left(u + \frac{N_3}{u}\right) \frac{du}{u} \quad . \tag{4.24}$$

Letting $y = u + \frac{N_3}{u}$, and $dy = (y^2 - 4N_3)^{1/2} \frac{du}{u}$ into Equations (4.17) and (4.20), one obtains:

$$P_{11} = \frac{\cos\bar{\omega}_1 a}{2} \int_{G_1}^{\infty} \frac{\sin y}{\sqrt{y^2 - 4N_3}} \, dy \tag{4.25}$$

and

$$P_{22} = \frac{\sin\bar{\omega}_1 a}{2} \int_{G_1}^{\infty} \frac{\cos y}{\sqrt{y^2 - 4N_3}} \, dy \quad , \tag{4.26}$$

where

$$G_1 = \frac{N_2^2 + N_3(T - \cos\phi)^2}{N_2(T - \cos\phi)} \quad .$$

Letting $y = u - \frac{N_3}{u}$, and $dy = (y^2 + 4N_3)^{1/2} \frac{du}{u}$ into Equations (4.18) and (4.19), one obtains:

$$P_{12} = \frac{\cos\bar{\omega}_1 a}{2} \int_{G_2}^{\infty} \frac{\sin y}{\sqrt{y^2 + 4N_3}}\, dy \qquad (4.27)$$

and

$$P_{21} = \frac{\sin\bar{\omega}_1 a}{2} \int_{G_2}^{\infty} \frac{\cos y}{\sqrt{y^2 + 4N_3}}\, dy \quad , \qquad (4.28)$$

where

$$G_2 = \frac{N_2^2 - N_3(T - \cos\phi)^2}{N_2(T - \cos\phi)} \quad .$$

Applying the same type of transformations as above to Equations (4.21) through (4.24), one obtains integrals identical to those in Equations (4.24) through (4.28) with different upper limits. Equations (4.24) and (4.26) can be rewritten as follows:

$$P_{11} = \frac{\cos\bar{\omega}_1 a}{2} \left[\int_{2\sqrt{N_3}}^{\infty} \frac{\sin y}{\sqrt{y^2 - 4N_3}}\, dy - \int_{2\sqrt{N_3}}^{G} \frac{\sin y}{\sqrt{y^2 - 4N_3}}\, dy \right]$$

$$= \frac{\cos\bar{\omega}_1 a}{2} \left[\frac{\pi}{2} J_o(2\sqrt{N_3}) - \int_{2\sqrt{N_3}}^{G_1} \frac{\sin y}{\sqrt{y^2 - 4N_3}}\, dy \right]$$

and

$$P_{22} = \frac{\sin\bar{\omega}_1 a}{2} \left[\int_{2\sqrt{N_3}}^{\infty} \frac{\cos y}{\sqrt{y^2 - 4N_3}}\, dy - \int_{2\sqrt{N_3}}^{G_1} \frac{\cos y}{\sqrt{y^2 - 4N_3}}\, dy \right]$$

$$= \frac{\sin\bar{\omega}_1 a}{2} \left[-\frac{\pi}{2} Y_o(2\sqrt{N_3}) - \int_{2\sqrt{N_3}}^{G_1} \frac{\cos y}{\sqrt{y^2 - 4N_3}}\, dy \right] \quad , \qquad (4.30)$$

where $J_o(x)$ and $Y_o(x)$ are the Bessel and Neumann functions, respectively. The integrals in Equations (4.29) and (4.30) can be evaluated by numerical methods. Equations (4.27) and (4.28) can be rewritten as follows:

$$P_{12} = \frac{\cos\bar{\omega}_1 a}{2}\left[\int_0^{200}\frac{\sin y}{\sqrt{y^2+4N_3}}\,dy + \int_{200}^{\infty}\frac{\sin y}{\sqrt{y^2+4N_3}}\,dy - \int_0^{G_2}\frac{\sin y}{\sqrt{y^2+4N_3}}\,dy\right], \quad \text{for } G_2 \gtrless 0 \tag{4.31}$$

and

$$P_{21} = \frac{\sin\bar{\omega}_1 a}{2}\left[\int_0^{\infty}\frac{\cos y}{\sqrt{y^2+4N_3}}\,dy \mp \int_0^{G_2}\frac{\cos y}{\sqrt{y^2+4N_3}}\,dy\right]$$

$$= \frac{\sin\bar{\omega}_1 a}{2}\left[K_o(2\sqrt{N_3}) \mp \int_0^{G_2}\frac{\cos y}{\sqrt{y^2+4N_3}}\,dy\right], \quad \text{for } G_2 \gtrless 0\,. \tag{4.32}$$

Since $y^2 >> 4N_3$, when $y \geq 200$, the second integral of Equation (4.31) can be approximated as follows:

$$\int_{200}^{\infty}\frac{\sin y}{\sqrt{y^2+4N_3}}\,dy \approx \int_{200}^{\infty}\frac{\sin y}{y}\,dy \quad , \text{ for } y^2 >> 4N_3 \quad ,$$

which turns out to be the Sine Integral function. The remaining

Equations (4.21) through (4.24). Substituting these results into Equation (4.16), one obtains an expression for the radiated pressure from an infinite elastic plate excited by a point force

$$Q(t) = f_o \cos\omega_1 t \; H(t_o - t) \quad .$$

The plots of the normalized radiated pressure versus time for $T > T_o$ and with $T_o = 0.5 \cos\phi$ and $T_o = \cos\phi - 0.1$ are shown in Figures 4.24 and 4.25, respectively. The other parameters for these plots were chosen as $\Omega_1 = \omega_1/\omega_o = 1.5$, $R/h = 50$ and $\phi = 30^o$. An expanded time scale for the results of Figure 4.25 is shown in Figure 4.26.

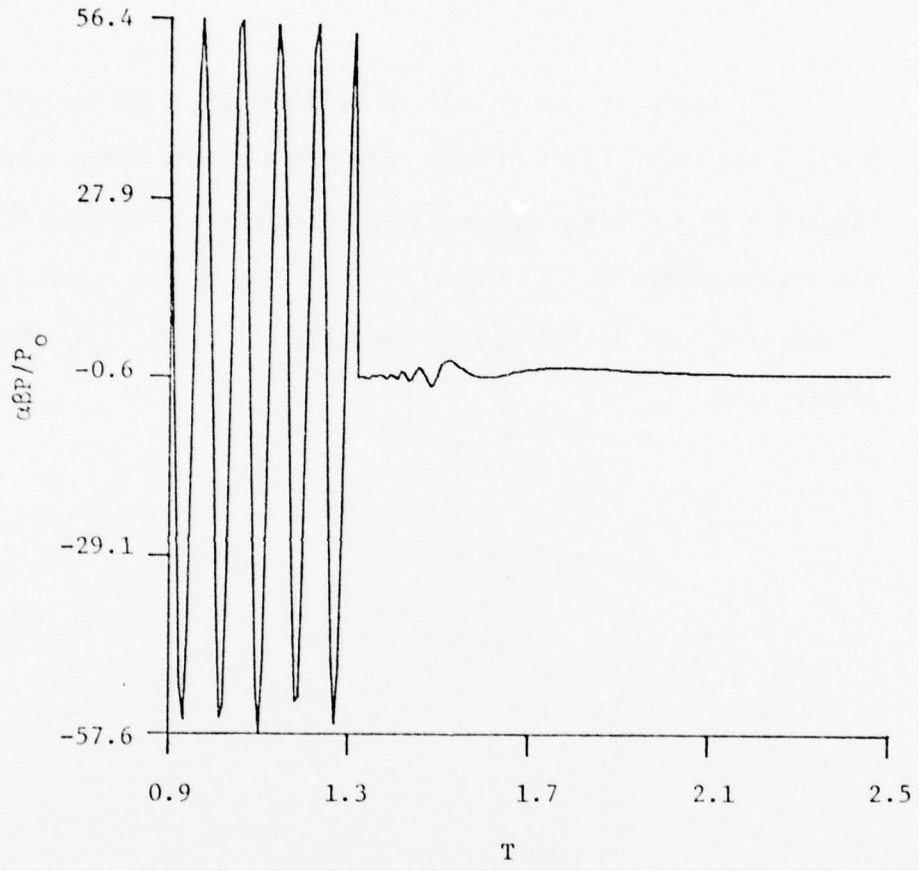


Figure 4.24 Normalized Radiated Pressure Versus Time at Observation Point $\phi = 30^{o}$ and $R/h = 50$ for a CW-Pulse Applied Load with Pulse Length $T_o = 0.5 \cos\phi$

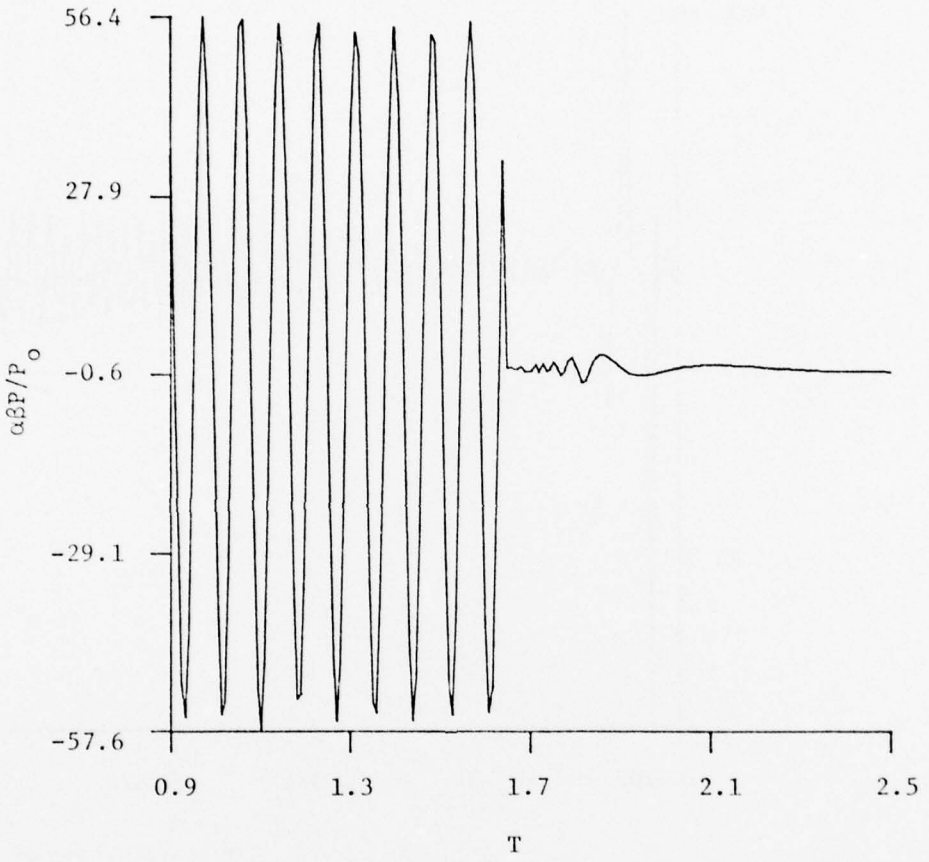


Figure 4.25 Normalized Radiated Pressure Versus Time at Observation Point $\phi = 30^{o}$ and $R/h = 50$ for a CW-Pulse Applied Load with Pulse Length $T_o = \cos\phi - 0.01$

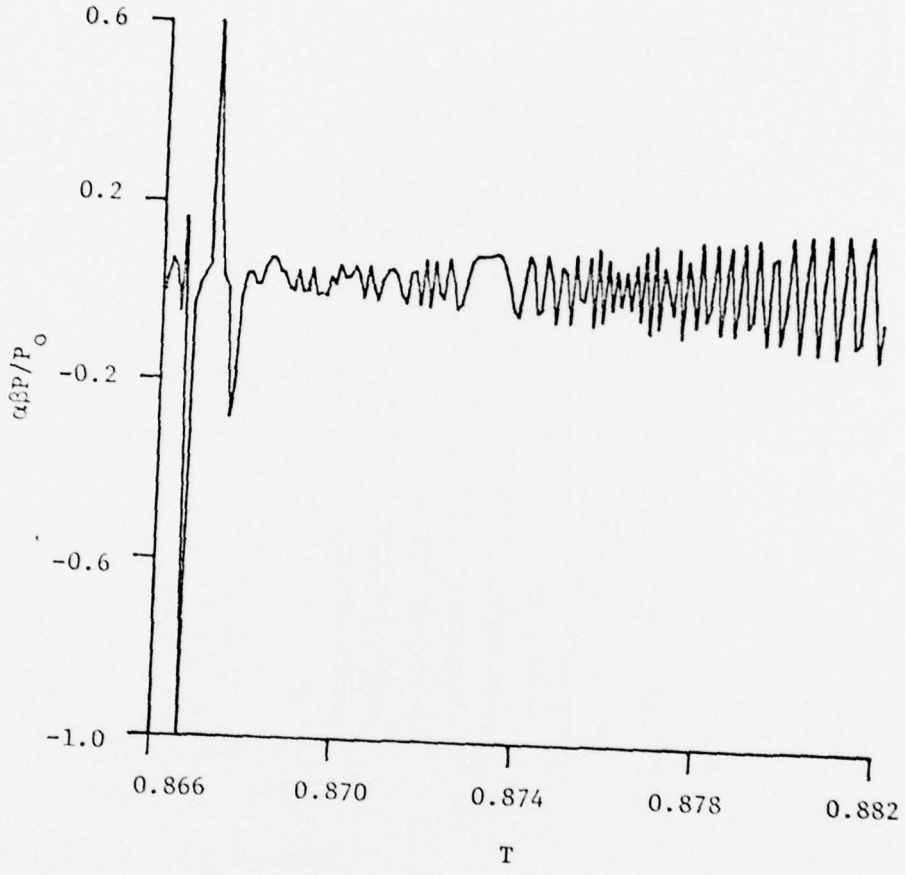


Figure 4.26 Normalized Radiated Pressure Versus Expanded Time Scale at Observation Point $\phi = 30^{o}$ and $R/h = 50$ for a CW-Pulse Applied Load with Pulse Length $T_o = \cos\phi - 0.1$

CHAPTER V

DISCUSSIONS OF THE RESULTS AND CONCLUSIONS

5.1 Discussion of the Impulse Response Solutions

The numerical results for the radiated pressure signature due to a unit impulse load are discussed first.

Equations (3.45) and (3.46) represent the solution for the radiated pressure from an infinite elastic plate in contact with an infinite acoustic medium occupying the space $z > 0$ and excited by impulsive point force for different observation angles and distances.

The expression for the unit impulse response consists of two terms, each exhibiting a damped sinusoidal oscillation where the period varies with time. The relative magnitude of these terms can be estimated from the numerical evaluation of the contribution of the first term as shown in Figures 4.1 and 4.2 to the contribution of the second term as shown in Figures 4.3 and 4.4, respectively, where the range R/h was 50 and observer angles are $\phi = 30^{o}$ and 60^{o} . These plots show that the ratio of peak value of the first term to that of the second term is $0(10^{2})$. Thus, the contribution of the second term can be neglected and solution is approximated by the first term only for all values of T . This is evidenced when one compares the total solution shown in Figures 4.5 and 4.6 with the contribution of the first term only in Figures 4.1 and 4.2, respectively. The general character of the solution is similar when $R/h = 100$ and 1000 and $\phi = 30^{o}$ as can be seen in Figures 4.7 and 4.8. Since the largest contribution to the impulse response comes from

the first term, one can explore the solution more fully by examining the first term only. The first term represents a damped sinusoidal oscillation, which decays to zero as $T \to \infty$. These oscillations are shown explicitly when one expands the time scale as shown in Figures 4.9 through 4.11 for $\phi = 30^{o}$ and $R/h = 50$, 100 and 1000. The period of oscillations varies with the elapsed time T, the observer angle ϕ and R/h. The period is very short at the first arrival of the acoustic wave and becomes larger later. The time of arrival T_n of the n^{th} peak can be deduced from the sinusoidal term in Equations (3.45) and (3.46), such that:

$$T_n = \frac{\alpha(R/h)\sin^2\phi}{2(2n+1)\pi} + \cos\phi \quad , \text{ where } n = 0,1,2,\ldots \quad . \quad (5.1)$$

The largest half-period between the last two observable peaks is given by the time difference between $T_{n=1}$ and $T_{n=2}$ as follows:

$$\Delta T = T_{n=1} - T_{n=2} = \frac{\alpha(R/h)\sin^2\phi}{15\pi} \quad .$$

The half-period ΔT is marked on each of Figures 4.9 through 4.11. Thus, the time interval between the last two observable peaks of an impulse response time signature of an elastic plate may be used to obtain an estimate of the observer distance R if the plate thickness h is known.

In absolute time scale, ΔT in seconds is given by:

$$\Delta T = \frac{R}{c_o}\Delta T = \frac{R^2}{30\pi c_o h} \quad ,$$

where $\alpha \approx 1.0$ and the mean value of $\sin^2\phi$ was taken to be 0.5 .

The last peak of the impulse response occurs at time $T_{n=0}$, after which no oscillation occurs in the time signature and it decays at T^{-1} .

The computation of the time signatures for the exact solutions has been discussed above. The most noticeable feature of the exact solution is the prediction of the first arrival of the acoustic pressure wave. The exact solution predicts a nondimensional arrival time of $T = \cos\phi < 1.0$ which, if translated to absolute time, is:

$$t = \frac{R}{c_o} \cos\phi = \frac{z}{c_o} < \frac{R}{c_o} \quad .$$

This means that the elastic wave in the plate would have travelled at an infinite phase velocity. Thus, the first vibration induced radiated acoustic pressure wave would have emanated from a point on the plate just below the receiver point (R,ϕ) and would have travelled in the acoustic medium a distance z only. Physically, the phase velocity in flexure cannot exceed the shear velocity of the elastic plate and thus one would expect the arrival time of the first pressure wave to have occurred later than $T = \cos\phi$. The reason for this underprediction of the first arrival is due to the Euler plate theory used as a model for the flexural vibration of the elastic plate. The Euler plate theory is an approximate theory of antisymmetric motion in a plate. This approximation assumes that the normal to the plate's mid-surface stays normal after deformation and that the flexural vibration involves no rotation of an element about its mid-surface. These approximations leading to the Euler plate theory gives one dispersion curve Ω vs $\bar{k}$ given in Equation (3.15a). Thus, the phase velocity v_p is given by the secant $v = \Omega/\bar{k}$, which increases without limit as $|\Omega| \to \infty$. Thus, the dispersion curve predicts an

infinite phase velocity as $\Omega \to \infty$. Since the Fourier transform in Equation (2.5) integrates over Ω from $-\infty$ to ∞ , one would expect an error when Ω is very large or when t is very small. Thus, the first arrival of the pressure wave would have travelled at infinite phase speeds when the integration covers $|\Omega| \to \infty$. It should be noted that the Euler theory is valid for wavelength-to-thickness ratio larger than eight, i.e., low frequencies. A more accurate theory of flexural vibration is the Timoshenko-Mindlin plate theory. This theory includes shear deformation and rotatory inertia, so that the two frequency spectra of this theory accurately predict the first two nonsymmetric spectra of the exact plate theory. Thus, the Timoshenko-Mindlin plate theory would accurately predict the flexural phase velocity as $\Omega \to \infty$ to be Rayleigh wave speed. Thus, the vibration in the plate would travel by Reyleigh speed first before travelling in the acoustic medium. Hence, the first arrival of the pressure wave would occur later than $T = \cos\phi$ but before the direct acoustic path arrival of $T = 1.0$, since the Rayleigh wave speed for metals is higher than that of the sound speed in water.

Approximate expressions for the radiated pressure were also obtained and given in Equations (B.9) and (B.10). This approximation parallels the development of similar solutions obtained by Magrab and Reader [20] and Stuart [12]. This approximation was obtained by the regular saddle-point method and henceforth will be referred to as RSP. A better approximation than the above, using the modified saddle-point method was given in Equations (B.14) and (B.15). These solutions will be referred to as MSP in the subsequent discussions. However, the two approximations predict similar time signatures, but the predicted

magnitudes of the radiated pressure were different. The two approximations predict an oscillating impulse response for $T < 1.0$ and a purely exponential decay in the response for $T > 1.0$. This is clearly in contrast to the character of the exact solution, which exhibits damped oscillations before and after $T = 1.0$ and up to time $T = T_{n=0}$, which is the time of arrival of the last peak of the oscillating impulse response. Furthermore, the exact solution predicts a time decay $1/T$ for $T > T_{n=0}$, which decays at a slower rate than the exponentially decaying response predicted by the approximate solutions. In addition, the approximate solutions cannot predict the first arrival of the acoustic wave, unlike that predicted by the exact solution.

The solutions predicted by MSP are shown in Figures 4.12 through 4.15 for $R/h = 50$ and 100 and $\phi = 30^{o}$ and 60^{o}. The MSP solutions predict acoustic pressure peak levels of the order $0(10^{-2})$ smaller than those predicted by the exact solutions for all T as can be seen when one compares Figures 4.12 through 4.15 to Figures 4.9 through 4.11. They also decay faster than the levels predicted by the exact solutions.

The solutions predicted by RSP are shown in Figures 4.16 through 4.19 for $R/h = 50$ and 100 and $\phi = 30^{o}$ and 60^{o}. The RSP solutions also predict acoustic pressure peak levels of the order $0(10^{-2})$ smaller than those predicted by the exact solutions for all T. Comparing solutions predicted by MSP and RSP, one can conclude that the two solutions predict similar time signatures, approximately the same peak levels and exhibit an exponentially decaying time signature after $T \geq 1.0$.

5.2 Discussion of the Radiated Pressure Due to Different Applied Loads

Using the unit impulse response given in Equations (3.45) and (3.46), one can obtain the solution for an applied point force with a designated time signature by use of the convolution theorem. In order that one can compare the relative magnitudes of the time signatures of the radiated pressure for different loads, the numerical values were normalized to the radiated pressure from an infinite elastic plate excited by harmonic point force at the coincidence frequency.

The normalized time signature from a plate excited by a constant load has been computed and shown in Figures 4.20 and 4.21 for $R/h = 50$ and $\phi = 30^{o}$. The response builds from a constant at first arrival and increases with T in an oscillatory manner as seen in the expanded scale in Figure 4.20. The oscillations are due to the continuous vibration of the plate after it had been excited at $T = 0$ by the constant load. The period of oscillation is zero at the arrival time and increases as time increases. The reason for zero or very short period at the arrival time can be traced to the inaccuracy of the Euler plate theory for high frequencies, which contribute mostly near the first arrival. After $T = 1.0$, the pressure increases to a maximum dynamic pressure and then decays monotonically as $1/T$ for $T \gg 1$ as seen in Figure 4.21. This is physically reasonable, since as $T \to \infty$, the influence of the constant load becomes quasi-static and, hence, no dynamic pressure results.

The response due to a square pulse is shown in Figures 4.22 and 4.23 for two pulse lengths. In Figures 4.22 and 4.23, the radiated pressure time signature due to pulse lengths $T_o = 0.5 \cos\phi$ and $T_o = \cos\phi - 0.1$ are shown, respectively. The response after the first

arrival at $T = \cos\phi$ and before the arrival of the pulse representing the time when the load is removed, i.e., $T = \cos\phi + T_o$ must necessarily resemble the response due to a constant applied load as shown in Figures 4.21 and 4.22. However, the response drops immediately by approximately 20 dB after the removal of the load. After the removal of the load, the plate oscillates freely and the peak value in the response corresponds to the peak value in the unit impulse response curve. The response for long times T again decays as $1/T$ for $T >> 1.0$ as clearly shown in Figure 4.23.

The normalized radiated pressure time signature due to CW-pulse load for $T_o = 0.5 \cos\phi$ and $T_o = \cos\phi - 0.1$ are shown in Figures 4.24 and 4.25, respectively. The response after the first arrival $T = \cos\phi$ is a sinusoid of the same period as the load. For $T > \cos\phi + T_o$, which represents the time when the load is removed, the response drops immediately as expected. After removal of the load, the plate oscillates with increasing periods in a manner similar to the impulse response. The response for long time T again decays as $1/T$ for $T >> 1.0$.

5.3 Conclusions

The prediction of the response of an elastic plate to time dependent point forces and the resulting time signatures of the radiated acoustic pressure was the main objective of this study. The radiated pressure was predicted for a unit impulse, a constant load, a square pulse and a CW pulse at different observer distances R/h and angles ϕ. The following conclusions can be drawn from the study of the analytic solutions and their numerical evaluation as follows:

AD-A076 772 PENNSYLVANIA STATE UNIV UNIVERSITY PARK APPLIED RESE--ETC F/G 20/1
TRANSIENT ACOUSTIC RADIATION FROM ELASTIC PLATES.(U)
APR 79 S M SENGERDY N00024-79-C-6043
UNCLASSIFIED ARL/PSU/TM-79-50 NL

2 OF 2
AD
A076772



END
DATE
FILMED
12-79
DDC

a. The predicted time for the first arrival $T = \cos\phi$ is shorter than the acoustic arrival $T = 1.0$, which is physically more realistic than the preceding studies since the elastic waves travel in an elastic plate at supersonic speeds at high frequencies. However, a more accurate prediction of the first arrival time would have been longer than $T = \cos\phi$ and shorter than $T = 1.0$ if one would have employed a more accurate theory of flexural response for the plate.

b. The time signature of the radiated acoustic pressure oscillates with an increasing period of oscillation due to the free vibration of the infinite plate after the application of the impulsive force. This was attributed to the dispersive nature of the frequency spectrum of the elastic plate.

c. The time signature of the radiated pressure always diminishes immediately after the removal of the load, which is physically reasonable.

d. The time difference between the last observable peaks can be measured and are directly related to the observer angle ϕ and the ratio R/h. Hence, one can get an approximate value for R from such a measurement if the average value of the observer angle ϕ is taken as 45^{o}.

5.4 Suggested Future Research

It was evident from the analytic solution thus developed that a Timoshenko-Midlin flexural plate theory would have made early time

predictions more accurate. However, even this more accurate theory would not be valid because it does not allow coupling of the flexural wave with longitudinal waves. A theory that includes such coupling would either be one of the higher order approximate theories of plate vibration developed by Mindlin or the exact theory of elasticity. In either case, such coupling would accur at high frequencies, which again would correct the short time response.

REFERENCES

1. Skudrzyk, E. J. Grundlagen der Akustik, Springer Verlag, Vienna, 1954.

2. Skudrzyk, E. J. "Sound Radiation of a System with a Finite or Infinite Number of Resonances," J. Acoust. Soc. Am. 30, (1958), 1152.

3. Heckl, M. "Schallabstrahlung von Platten Bei punktförmiger Anregung," [Trans.: "Sound Radiation from Point Excited Plates."] Acoustica 9, (1959), 371-380.

4. Heckl, M. "Untersuchungen an orthotropen Platten," [Trans.: "Studies of Orthotropic Plates."] Acoustica 10, (1960), 109-115.

5. Heckl, M. "Abstrahlung von Einer punktförmig Angeregten Unendlich Grossen Platte unter Wasser," [Trans.: "Radiation from a Point Excited Infinitely Large Plate Under Water."] Acoustica 13, (1963), 182.

6. Thompson, Jr., W. and Rattaya, J. V. "Acoustic Power Radiated by an Infinite Plate by a Concentrated Moment," J. Acoust. Soc. Am. 36, (1964), 1488-1490.

7. Gutin, L. Y. "Sound Radiation from an Infinite Plate Excited by a Normal Point Force," Sov. Phys. Acoust. 10 (4), (1965), 369-371.

8. Feit, D. "Sound Radiation from Orthotropic Plates," J. Acoust. Soc. Am. 47 (1), (1970), 388-389.

9. Skudrzyk, E. J. Simple and Complex Vibrating Systems, The Pennsylvania State University Press, University Park, PA, 1968.

10. Maidanik, G. and Kerwin, Jr., E. M. "Influence of Fluid Loading on the Radiation from Infinite Plates Below the Critical Frequency," J. Acoust. Soc. Am. 40, (1966), 1034-1038.

11. Feit, D. "Pressure Radiation by a Point-Excited Elastic Plate," J. Acoust. Soc. Am. 40 (6), (1966), 1489-1494.

12. Stuart, A. D. "Acoustic Radiation from a Point Excited Infinite Elastic Plate," Ph.D. thesis, The Pennsylvania State University, June 1972.

13. Stuart, A. D. "Acoustic Radiation from Submerged Plates. I. Influence of Leaky Wave Pole," J. Acoust. Soc. Am. 59 (5), (1976), 1160-1169.

14. Stuart, A. D. "Acoustic Radiation from Submerged Plates. II. Radiated Power and Damping," J. Acoust. Soc. Am. 59 (5), (1976), 1170-1174.

15. Romanov, V. N. "Radiation of Sound by an Infinite Plate with Reinforcing Beams," Sov. Phys. Acoust. 17, (1971), 92-96.

16. Feit, D. and Saurenman, H. J. "Sound Radiation by Beam Stiffened Plates," Cambridge Acoustical Associates, Inc., Cambridge, MA, Report No. U-356-213, August 1971.

17. Gorman, R. M. "Vibration of and Acoustic Radiation from Line Excited Rib-Stiffened Damped Plates in Water," Ph.D. thesis, The Pennsylvania State University, June 1974.

18. Garrelick, J. M. and Lin, G. F. "Effect of the Number of Frames on the Sound Radiation by Fluid-Loaded, Frame-Stiffened Plates," J. Acoust. Soc. Am. 58, (1975), 499-500.

19. Lin, G. F. and Hayek, S. I. "Acoustic Radiation from Point Excited Rib-Reinforced Plate," J. Acoust. Soc. Am. 62, (1977), 72-83.

20. Magrab, E. B. and Reader, T. W. "Farfield Radiation from an Infinite Elastic Plate Excited by a Transient Point Loading," J. Acoust. Soc. Am. 44, (1968), 1623-1627.

21. Jones, L. Y. The Theory of Electromagnetism, The Macmillan Company, New York, 1964.

22. Gradshteyn, I. S. and Ryzhik, I. M. Table of Integrals, Series and Products, Academic Press, New York, 1965.

APPENDIX A

ACOUSTIC PRESSURE RESPONSE IN THE VICINITY OF THE VERTICAL AXIS

To obtain a solution for the radiated pressure when the observation point falls on vertical axis $\phi = 0$, one can substitute $J_o(kR\sin\phi) = 1.0$ in Equations (3.29) and (3.31), yielding:

$$I_1(R,0,t) = \int_0^\infty \left\{ \frac{i}{2\alpha^5} + \frac{2\alpha^5\Omega_{p1}\overline{\Gamma}_{p1} - i[3\alpha^6\Omega_{p1}^2 - 2\alpha^4\overline{k}^2 - \alpha^2\overline{k}^4 + 2\alpha^4\beta\overline{\Gamma}_{p1}]}{2\alpha^5(3\alpha^6\Omega_{p1}^2 - 2\alpha^4\overline{k}^2 - \alpha^2\overline{k}^4 + 2\alpha^4\beta\overline{\Gamma}_{p1})} \right\}$$

$$\times \exp\{\Gamma_{p1}z - i\omega_o\Omega_{p1}t\}\, kJ_o(k,r)dk \quad , \qquad (A.1)$$

and

$$I_2(R,0,t) = \int_0^\infty \left\{ -\frac{i}{2\alpha^5} + \frac{2\alpha^5\Omega_{p2}\overline{\Gamma}_{p2} + i[3\alpha^6\Omega_{p2}^2 - 2\alpha^4\overline{k}^2 - \alpha^2\overline{k}^4 + 2\alpha^4\beta\overline{\Gamma}_{p2}]}{2\alpha^5(3\alpha^6\Omega_{p2}^2 - 2\alpha^4\overline{k}^2 - \alpha^2\overline{k}^4 + 2\alpha^4\beta\overline{\Gamma}_{p2})} \right\}$$

$$\times \exp\{\Gamma_{p2}z + i\omega_o\Omega_{p2}t\}\, kJ_o(kr)dk \quad . \qquad (A.2)$$

Using the modified saddle-point method and following the same procedures as outlined in Section 3.2.2 to evaluate the above integrals, one obtains the normalized radiated pressure from an infinite elastic plate excited by an impulse point force $Q(t) = F_o\delta(t)$ given by:

$$\frac{P(2\pi h^2)}{F_o(c_o/h)} = \frac{\alpha\beta}{2}\,\delta(T-1.0 + \frac{k_s \pi\beta\alpha^3 \bar{k}_s - \bar{k}_p)(A_1^2+A_2^2)^{1/2}(a_1^2+x_2^2)^{1/2}}{2(B_1^2+B_2^2)^{1/2}}$$

$$\times \exp\left\{\frac{R}{h}\left[\bar{\Phi}_1 + \frac{1}{2}(\bar{k}_p - \bar{k}_s)^2\Phi''_a\right]\right\}$$

$$\times \cos\left\{\psi_1 + \psi_2 + \frac{R}{h}\bar{\Phi}_2 + \frac{R}{2h}(\bar{k}_p - \bar{k}_s)^2\Phi''_b - \xi\right\} H(T-1.0) \,. \qquad (A.3)$$

The definitions of the terms in Equation (A.3) are given in Section 3.2.3 with ϕ set to zero.

APPENDIX B

APPROXIMATE SOLUTIONS

Using the methods of solution employed by Magrab and Reader [20] and Stuart [12] to evaluate the radiated pressure from an infinite elastic plate excited by a transient force, one can compare such solutions with the solutions obtained in Chapter III. Applying the inverse Hankel transform to Equation (2.20), one obtains:

$$\bar{P}(r,z,\omega) = \int_0^\infty \frac{\rho_o \omega^2 Q(\omega) e^{\Gamma z} k J_o(kr)\,dk}{2\pi D\left\{(k^4 - \frac{\omega^2}{h^2 c_p^2})\Gamma + \frac{\omega^2 \rho_o}{D}\right\}} \quad . \tag{B.1}$$

Letting

$$J_o(kr) = \frac{1}{2}[H_o^{(1)}(kr) + H_o^{(2)}(kr)] \quad , \tag{B.2}$$

$$H_o^{(1)}(kr) \approx \sqrt{\frac{2}{kr\pi}}\, e^{i(kr - \frac{\pi}{4})} \quad , \tag{B.3}$$

$$r = R\sin\phi \quad , \quad z = R\cos\phi \quad , \quad \Omega = \frac{\omega}{\omega_o} \quad ,$$

and substituting Equations (B.2) and (B.3) into Equation (B.1) yields:

$$\bar{P}(R,\phi,t) = \frac{\beta\alpha^4\Omega^2 Q(\omega_o\Omega)\sqrt{2}\, e^{\frac{-i\pi}{4}}}{4\pi\sqrt{\pi R\sin\phi}} \int_{-\infty}^{\infty} \frac{k^{1/2}\exp\{R(\Gamma\cos\phi + ik\sin\phi)\}dk}{(\bar{k}^4 - \alpha^4\Omega^2)\bar{\Gamma} + \beta\alpha^4\Omega^2} \quad , \tag{B.4}$$

where $\bar{\Gamma} = (\bar{k}^2 - \alpha^2\Omega^2)^{1/2}$.

One can extend the real variable k to the complex plane and use the saddle-point method to evaluate the integral in Equation (B.4). The choice of the branch cuts, path of steepest descent, etc., are enumerated below.

Branch Point and Branch Cuts. Branch points are defined by $\Gamma = 0$, which yields $\bar{k}_B = \pm \alpha\Omega$ located on the real axis. The branch points and branch cuts are shown in Figure B.1 and, for detailed determination of the branch cuts, see Section 2.1.1a.

Saddle Points and Path of Steepest Descent (PSD). The saddle point(s) k_s of the integral in Equation (B.4) is defined as that value of k for which the first derivative with respect to k of the exponential term is zero; hence,

$$\bar{k}_s = \pm \alpha\Omega\sin\phi \quad . \tag{B.5}$$

The saddle point and PSD are shown in Figure B.2 and, for detailed discussion and determination of PSD and poles, see Stuart [12].

One can use one of two methods to evaluate these integrals. The first method involves the use of the regular saddle-point method which does not take into account contribution of the pole when it appears near the saddle point. The second method involves the use of the modified saddle-point method which takes into account contribution of this pole and, hence, gives more accurate results than the first.

(a) Radiated Pressure Obtained by Regular Saddle-Point Method (RSP). Evaluating the integration in Equation (B.4) by the regular saddle-point method, one obtains:

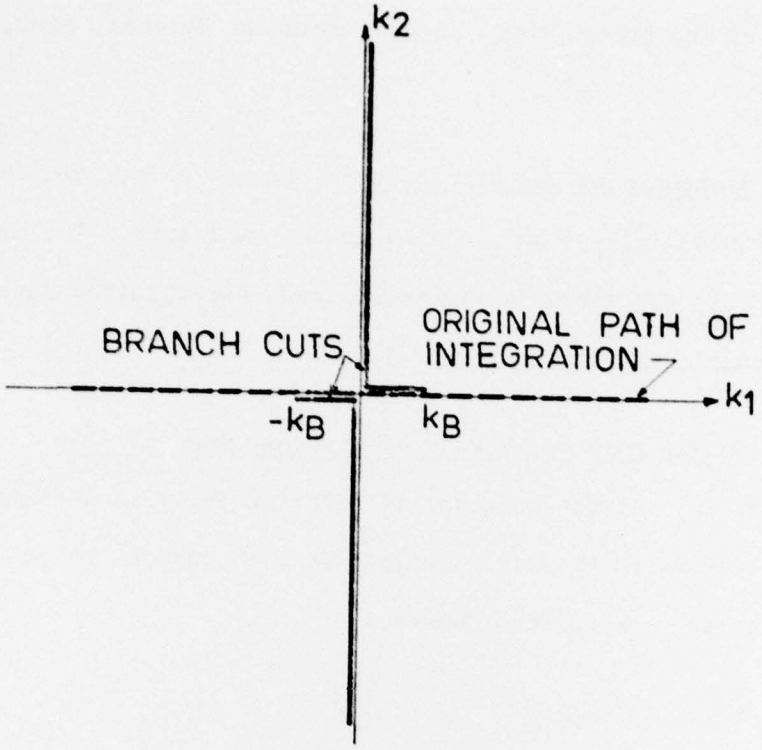


Figure B.1 Branch Cuts and Branch Point in the k-Plane for Integral $\bar{P}$

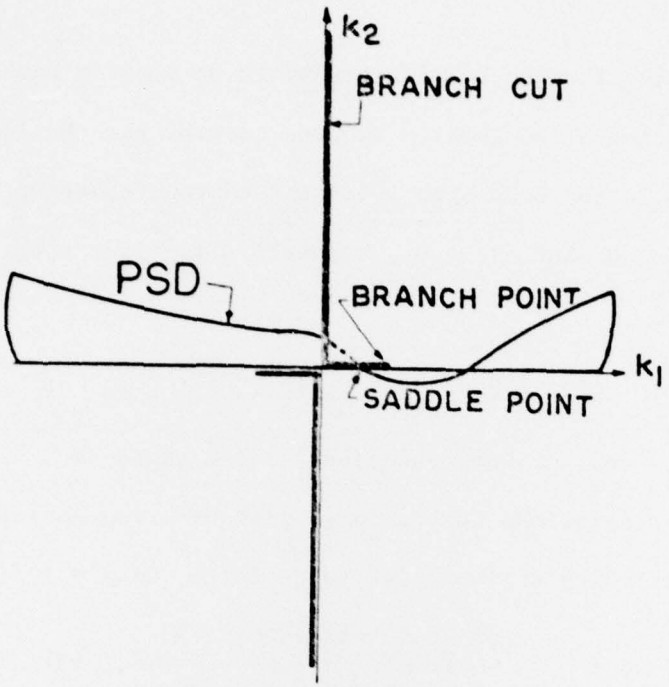


Figure B.2 Path of Integration and Path of Steepest Descent (PSD) in the k-Plane for Integral $\overline{P}$

$$\bar{P}(R,\phi,\Omega) = \frac{i\beta\alpha\cos\phi}{2\pi Rh}\left\{\frac{\Omega\bar{Q}(\omega_o\Omega)e^{iR\alpha\Omega/h}}{i\alpha\Omega\cos\phi(\Omega^2\sin^4\phi - 1) + \beta}\right\} \quad . \qquad (B.6)$$

Applying the inverse Fourier transform on time in Equation (B.6), Cauchy contour integration theorem is used to evaluate the integration. Figures B.3a and B.3b show poles and contour of integration for retarded times $\tau_1 > 0$ and $\tau_1 < 0$, respectively. It can be shown that the poles are:

$$\Omega_{p1} = \varepsilon_1 + i\varepsilon_2 \ , \quad \Omega_{p2} = -\varepsilon_1 + i\varepsilon_2 \quad \text{and} \quad \Omega_{p3} = -i2\varepsilon_2 \quad ,$$

where ε_1 and ε_2 are functions of the angle ϕ.

The solutions for radiated pressure from an infinite elastic plate excited by an impulsive point force $Q(t) = f_o\delta(t)$ become:

$$P(R,\phi,t) = \frac{\alpha\beta c_o\varepsilon_2 F_o \exp\{-2R\alpha\varepsilon_2\tau_1/h\}}{\pi Rh^2[12\varepsilon_2^2\sin^4\phi + 1.0]} \ , \quad \text{for } \tau_1 > 0 \ , \qquad (B.7)$$

and

$$P(R,\phi,t) = -\frac{\alpha\beta c_o(\varepsilon_1^2 + \varepsilon_2^2)^{1/2} F_o e^{R\alpha\varepsilon_2\tau_1/h}}{2\pi Rh^2(a_1^2 + a_2^2)^{1/2}} \sin[\bar{\theta} + \frac{R}{h}\alpha\tau_1\varepsilon_1 - \psi] \ ,$$

$$\text{for } \tau_1 < 0 \ , \qquad (B.8)$$

where

$$a_1 = 3(\varepsilon_1^2 - \varepsilon_2^2)\sin^4\phi - 1 \quad ,$$

$$a_2 = 2\varepsilon_1\varepsilon_2 \quad ,$$

$$\bar{\theta} = \arctan(\varepsilon_2/\varepsilon_1) \quad ,$$

$$\psi = \arctan(a_2/a_1)$$

and

$$\tau_1 = T - 1 \quad .$$

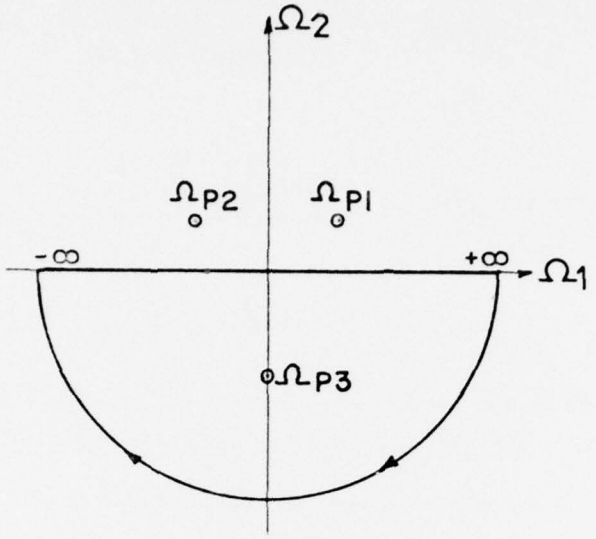


Figure B.3a Integration Path in Ω-Plane for $\tau_1 > 0$

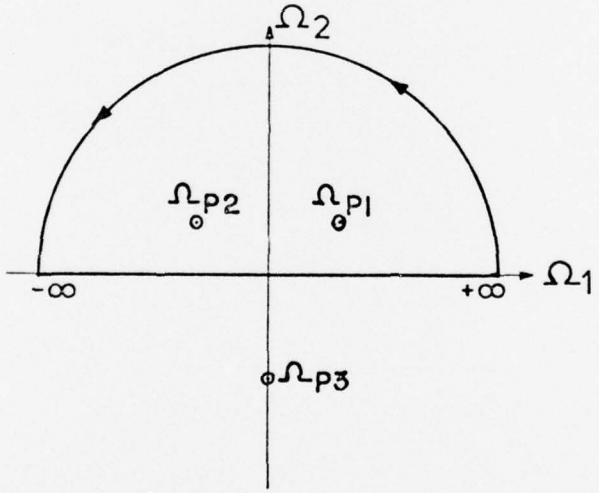


Figure B.3b Integration Path in Ω-Plane for $\tau_1 < 0$

The normalized radiated pressure is given by:

$$\frac{P(2\pi h^2)(R/h)}{F_o(c_o/h)} = \frac{2\alpha\beta\exp[2\bar{\alpha}\varepsilon_2\tau_1(R/h)]}{[12\varepsilon_2^2\sin^4\phi + 1.0]} \quad , \text{ for } \tau_1 \leq 0 \qquad (B.9)$$

and

$$\frac{P(2\pi h^2)(R/h)}{F_o(c_o/h)} = -\frac{\alpha\beta(\varepsilon_1^2 + \varepsilon_2^2)^{1/2}\exp[-(R/h)\bar{\alpha}\tau_1\varepsilon_2]}{(a_1^2 + a_2^2)^{1/2}}$$

$$\times \sin[\bar{\theta} + \frac{R}{h}\alpha\tau_1\varepsilon_1 - \psi] \quad , \text{ for } \tau_1 > 0. \qquad (B.10)$$

(b) Radiated Pressure Obtained by Modified Saddle-Point Method (MSP). Using Jones' [21] modified saddle-point method for the evaluation of the integral in Equation (B.4), one obtains:

$$\bar{P}(R,\phi,\Omega) = \frac{i\beta\bar{Q}(\omega_o\Omega)\sqrt{2}e^{\frac{-i\pi}{4}}}{4\pi\sqrt{\pi Rh}}$$

$$\times \left\{ \frac{(\alpha\Omega\sin\phi - \bar{k}_p)(\alpha\Omega)^{1/2}\{-2H(Rez) + \operatorname{erfc}[-(\frac{1}{2}\frac{R}{h})^{1/2}z]\}}{i\alpha\Omega\cos\phi(\Omega^2\sin^4\phi - 1) + \beta} \right.$$

$$\left. \times \exp\left(\frac{R}{h}\left[i\alpha\Omega + \frac{1}{2}(\bar{k}_p - \alpha\Omega\sin\phi)^2\left\{\frac{-1i}{\alpha\Omega\cos^2\phi}\right\}\right]\right)\right\} \quad , \qquad (B.11)$$

where k_p = pole close to saddle point ,

$$z = (\bar{k}_p - \alpha\Omega\sin\phi)\left\{\frac{-i}{\alpha\Omega\cos^2\phi}\right\}^{1/2}$$

and

$H(x)$ = Heaviside function.

Applying the inverse Fourier transform to Equation (B.11) and using Cauchy contour integration theorem, one can evaluate the resulting

integration. Figures B.3a and B.3b show the poles and the contour of integration for $\tau_1 > 0$ and $\tau_1 < 0$, respectively.

The solutions for the radiated pressure from an infinite elastic plate excited by an impulse point force $Q(t) = f_o\delta(t)$ are:

$$P(R,\phi,t) = \frac{\alpha\beta c_o \cos\phi \sqrt{\alpha\varepsilon_2}}{2\pi\sqrt{\pi Rh}} \left\{ \frac{\exp[-2\alpha R\varepsilon_2\tau_1]}{-4\varepsilon_2^2[-5\sin^3\phi\cos^2\phi + \sin^3\phi] - \sin\phi} \right\} ,$$

$$\text{for } \tau_1 > 0 . \qquad \text{(B.12)}$$

and

$$P(R,\phi,t) = -\frac{\alpha\beta c_o \sqrt{2\alpha}\cos\phi(\varepsilon_1^2 + \varepsilon_2^2)^{1/4} \exp(R\alpha\varepsilon_2\tau_1)}{4\pi h^2\sqrt{\pi Rh}\,(a_{11}^2 + a_{22}^2)^{1/2}}$$

$$\times \cos\left\{\frac{\bar{\theta}_1}{2} + R\alpha\tau_1\varepsilon_1 - \frac{\pi}{4} - \bar{\theta}_2\right\} , \text{ for } \tau_1 < 0 .$$

(B.13)

where

$$a_{11} = \mathrm{Re}\{-5\Omega_{p1}^2\sin^3\phi\cos^2\phi + \Omega_{p1}^2\sin^3\phi - \sin\phi\} ,$$

$$a_{22} = \mathrm{Im}\{-5\Omega_{p1}^2\sin^3\phi\cos^2\phi + \Omega_{p1}^2\sin^3\phi - \sin\phi\} ,$$

$$\bar{\theta}_1 = \arctan(\varepsilon_2/\varepsilon_1)$$

and

$$\bar{\theta}_2 = \arctan(a_{22}/a_{11}) .$$

The normalized expressions for the radiated pressure become:

$$\frac{P(2\pi h^2)(R/h)}{F_o(c_o/h)} = \frac{\beta\alpha\sqrt{\alpha(r/h)}}{\sqrt{\pi}}\cos\phi \left\{ \frac{\exp[(R/h)(-2\alpha\varepsilon_2\tau_1)]}{-4\varepsilon_2^2\sin^3\phi[-5\cos^2\phi + 1] - \sin\phi} \right\} ,$$

$$\text{for } \tau_1 > 0 \qquad \text{(B.14)}$$

and

$$\frac{P(2\pi h^2)(R/h)}{F_o(c_o/h)} = -\frac{\beta\alpha\sqrt{\alpha(R/h)}}{\sqrt{2\pi}}\cos\phi\left\{\frac{(\varepsilon_1^2+\varepsilon_2^2)^{1/2}\exp[(R/h)\alpha\tau_1\varepsilon_2]}{(a_{11}^2+a_{22}^2)^{1/2}}\right\}$$

$$\times\cos\left\{-\bar{\theta}_2+\frac{\theta_1}{2}+\frac{R}{h}\alpha\varepsilon_1\tau_1-\frac{\pi}{4}\right\}, \quad \text{for} \quad \tau_1<0\,. \tag{B.15}$$

DISTRIBUTION

Commander (NSEA 09G32)
Naval Sea Systems Command
Department of the Navy
Washington, DC 20362 — Copies 1 and 2

Commander (NSEA 0342)
Naval Sea Systems Command
Department of the Navy
Washington, DC 20362 — Copies 3 and 4

Defense Documentation Center
5010 Duke Street
Cameron Station
Alexandria, VA 22314 — Copies 5 through 16